UDC 66.021.1:532.5,661.15,661.15 66.021.1:532.5
No of state registration 0119U100834
Inv. No

Ministry of Education and Science of Ukraine
Sumy State University
40007, Sumy, R.-Korsakova str., 2;
phone. (0542) 33-41-08/33-40-49

APPROVED
Vise-rector for scientific work
D.Sc. (physics and mathematics),
professor
_____ A.M. Chornous

REPORT
ON RESEARCH WORK

# SMALL-SCALE ENERGY-SAVING MODULES WITH THE USE OF MULTIFUNCTIONAL DEVICES WITH INTENSIVE HYDRODYNAMICS FOR THE PRODUCTION, MODIFICATION AND ENCAPSULATION OF GRANULES

(final)

Manager of research work
Ph.D. (technical sciences),
assoc. prof., senior researcher A.E. Artyukhov

2021

The manuscript was complete on December 20, 2021.

The results of this work were considered by the Scientific Council, Minutes from 2019.12.23 No. 7

# LIST OF AUTHORS

Manager of research work
Ph.D. (technical sciences) A.E. Artyukhov
(introduction, sections 1-3, conclusions)

Responsible performer:
Junior Researcher A.S. Manzharov
(introduction, section 1, 4-6, conclusions)

# ABSTRACT

Report on research work: 121 p., 51 figures, 5 tables, 67 references.

DIRECTIONAL MOTION OF THE FLUIDIZED BED, FREE AND CONSTRAINT MOTION, GRANULATOR, HYDRODYNAMIC OF FLOW MOVEMENT, JET DECAY, MELT DISPERSION PROCESS, NUMERICAL METHODS, OPTIMIZATION, ROTATING PERFORATED SHELL ACTIVE HYDRODYNAMIC REGIME, TRAJECTORY, VIBRATION, NANOPOROUS STRUCTURE, AMMONIUM NITRATE, HUMIDIFICATION, VORTEX GRANULATOR, TWO-COMPONENT FERTILIZERS, POROUS STRUCTURE, MICROPORES AND MACROPORES, POROSITY, EFFECTIVE COEFFICIENT OF THERMAL CONDUCTIVITY, TEMPERATURE PROFILE, HEATING TIME, TEMPERATURE REGIME.

Research object – hydrodynamic and heat-mass exchange characteristics of the target and supporting processes in the granulation modules with intensive hydrodynamics.

The aim of the research is a theoretical description and experimental study of the equipment for the production of monodisperse droplets from solutions and melts with vibrating influence on the melt stream and the granulation and drying of mineral fertilizers in the devices with active hydrodynamics.

Methodology. Mathematical modeling of hydrodynamic flows was carried out based on the points of classical fluid and gas mechanics and technical hydromechanics. Reliability of the obtained experimental results is based on the application of time-tested in practice methods.

Hydrodynamic properties of the liquid jet outflow were obtained. The presented mathematical model allows calculation of the radial component of the jet outflow velocity, as well as determination of the influences of physical and chemical properties of the liquid and the outflow hole diameter on the jet length and flow velocity along the axis to its disintegration into separated drops. The developed mathematical model

extended with the theoretical description of the melt dispersion process from rotating perforated shells allowed us to improve design of the granulator to stabilize hydrodynamic parameters of the melt movement. The nitrogen fertilizers melt disperser was investigated regarding industrial-scale production and operating parameters of the process of jet decay into drops, drop size and monodispersity level were optimized.

*Stage 1 (2019)*

The results of the optimization calculation of devices with active hydrodynamics let to provide:

– a minimum "hydrodynamic" residence time of the particle in the device, which will not exceed "thermodynamic" time (minimum time of particles dehydration to the normative index is determined by the dehydration kinetics laws, thermodynamic indices of the dehydration process);

– implementation of different temperature and humidity potential of the heat transfer agent in some sections in the devices;

– variety of the device construction;

– possibility to use the recirculation of the heat transfer agent.

The original methods of the equipment engineering calculation with the directed fluidized bed as a part to obtain the granulated products are found.

The main recommendations to improve the technological equipment construction of the granulation unit have been implemented in the new methods of granulation and drying.

*Stage 2 (2020)*

The following new scientific results were obtained during the research:

1. A theoretical model of the conditions for the formation of the porous structure of ammonium nitrate granules and the application of an organic shell in a vortex granulator has been created. The influence of the porosity of the granules on the intensity of heat transfer in them is shown.

2. Experimental data of research conditions of formation of the porous structure of granules of ammonium nitrate in the vortex granulator are received. The influence of

hydrodynamic and thermodynamic conditions of the process implementation on the peculiarities of the formation of the porous structure in the granule of porous ammonium nitrate (size, depth, the shape of pores, relative porous surface, etc.) is established.

3. The experimental data of research of the drying of granules of porous ammonium nitrate in multistage shelf devices is received. The influence of the construction of perforated shelf contacts on the residence time of the granules in the apparatus and the morphology of the granule's porous surface is shown.

4. Data on the effect of wetting intensity of ordinary ammonium nitrate granules on the nanoporous structure of granules are obtained. The compositions of solutions for the stage of wetting the granules are proposed.

*Stage 3 (2021)*

1. The authors proposed a modified scheme of the installation for porous ammonium nitrate granulation. They showed the potential for the energy efficiency of the new system compared to the basic one (used in practice) through the exergy analysis. The study of heat and mass exchange processes, chemical transformations, and changes in the phase composition of flows in these devices is of particular interest. One of the directions for further research is to improve the method for obtaining porous ammonium nitrate, particularly the organization of the optimal technological and constructive solution for the humidification and drying stages.

2. The main innovative solutions in the modified scheme are vortex granulator with the new organization of flows' interactive, an ejector module for the utilization of substandard flow; the use of heat and mass exchangers of indirect regenerative evaporative cooling as recuperative, cooling and humidifying equipment; a power generation and heat recovery module based on a sub-atmospheric inverse Brayton cycle. The calculations showed a significant energy efficiency of the proposed solutions.

# TABLE OF CONTENTS

# INTRODUCTION

*Report section "Introduction" is prepared in according to data [1,14] and references in this work.*

Liquid dispersion processes forming micro- or macro drops are used in power generation, medicine, chemical industry, agriculture and other spheres of human activity. Efficiency of these technological processes and equipment is largely determined by the quality of liquid dispersion, which usually involves obtaining monodisperse drops.

This fully applies to the production of the commodity form of nitrogen fertilizers, which is carried out in two main ways:

– granulation starting from the liquid phase by dispersing it on the surface of suspended particles in a fluidized bed that can be variously configured (technologies of Casale S.A., Switzerland; Kahl Group, Germany; Stamicarbon, Netherlands; Toyo Engineering Corporation, Japan; Thyssenkrupp Fertilizer Technology GmbH, Germany, etc.), including vortex granulation;

– granulation starting from the liquid phase by dispersing into drops followed by crystallization of the solute by dewatering and cooling (prilling) (devices of Norsk Hydro, Norway; Didier Engineering GmbH, Germany; Imperial Chemical Industries, UK; Kaltenbach-Thuring S. A., France, etc.).

In these methods, among others, devices with different forms of a perforated shell, generally being axially symmetrical, can be used for dispersion of the nitrogen fertilizer melt.

Melt dispersion devices can be classified by the form of the working part (*i.e.* perforated shell) and by the presence of internal devices in the perforated shell. Additionally, these devices differ in the nature of force acting on the melt and can be static, swirl (tangential introduction of the melt into a perforated shell or to the turbine for the melt spin), and dynamic (rotating).

In recent years, preference is mainly given to conical or cylindrical rotating devices and devices with the cup-shaped shell. This is due to simplicity of operation and high uniformity of resulting liquid drops and commodity granules in comparison to analogue

devices. For example, ammonium nitrate granulators (dispersers), which are currently in operation, provide manufacturing of products with following granulometric composition in terms of mass fraction: 0.5 - 1.5 % of granules < 1.0 mm in size, 90 – 98 % of granules in the size range 2.0 - 4.0 mm, where granules in the size range 2.0 - 2.5 mm comprise 42 – 71 % and granules in the size range 2.0 - 3.0 mm comprise 85 - 95 %. Dispersion of melts producing more than 2 % of dust-forming particles of less than 1.0 mm as well as those over 3.5 mm in size, which can be also destructed making dust, leads to dust formation of nitrogenous fertilizers in air in the tower.

In existing equipment, calculation of hydrodynamic characteristics of the liquid jet that is dispersed, is often not performed, resulting in sub-optimal uniformity of the obtained drops. Hydrodynamic parameters of the liquid jet issuing from a single hole or holes of the perforated shell, and design features of devices for fluid dispersion influence the process of jet decay into drops.

The problem of creating the adequate model of jet decay into drops at the opening in a thin wall is highly relevant for dispersion improvement in granulation devices in the mineral fertilizers production. By controlling the jet decay process, we can optimize performance of the disperser and create favourable conditions to produce a product with a high degree of monodispersity.

The granulated ammonium nitrate has been widely used in agriculture as an effective nitrogen fertilizer. The native industry produces an ordinary ammonium nitrate by the proven technologies, which have been improved for more than fifty years. At the same time, the ammonium nitrate is used as a component of the industrial explosive substance ANFO (ammonium nitrate / fuel oil) in the industry. Such ammonium nitrate, called porous ammonium nitrate (PAN), differs significantly by its properties from the ordinary ammonium nitrate. The ordinary ammonium nitrate can also be a component of ANFO, however, it has several disadvantages:

1. The ordinary ammonium nitrate is covered with a special shell, which prevents the premature dissolution of the granules after its addition into the soil. The protective shell prevents access to the inner pores of the granules.

2. The ordinary ammonium nitrate can be chalked, causing a significant reduction (and, in fact, loss) of the ability to explode in a mixture with diesel fuel.

3. The ordinary ammonium nitrate does not have sufficient porosity for successful retention of the diesel fuel distillate inside the granule.

4. The ordinary ammonium nitrate has a certain number of pores, but their nature is mechanical, not modifying. These are the pores that are obtained as a result of the destruction of the granules (cracks, chips, caverns). Such pores are large enough ($10^{-6}$-10-4 m) and it is difficult to hold the diesel fuel distillate (when transporting ANFO to the blasting places, the diesel fuel distillate flows out of the granule and ideally stays on the surface, at worst - leaves the surface of the granule).

The production of PAN from the ordinary ammonium nitrate by the method of humidification and heat treatment (the method is one of the most energy-efficient and environmentally safe) requires special hydrodynamic and thermodynamic conditions, as well as rational selection of the type and construction of the main technological equipment in granulation. The main task of the technology to produce PAN from the ordinary ammonium nitrate is to form a network of nanopores on the granule surface and in the surface layers, keeping the strength of the core. Vortex granulators have the following advantages:

- the possibility significantly to reduce the overall dimensions (in particular, the height) of the workspace due to the variable height of the cross-sectional area and the possibility of internal circulation of the seeding agent;

- control of the granules' residence time in the workspace;

- the ability to control the motion of granules in the workspace;

- the possibility to create intensive turbulence in the workspace;

- universality (the ability to carry out granulation and drying processes in one device);

- processability and ease of production;

- possibility of fast adjustment and change of constructive and technological parameters if necessary.

# 1 RESEARCH OF THE EQUIPMENT FOR THE PRODUCTION OF MONODISPERSE DROPLETS FROM SOLUTIONS AND MELTS WITH VIBRATING INFLUENCE ON THE MELT STREAM

## 1.1 Decay of the melt stream during dispersion

*This report section is prepared in according to data [1].*

*Experimental rotating vibration granulator*

A rotating vibration granulator is the main unit of the experimental system (figure 1), which consists of a variable perforated membrane 1 with holes to discharge the fluid, housing 2 with a distributive drive 3 and a pipe 4 for introducing air from the fan 5. The housing 2 is also supplied with a fixed liquid distributor 6 with a pipe 7 and a filter element 8.

At the top of the fluid atomizer, a mechanical, electrical or electromagnetic vibrator 9 is installed, which is connected by a rod 10 with the resonator 11 in the form of an elastic disc or plate.

When the granulator is working, liquid that goes through the pipe 7 and the distributor 6 to the bottom part of the granulator flows out of the holes of the perforated membrane. Simultaneously, air at a given pressure is supplied by the fan 5 through the pipe 4 into the cavity of the granulator.

The installation is equipped with a buffer bunker 12 for liquid with a circulation pump 13. Valve 14 and rotameter 15 are used to regulate and measure the liquid flowrate. The oscillations sensor 16 is connected with an oscillograph 17 to observe fluctuations while the digital frequency meter 18 is used to measure the oscillation frequency. When the electrodynamic or electromagnetic vibrator is used, regulation of oscillations is carried out by the electronic controller 19. A stroboscope (20 and 21) is installed for visual observation of the process of liquid dispersion into drops. Measurements of the liquid pressure in holes and air at the free surface of the liquid are carried out by manometers 22 and 23, respectively. The controller 24 is aimed to regulate the air pressure in the granulator.

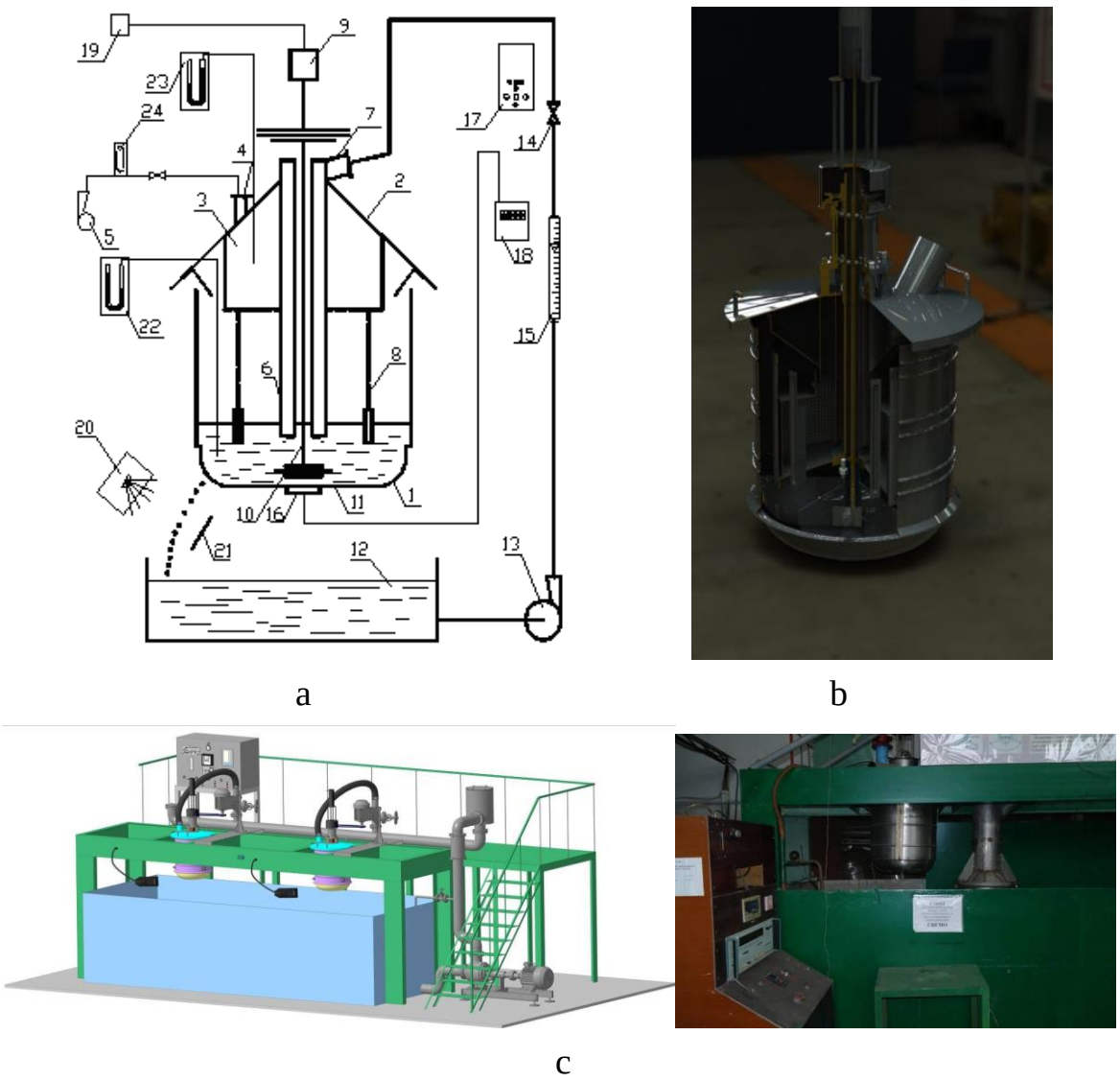


a b

c

Figure 1 – Experimental installation of the rotating vibration granulator: a) a schematic presentation of the granulator: 1- perforated membrane (diameters of holes are 1.0 mm, 1.1 mm, 1.2 mm, 1,3mm, 1,4 mm, number of holes is 1800-2300, bottom shape is toroidal, length is 650 mm, diameter is 560 mm), 2 – housing (height is 590 mm, diameter is 560 mm), 3 – distributive drive, 4 – pipe (diameter is 45 mm), 5 – fan, 6 – liquid distributor, 7 – pipe (diameter is 100 mm), 8 - filter element (metal grid), 9 – vibrator (MFR OTY 77 actuator, range of output frequency 120-1200 is Hz), 10 – rod, 11 - resonator, 12 - buffer bunker, 13 – circulation pump (model Calpeda NC3 25-50/180), 14 – valve, 15 – rotameter (model Raifil RF FM 10), 16 - oscillations sensor, 17 – oscillograph (model C1-65A), 18 – digital frequency meter (model VC3165), 19 – electronic controller, 20, 21 – elements of stroboscope, 22, 23 – manometers (model МТ-2У), 24 – controller (model Euroaqua SKD-1); b) 3D model of the vibrating granulator; c) 3D model and a photograph of the experimental installation

Next, the electronic oscillator 19 is switched on and the electrodynamic vibrator 9 started resulting in vibration of the resonator at a certain frequency, which is fixed and

recorded by the digital frequency meter 18, which is connected to the vibration sensor 16 of the granulator basket. Air is supplied into the granulator by turning the fan 5 on, and when the interstitial position is changed, the certain pressure is installed based on manometer data. The process of jets dispersion into drops is simultaneously monitored by using a stroboscope 20. When formation of monodisperse drops (without satellite droplets) is observed, measurements are recorded at the manometer 22, which corresponds to the total liquid pressure in the leakage holes, and at the digital frequency meter 18 showing the vibration frequency (upper limit). These liquid and air parameters are varied by changing the vibration frequency by the electronic generator 19 at the lower limit of the granulator stable operation range. Ranges of stable operation are determined for different liquid leakage velocities from holes in the basket, which can be achieved by changing the granulator performance under the constant air pressure or by changing the air pressure by using the pressure regulator at the constant granulator performance. When operating the rotating vibration granulator at different liquid leakage velocities, the fluid flow rate is measured by a graduated cylinder.

Physical modeling is based on methods of the similarity theory. The geometric similarity is maintained by equality of appropriate constants and invariants.

The special frequency generator is designed to generate vibration on the radiator of the rotating vibration melting granulator by feeding electric signals of a special shape on the MFR OTY 77 actuator.

*Processing of the experimental results*

Velocity, V, of the liquid leaking from the granulator holes is calculated as:

$$V = \phi\sqrt{2gH}\ , \qquad (1)$$

where φ is the discharge coefficient and set to 0.96-0.98.

According to experimental data of upper $f_1$ and lower $f_2$ limits of the frequency, which provide a monodisperse liquid jet decay, the maximum and minimum lengths of the wave are calculated:

$$\lambda_{max} = V/f_1;\ \lambda_{min} = V/f_2 \tag{2}$$

The melt flowrate, $G_S$, through the granulator hole is calculated from the measured leaked melt volume, $G_\tau$ and time, $\tau$:

$$G_s = G_\tau/\tau\ . \tag{3}$$

Diameter of drops, formed by the decay of liquid jets at the average vibration frequency of the granulator, $f_{avi}$, is determined from the material balance according to the equation:

$$d_{dr} = \sqrt[3]{\frac{6G_s}{\pi f_{avi}}}\ . \tag{4}$$

The absolute difference of drop diameters and a relative deviation of drop diameters from the average drop diameter at the granulator maximum and minimum productivity are calculated as follows:

$$\Delta d_{dr}^{ab} = d_{dr}^{max} - d_{dr}^{min} \tag{5}$$

$$\Delta d_{dr}^{rel} = \frac{2(d_{dr}^{max} - d_{dr}^{min})}{d_{dr}^{max} + d_{dr}^{min}} \tag{6}$$

To define the optimal number of experiments and the highest accuracy degree and reliability of the obtained results, as well as for the processing of these results, methods of mathematical statistics were used.

*Theoretical model*

The model of the jet decay is based on the solution of Navier-Stokes equations (7)-(8) and the flow continuity equation (9) in cylindrical coordinates [9], with the following simplifications:

– flow is axially symmetrical;

– cross-section of the jet is circular, there is only jet restriction and extension (the tangential component of jet velocity $\upsilon_\theta$=0).

$$\upsilon_r \frac{\partial \upsilon_r}{\partial r} = -\frac{1}{\rho}\frac{\partial p}{\partial r} + \nu\left[\frac{\partial^2 \upsilon_r}{\partial z^2} + \frac{\partial}{\partial r}\left(\frac{\frac{\partial}{\partial r}(r\upsilon_r)}{r}\right)\right] \tag{7}$$

$$\upsilon_z \frac{\partial \upsilon_z}{\partial z} = -\frac{1}{\rho}\frac{\partial p}{\partial z} + \nu\left[\frac{\partial^2 \upsilon_z}{\partial z^2} + \frac{1}{r}\frac{\partial}{\partial r}\left(r\frac{\partial \upsilon_z}{\partial r}\right)\right] \tag{8}$$

$$\frac{\partial \upsilon_z}{\partial z} + \frac{1}{r}\frac{\partial}{\partial r} r\upsilon_r = 0 \tag{9}$$

By assuming that the axial velocity component at the time of leaving the hole varies parabolically with the radial coordinate:

$$\upsilon_z = A_1 r^2 z^2 + A_2 r + A_3 \tag{10}$$

And transforming the equation (9), we obtain the value of the radial component of the jet velocity:

$$\upsilon_r = \frac{-\frac{1}{2}A_1 r^4 z + F_1(z)}{r} \tag{11}$$

where $F_1(z)$ is a polynomial function.

Given the fact that the pressure change in a jet in the radial direction is insignificant compared to the axial component, and by substituting (10) into (8) we get:

$$2\left(A_1 r^2 z^2 + A_2 r + A_3\right) A_1 r^2 z = \frac{1}{\rho}\frac{dp}{dz} + \nu\left(2A_1 r^2 + \frac{4A_1 r z^2 + A_2}{r}\right) \tag{12}$$

By solving the equation (12) for d$p$/d$z$ and by integration the expression for pressure change along the jet axis it is obtained:

$$p(z) = -\frac{1}{3}\rho\left(\frac{1}{3}A_1^2 r^5 z^4 + A_1 r^4 z^2 A_2 + A_1 r^3 z^2 A_3 - 2\nu A_1 r^3 z - \frac{4}{3}\nu A_1 r z^3 - \nu A_2 z\right) + C_1 \tag{13}$$

By setting the origin of the coordinate system at the hole exit ($z$ = 0) and by introducing the assumption that the liquid outflow occurs at a constant pressure ($p$ = const), then according to (13) it is obtained that $C_1 = p_1$.

After insertion of this constant we get:

$$p(z) = -\frac{1}{3}\rho\left(\frac{1}{3}A_1^2 r^5 z^4 + A_1 r^4 z^2 A_2 + A_1 r^3 z^2 A_3 - 2\nu A_1 r^3 z - \frac{4}{3}\nu A_1 r z^3 - \nu A_2 z\right) + p_1 \tag{14}$$

By inserting (14) into (7) we obtain the differential equation of total derivatives in respect to the function $F_1(z)$:

$$\frac{\left(-\frac{1}{2}A_1r^4z+F_1(z)\right)\left(-2A_1r^2z-\frac{-\frac{1}{2}A_1r^4z+F_1(z)}{r^2}\right)}{r}=-\frac{1}{\rho}\left(\frac{1}{r^2}\rho\left(\frac{1}{2}\right)A_1^2r^5z^4+A_1r^4z^2A_2+\right.$$

$$+A_1r^3z^2A_3-2\nu A_1r^3z-\frac{4}{3}\nu A_1rz^3-\nu A_2z\left(-\frac{1}{r}\rho\left(\frac{5}{2}\right)r^4A_1^2z^4+4A_1r^3z^2A_2+\right.$$

$$\left.+3A_1r^2z^2A_3-6\nu A_1r^2z-\frac{4}{3}\nu A_1z^3+\nu\left(\frac{1}{r}\right)\frac{d^2F_1(z)}{dz^2}-4A_1rz\right) \qquad (15)$$

Based on the fact, that the derivative $d\upsilon_r/dz$ is equal to:

$$\frac{d\upsilon_r}{dz}=\frac{-\frac{1}{2}A_1r^4z+\frac{dF_1(z)}{dz}}{r} \qquad (16)$$

And the radial velocity component of the jet at $z=0$ becomes $\upsilon_r=0$, we obtain:

$$\frac{1}{2}A_1r^4z=\frac{dF_1(z)}{dz}. \qquad (17)$$

By using the boundary conditions $F_1(z=0)=0$ and $dF_1/dz\ (z=0)=0$, and putting them into the equation (10) we obtain the value of the function $F_1$ as a polynomial:

$$F_1(z)=\frac{(-A_2+8A_1r^3)z^3}{6r}+\frac{A_1r^2(3A_1r^4-12A_2r-8A_3)z^4}{48\nu}. \qquad (18)$$

Substituting the relation (18) in the equation (11) leads to:

$$\upsilon_r=\frac{z\left(24A_1r^5\nu-8\nu z^2A_2+64\nu z^2A_1r^3+3A_1^2r^7z^3-12A_1r^4z^3A_2-8A_1r^3z^3A_3\right)}{48\nu r^2}. \qquad (19)$$

The coefficient $A_2$ can be found by assuming that on the jet surface $r=r_s$ the pressure p is equal to the pressure of the surrounding environment $p_0$. This boundary condition can be written as:

$$p_0 = -\frac{1}{r_s}\left(\frac{1}{3}\rho\left(\frac{1}{2}A_1^2 r_s^5 z^4 + A_1 r_s^4 z^2 A_2 + A_1 r_s^3 z^2 A_3 - 2\nu A_1 r_s^3 - \frac{4}{3}\nu A_1 r_s z^3 - \nu A_2 z\right)\right) + p_1 \quad (20)$$

Thus, the coefficient $A_2$ is now calculated as:

$$A_2 = -\frac{(r_s(3z^4 A_1^2 \rho r_s^4 + 6z^2 A_1 \rho r_s^2 A_3 - 12zA_1\rho\nu r_s^2 - 8\rho\nu A_1 z^3 - 6p_1 + 6p_0))}{6\rho z(A_1 r_s^4 z - \nu)}. \quad (21)$$

The coefficient $A_3$ can be defined by assuming that that if $r=0$, $\upsilon_r=0$:

$$A_3 = -\frac{3z^4 A_1^2 \rho r_s^4 + 6p_0 - 12zA_1\rho\nu r_s^2 - 8\rho\nu A_1 z^3 - 6p_1}{6z^2 r_s^2 \rho A_1}. \quad (22)$$

Accordingly,

$$\upsilon_z = A_1 r^2 z^2 - \frac{3z^4 A_1^2 \rho r_s^4 + 6p_0 - 12zA_1\rho\nu r_s^2 - 8\rho\nu A_1 z^3 - 6p_1}{6z^2 r_s^2 \rho A_1}. \quad (23)$$

The coefficient $A_1$ is determined by assuming that at a point close to the origin of the coordinate system $z = z_0$, the exhaust velocity has not yet changed its value and is equal to the flow velocity jet in the hole $\upsilon_z = \upsilon_{z0}$ that is:

$$\upsilon_{z_0} = \frac{6A_1^2 r^2 z_0^4 r_s^2 - 3z_0^4 A_1^2 \rho r_s^4 - 6p_0 - 12z_0 A_1 \rho\nu r_s^2 + 8\rho\nu A_1 z_0^3 + 6p_1}{6z_0^2 r_s^2 \rho A_1}. \quad (24)$$

When we solve the resulting equation (24) for the coefficient $A_1$, we obtain:

$$A_1 = \frac{1}{3z_0^3 r_s^2 \rho(2r^2 - r_s^2)}(-4\nu\rho z_0^2 + 3\upsilon_{z0} r_s^2 \rho z_0 - 6\rho\nu r_s^2 + (16\nu^2\rho^2 z_0^4 -$$

$$-24\nu\rho^2 z_0^3 \upsilon_{z0} r_s^2 + 48\nu^2\rho^2 z_0^2 r_s^2 + 9\upsilon_{z0}^2 r_s^4 \rho^2 z_0^2 - 36\upsilon_{z0} r_s^4 \rho^2 z_0 \nu + 36\rho^2\nu^2 r_s^4 +$$

$$36z_0^2 r^2 r_s^2 \rho p_0 - 36z_0^2 r^2 r_s^2 \rho p_0 - 36z_0^2 r^2 r_s^2 \rho p_1 - 18z_0^2 r_s^4 \rho p_0 + 18z_0^2 r_s^4 \rho p_1)^{1/2}) \qquad (25)$$

The presented mathematical model allows calculating radial and axial components of the velocity jet outflow, as well as to establish the influence of physical and chemical properties of the liquid and the hole diameter on the jet length and velocity along the axis to its disintegration into separate drops (figures 2, 3).

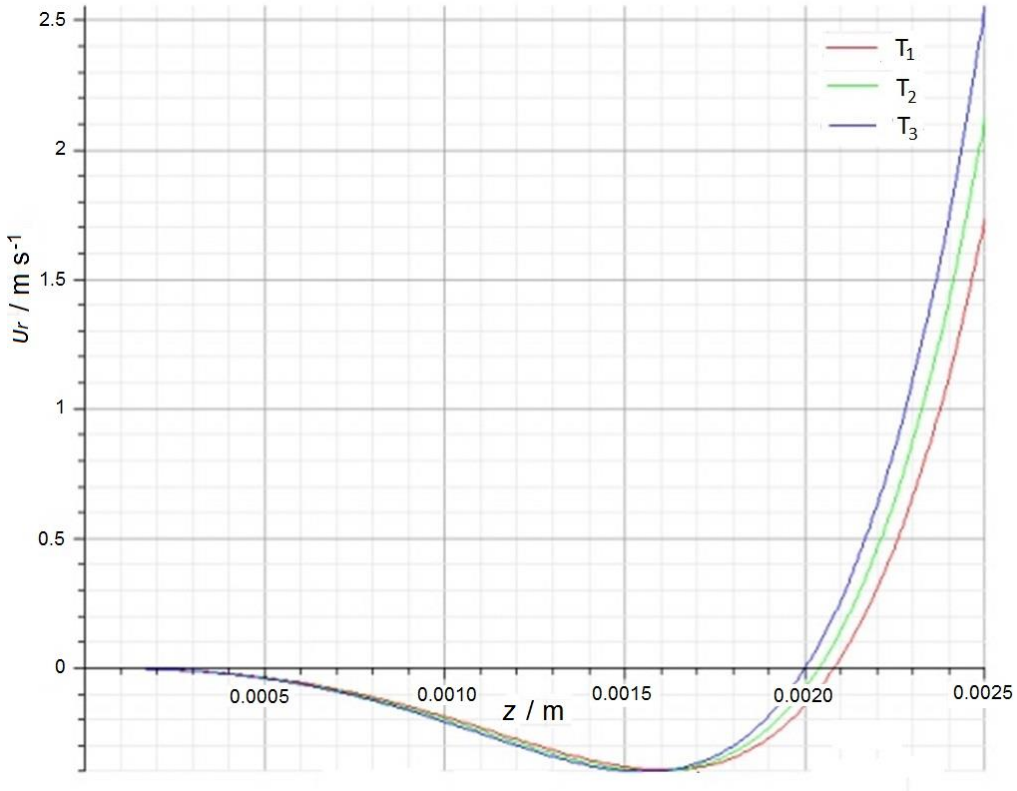


Figure 2 – Dependence of the radial component of the jet velocity of the ammonium nitrate melt on the axial distance, z, from the hole 1.3 mm in diameter at different temperatures of the melt at $T_1$ = 175°C, $T_2$ =180°C, $T_3$ = 185°C and the vibration frequency of 340 Hz (viscosities were 5.36, 5.03, 4.74 mPa·s, densities were 1434, 1431, 1428 kg/m$^3$ respectively)

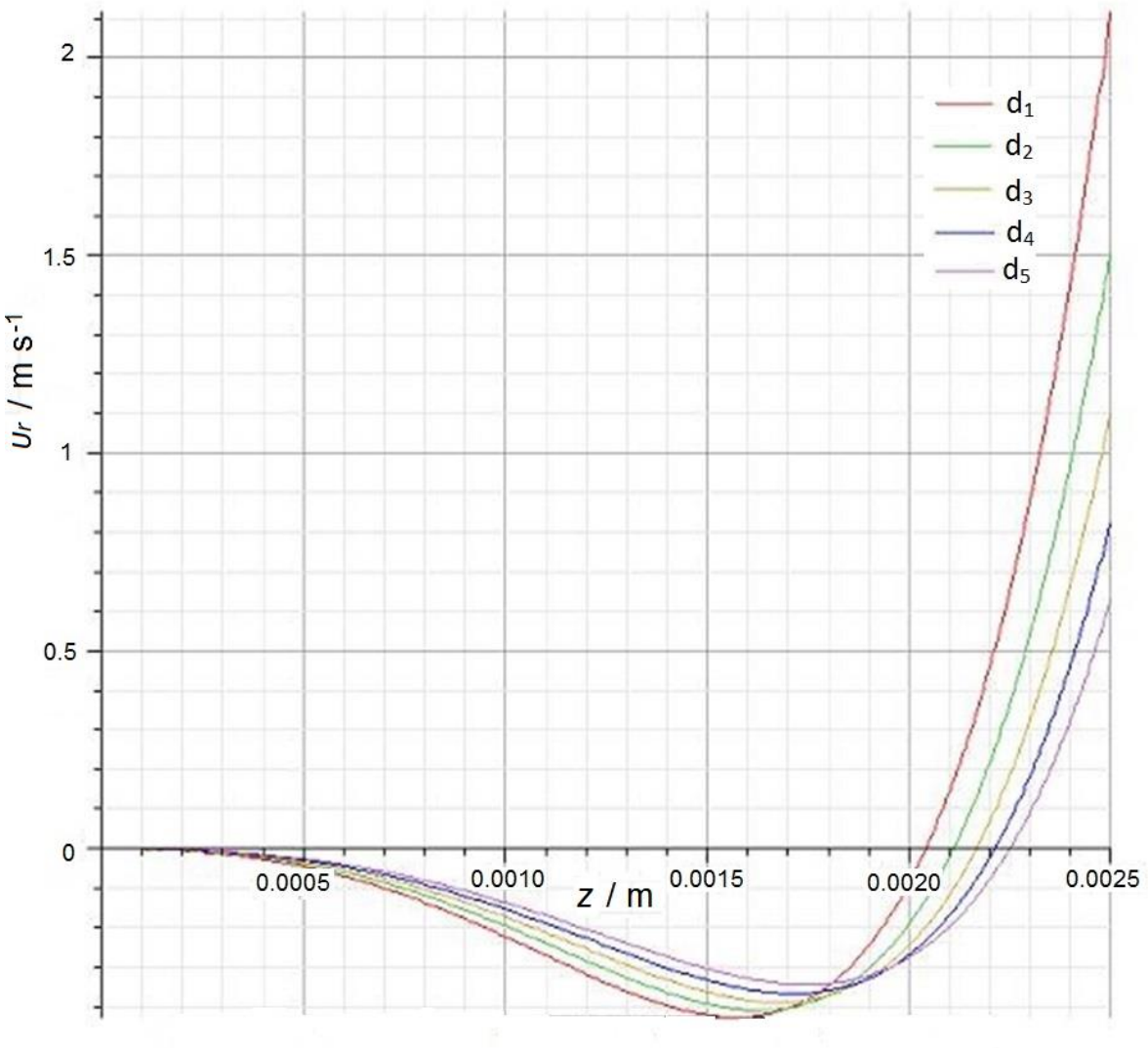


Figure 3 – Dependence of the radial component of the jet velocity of the ammonium nitrate melt on the axial distance, z, from the holes of different diameters: $d_1$=1.0 mm, $d_2$=1.1 mm, $d_3$=1.2 mm, $d_4$=1,3mm, $d_5$=1,4 mm at the temperature of 185°C (viscosity was 4.74 mPa·s, density was 1428 kg/m$^3$) and the vibration frequency of 340 Hz

For the granulator basket rotation velocity of $n$ = 60 rpm and a load of 37 t/h optimal diameter of the hole is $d$ = 1.2 mm and the melt temperature is 185 °C.

An example of comparison of theoretical calculations and experimental results of velocity radial component measurement is shown in table 1.

Basket tests of the granulator confirmed the theoretical research and provided a basis for modernization of the equipment construction. During the tests, a stable jet breakup

into drops at a distance of 2-5 mm from the wall of the perforated shell was obtained (figures 4, 5).

Table 1 – An example of comparison of theoretical calculations and experimental results of $\upsilon_r$ measurement (hole diameter was 1.3 mm, temperatures of the melt was 175°C (viscosity was 5.36 mPa·s, density was 1434 kg/m$^3$), vibration frequency was 340 Hz, granulator basket rotation velocity was n = 60 rpm and a load was 37 t/h**)**

| $\upsilon_{r.theor}$ / m s$^{-1}$ | No of measurement | $\upsilon_{r.exp}$ / m s$^{-1}$ | $\upsilon_{r.theor}$ / m s$^{-1}$ | No of measurement | $\upsilon_{r.exp}$ / m s$^{-1}$ |
|---|---|---|---|---|---|
| *z* = 0 m | | | *z*= 0.0005 m | | |
| 0 | 1 | 0 | -0.05 | 1 | -0.04 |
| 0 | 2 | -0.003 | -0.05 | 2 | -0.02 |
| 0 | 3 | 0.002 | -0.05 | 3 | -0.08 |
| 0 | 4 | 0 | -0.05 | 4 | -0.07 |
| 0 | 5 | 0.004 | -0.05 | 5 | -0.09 |
| 0 | 6 | -0.005 | -0.05 | 6 | -0.04 |
| *z* = 0.001 m | | | *z* = 0.0015 m | | |
| -0.2 | 1 | -0.21 | -0.4 | 1 | -0.4 |
| -0.2 | 2 | -0.19 | -0.4 | 2 | -0.42 |
| -0.2 | 3 | -0.19 | -0.4 | 3 | -0.39 |
| -0.2 | 4 | -0.19 | -0.4 | 4 | -0.38 |
| -0.2 | 5 | -0.18 | -0.4 | 5 | -0.4 |
| -0.2 | 6 | -0.2 | -0.4 | 6 | -0.41 |
| *z* = 0.002 m | | | *z* = 0.0025 m | | |
| 0 | 1 | -0.01 | 2.5 | 1 | 2.44 |
| 0 | 2 | 0.01 | 2.5 | 2 | 2.53 |
| 0 | 3 | 0.02 | 2.5 | 3 | 2.51 |
| 0 | 4 | 0 | 2.5 | 4 | 2.41 |
| 0 | 5 | -0.03 | 2.5 | 5 | 2.56 |
| 0 | 6 | 0 | 2.5 | 6 | 2.6 |

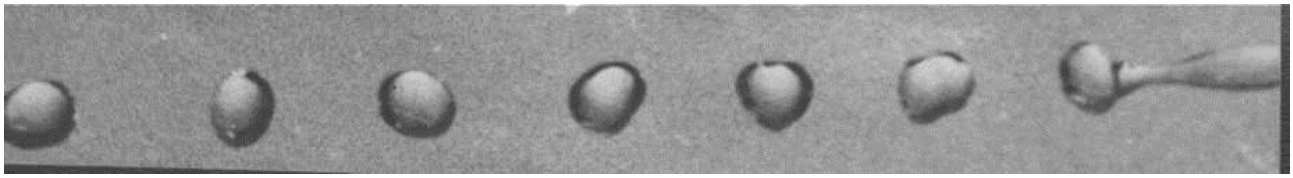

a

b

Figure 4 – Jet disintegration into drops after the outflow from the perforated shell: a) ammonium nitrate drops, vibration frequency of 200 Hz; b) ammonium nitrate drops, vibration frequency of 340 Hz. Diameter of the hole was 1.1 mm and the temperature was 185°C (viscosity was 4.74 mPa·s, density was 1428 kg/m$^3$). Granulator basket rotation velocity was n = 60 rpm and a load of 37 t/h

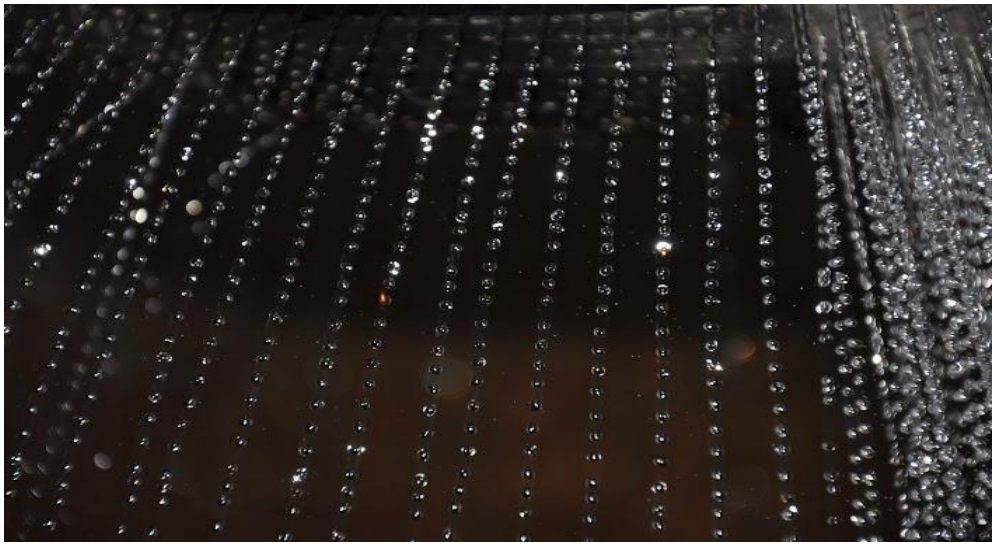

Figure 5 – Steady jet disintegration into drops after the outflow from the perforated shell: ammonium nitrate drops, vibration frequency of 340 Hz. Diameter of the hole was 1.1 mm and the temperature was 185°C (viscosity was 4.74 mPa·s, density was 1428 kg/m$^3$). Granulator basket rotation velocity was n = 60 rpm and a load of 37 t/h

The developed mathematical model was extended with the theoretical description of the melt dispersion process from rotating perforated shells, which allowed us to improve the granulator design to stabilize hydrodynamic parameters of the melt movement within

it. By applying of a weighted vortex layer in combination with the vibrating material liquid spray and rotation of liquid jets by their decay should further improve the quality of the granulated product.

A scheme of the modernized granulator is shown in figure 6, and layout solutions for the granulator installation in a granulation tower in figure 7. Similarity of respective particles movements and their trajectories in the industrial design and in the experimental granulator is maintained.

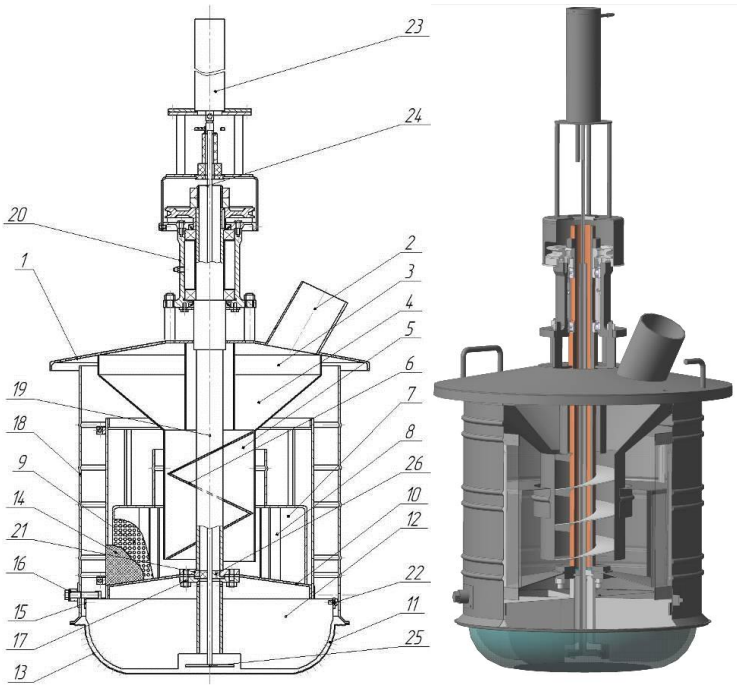


Figure 6 – The improved rotating vibration granulator of solutions (melts): 1 - housing; 2 - pipe for introducing the solution (melt); 3 - ring collector; 4 - reverse cone; 5 - annular channel; 6 - auger; 7 - distributor of the solution (melt); 8 - directing blades; 9 - perforated cylinder; 10 - directing cone for the solution (melt); 11 - perforated bottom (basket); 12 - pressure blades; 13 - hole; 14 - mesh for the final melt filtration; 15 - ring; 16 - bolts; 17 - pins; 18 - cylindrical chamber; 19 - hollow shaft; 20 - bearing assembly; 21 - flange connection; 22 - bulge for centering the cylindrical chamber; 23 - vibration device; 24 - rod; 25 - disc radiant; 26 - hub

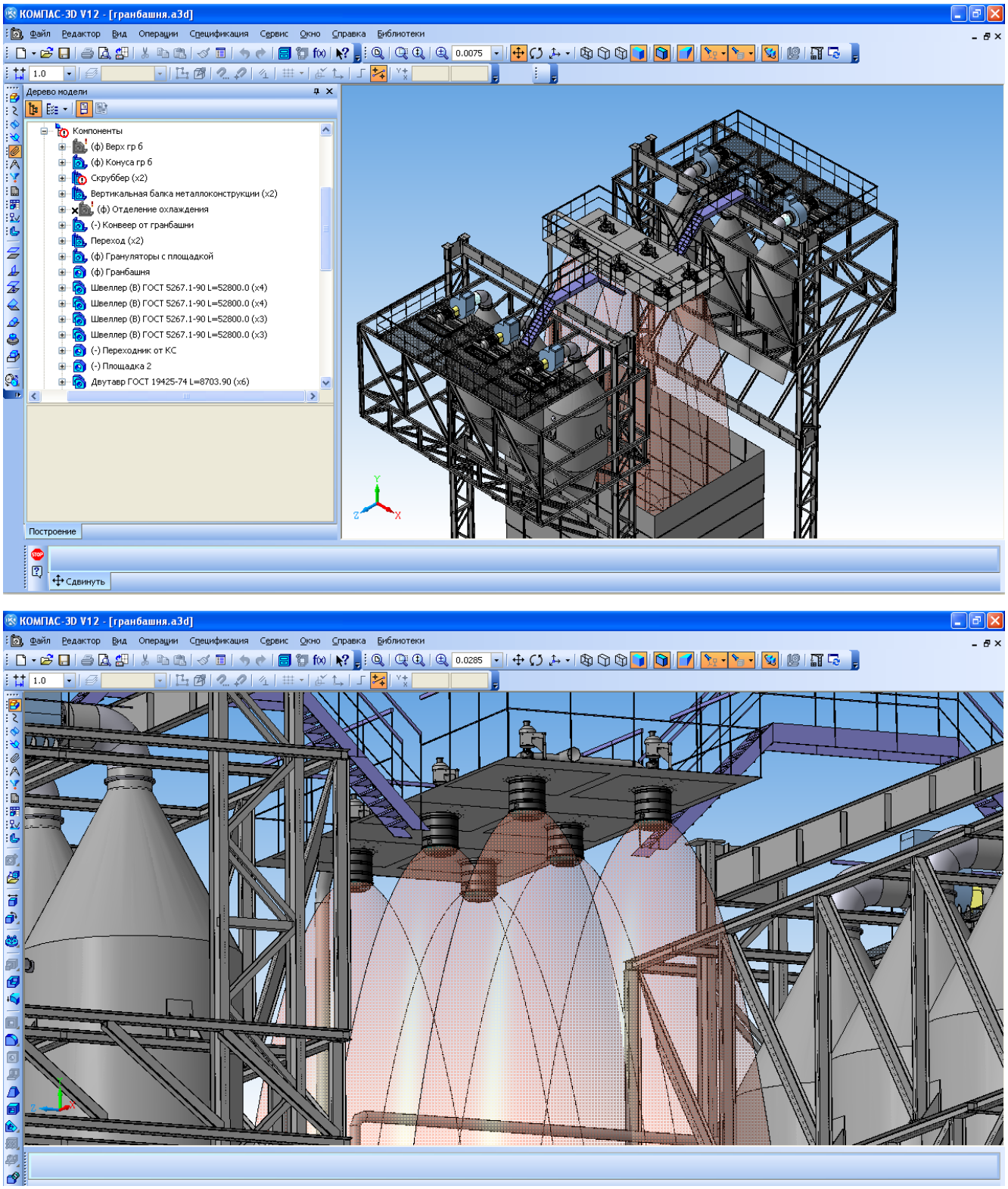


Figure 7 – Layout solutions for granulator installation in a granulation tower

The improved granulator has a guiding element in the form of an auger installed, so when the melt contacts the shoulder blade, the total melt pressure is increased by

transforming the screw mechanical energy into the melt kinetic energy and then turning it into the internal energy. Possibility of screw rotation provides an option for increasing the pressure in front of the outflow holes.

Pilot testing of the improved granulator of the total capacity of 37 t/h in production of ammonium nitrate at different climatic conditions (humid and hot climate, temperate continental climate) showed a high yield of marketable fractions and reduction of dust content in flue gases. High level of monodispersity of granules is achieved by improving the fusion hydrodynamics in the granulator and by applying vibration to the jets leaking from the basket perforated bottom. Also the improved granulator significantly reduced the dust level in the air leaving the tower. Axial flow fans capture from 16 to 38 mg/m$^3$ of dust so that the granulator enables reduction of costs needed for purchasing expensive new equipment for treatment of the exhaust air.

Results of basic tests of the improved granulator are shown in figures 8 and 9. Analysis of figures 8 and 9 provides determination of an optimal (operating) vibration frequency (frequency range), at which the maximal degree of drop monodispersity is achieved. At these conditions, the melt jet disintegrates evenly and without formation of drop satellites.

The monodispersion process introduces a fundamental improvement in the fertilizer production technology. Use of uniform (monodisperse) granules, for example in agriculture, provides even distribution of the fertilizer on the fertilized area resulting in additional yields up to 10 % [10-12].

Vibrating granulators provide production of strong monodisperse granules with a smooth glossy surface (the monodispersity degree is up to 99 %). Thus, these devices open possibilities to intensify the granulation process and essentially improve the agrotechnical value of fertilizers.

Table 2 shows a comparative analysis of granulometric compositions of final products obtained in different types of granulators.

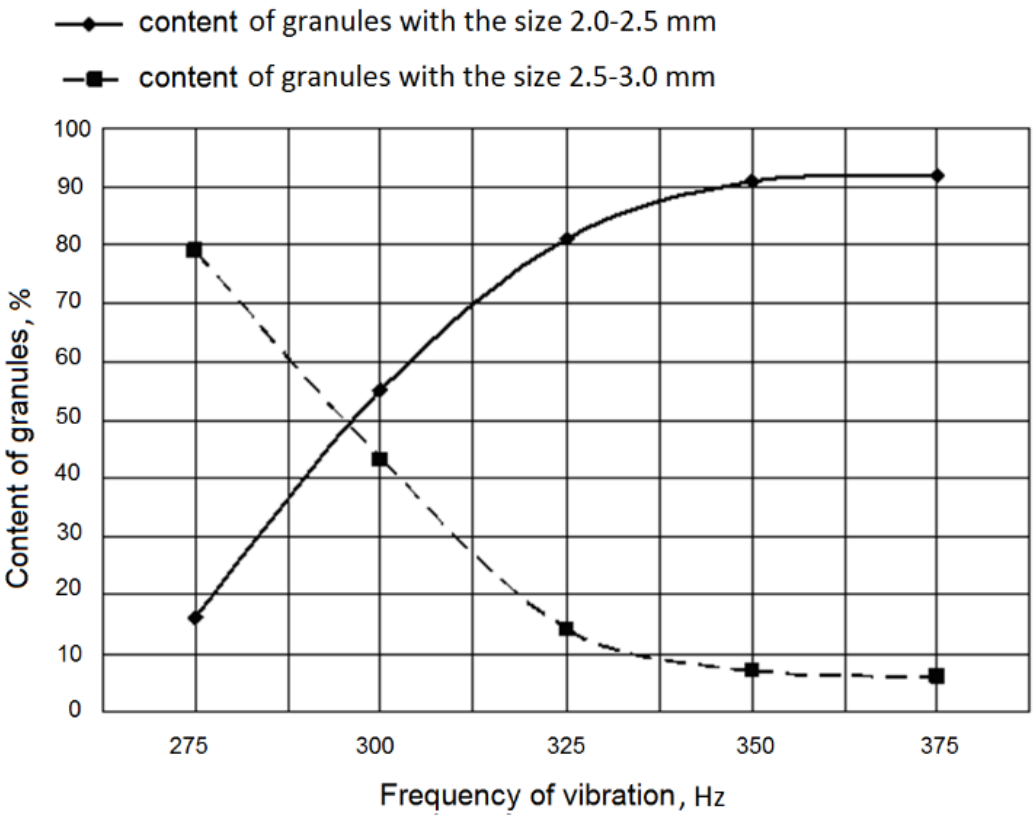


Figure 8 – Mass fractions of ammonium nitrate granules with sizes 2.0 – 2.5 mm and 2.5 - 3.0 mm as functions of the vibration frequency at the granulator basket rotation velocity of n = 60 rpm, load of 37 t/h and 1.2 mm hole diameter

Table 2 – Comparison of granulometric content of products obtained in the improved rotating vibration granulator and in world analogues of the granulation equipment

| Granule size range, mm | Granulometric content of products, % | | |
|---|---|---|---|
| | Centrifugal granulator, company "Kreber" (Netherlands) [2] | Acoustics granulator designed by Research Institute at the Chemical plant (Russia) [3] | Improved rotating vibration granulator |
| 1 - 4 | 97-99 | 98-99 | more than 99 |
| 2 - 4 | 83-92 | 85-95 | 90-97 |
| 2 - 3 | 75-90 | 80-90 | more than 90 |
| 2.0 - 2.5 | 40-50 | 45-65 | more than 80 |
| less than 1 | 0.8-2.5 | 0.8-1.5 | 0.1-0.8 |

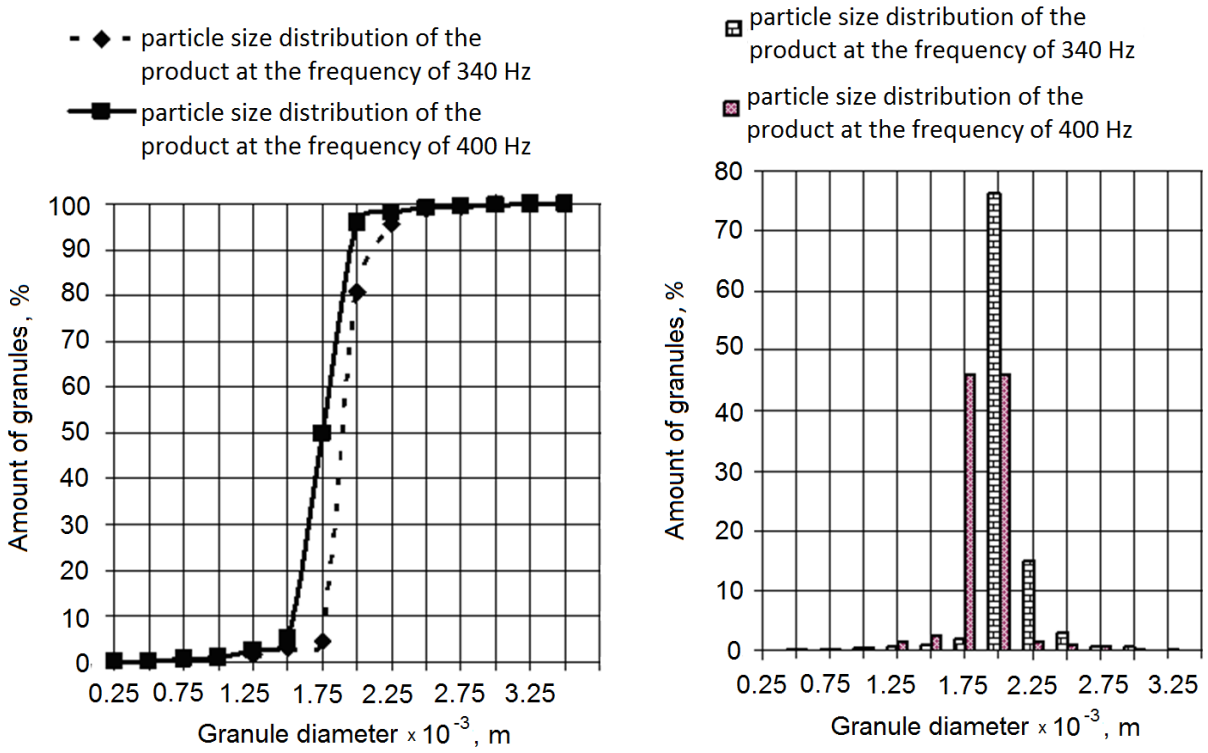


a b

Figure 9 – The integral particle size distribution of ammonium nitrate granules at vibration frequencies of 340 and 400 Hz and the granulator basket rotation velocity of n = 60 rpm, load of 37 t/h and the hole diameter of 1.2 mm: a) line graph b) bar chart

The improved granulator has following advantages over other granulator types:

– high safety in operation;
– production of more competitive uniform granules;
– avoidance of product's sticking in towers;
– decrease of dust;
– increase of the agro-technical value of fertilizers.

The improved vibrating granulators have a reliable vibration system, which provides a stable imposition of oscillations on fluid jets flowing out of perforated shell holes, regardless the changes in the load on the melt disperser. This vibration system provides measurements of the level of melt in the granulator and thereby, control of the clogging degree and melt outflow velocity from the holes of the perforated shell.

The improved vibrating granulator (figure 6) with an electromagnetic vibration system (vibration frequency of 340 Hz) provided production of a product with the following granulometric composition as mass fractions: 0.02 - 0.2 % of granules < 1.0 mm and over 96 % of granules 2.0 - 4.0 mm in size. Also, the fraction of granules in the size range 2.0 - 2.5 mm was not lower than 88 % with the main size in the range 2.1 - 2.5 mm. When the vibration frequency was changed to 400 Hz, the granulator provided a product with the main granule fraction (over 65 %) in the size range 2.5 - 3.0 mm with a simultaneously obtained increased granule hardness.

Similar granulometric compositions of products were obtained by using vibrating granulators with electromagnetic vibration systems in the ammonium nitrate production at tropical conditions in Cuba and in urea production with hydrohumates as foaming additives. During the industrial operation over one month the product (urea) was stably obtained with the following granulometric composition in mass fractions: 0.1 - 0.3 % of granules < 1.0 mm, 99.7 - 99.9 % of granules in the size range 1.0 - 4.0 mm where granules in the size range 2.0 - 4.0 mm comprised 96.5 - 98.9 % while granules larger than 4.0 mm were absent.

Consideration of hydrodynamic parameters of the liquid jet flowing out of holes of a perforated membrane allowed us to affect the process of jet decay into drops and resulting drop size and dispersity and consequently to improve the construction of nitrogen fertilizers melt granulator.

Main results:

– a mathematical model was derived to calculate hydrodynamic properties of the melt jet expiration process from a perforated shell;

– influences of the hole diameter and melt properties on the radial velocity field were determined and shown;

– optimal conditions for prilling in a rotating vibration granulator for a given capacity of 37 t/h are defined: the rotation velocity of the basket (60 rpm), the diameter of holes in the perforated shell (1.2 mm), the melt temperature (185 $^{o}$C), the frequency range of the actuator’s oscillation (340-400 Hz);

– the experimental studies and mathematical modeling provided possibilities for construction of a modernized rotating vibration granulator;

– industrial tests of the modernized vibrating granulator confirmed optimal conditions of the prilling resulting in the improved product.

## 1.2 Improving of the electronic intellectual cleaning system of holes in perforated shells of the priller

This report section is prepared in according to data [4].

The improvement of the prillers operation and quality of the obtained product has been achieved by creating the intellectual system to form the monodispersed drops in the dispersed devices, based on the electromagnetic vibrator [5]. This system enabled:

– to regulate the average size of the obtained granules, depending on the air temperature at the entrance to the granulation tower;

– to receive the stable size of granules, which does do not depend on the load (flow rate) of the fusion for priller;

– to reduce the heating load on the tower;

– to decrease the fraction content of granules of less than 1.0 mm in the product to 0.1-0.2% and dust in the air at the entrance of the tower by 20-60%.

At the same time, the market demands led to the necessity to produce goods with additives (for example porous ammonium nitrate, calcium-ammonium nitrate of the CAN trademark containing 25-28% of nitrogen). In the production of these fertilizers the powdered substances or liquid components, which contain particles larger than 0.4 mm, are fed into the nitrogen fertilizer fusion. These particles come to the holes of the perforated shell and cause full or partial clogging. It leads to:

– increase of the fusion level in the perforated shell of the priller;

– changes in the jet motion trajectory, that causes the sticking of the product to the workspaces in the tower;

– vibration system of the priller works in the non-optimal mode in case of the increased fusion level;

– deterioration of the granulometric composition of the product.

Table 3 –Description of the priller operation

| | | | |
|---|---|---|---|
| Load on the priller by the fusion of the ammonium nitrate, t/hour | 40 | 41 | 40 |
| Level of the fusion in the perforated shell of the prillers, m | 0.150 | 0.240 | 0.290 |
| The fraction content is less than 1.0 mm in the product | 0.1 | 0.4 | 1.1 |

As it is seen from the demonstrated data regarding the priller operation, the clogging of the holes in the perforated shell leads to the great increase of the fusion level in it and dust content rise in the product.

In order to remove the clogging of holes in the priller, the melt is stopped to flow and steam is fed or it is stopped to work, is demounted. The perforated shell and inner constructions of the priller are cleaned. During one day such cleaning can be carried out 3–15 times. It leads to the great losses of goods, unstable production.

In order to clean the holes in the perforated shell of the priller without stopping its work, it is reasonable to use high-frequency vibration. Such frequency can be periodically transmitted to the perforated shell of the priller.

Based on the above, the main aim of this research is to create the electronic intellectual system to regulate the formation of the monodispersed drops in the granulation devices and to clean their holes when they are clogged.

The high-frequency vibration is imposed on the perforated shell 6 by the high-frequency vibrator 9 (figure 1) in two modes:

– periodically in some time τ;

– when a certain level of the liquid is achieved in the perforated shell 6.

In the first mode of the holes cleaning in the perforated shell, the variable parameters included the duration of the high-frequency vibrator impulse, its amplitude, vibration frequency, the liquid level in the shell before and after the vibration overlay.

In the second mode of the holes cleaning in the perforated shell, the variable parameters included the amplitude of the high-frequency vibrator impulse and its vibration frequency. The operation o the high-frequency vibrator was based on the intellectual system and carried out to the value of the liquid level in the basket which was closer to the total cleaning of the holes.

The monodispersed fragmentation of drops was fixed as indicators of the device operation.

The level of liquid in the perforated shell

$$H = \frac{\left(\frac{4G}{n\pi d^2 \varphi}\right)^2}{2g}, \qquad (26)$$

where $G$ – flow rate of the liquid phase, $m^3$/hour;

$n$ – number of holes in the perforated shell;

$d$ – diameter of holes in the perforated shell, m;

$\varphi$ – jet compression coefficient;

g – gravitational acceleration, $m/s^2$.

The structure and operating principle of the cleaning system of the holes in the perforated shell

The cleaning system of the holes in the perforated shell consists of the control panel and the high-frequency generator. The high-frequency generator is used to generate vibrations on the perforated shell of the priller.

Block-diagram of the high-frequency vibrator operation according to the second variant:

1. The income parameters: the liquid level in the perforated shell H, liquid flow rate G.

2. Determining of H.

3. Comparing

if Hi < H + xH →yes → to turn off the high-frequency vibrator;

→no → to switch on the high-frequency vibrator.

The main parameters and properties:

- Microprocessor – PIC16F877A:
- Frequency interval – 10Hz-10MHz;
- The frequency setting error of the high-frequency signal generator – 0.01.
- Frequency instability in 5 minutes of the work – $1 \cdot 10^{-5} f$.
- Signal output level – 2W.
- The output level setting error of the high-frequency signal generator – 10%.
- Harmonic components level – 30dB.
- Parasitic amplitude modulation – 0.3%.
- Parasitic numerical modulation of a high-frequency signal generator – $3 \cdot 10^{-6} f$.

Amplitude modulation mode:

- modulation coefficient – 0%-99%;
- error of the device / installation error – 10%;
- modulating frequency range – 0,05kHz-10kHz.

The cleaning system consists of the control panel and the high-frequency vibrator.

The control panel regulates the liquid level in the perforated shell of the priller, amplitude and frequency of vibration. The panel is implemented on the microprocessor. Thereby, it possesses high stability in the work and installation simplicity. The device lets to keep settings in the non-volatile memory, which can be easily changed depending on the exploitation conditions of the priller. The control panel has a built-in protection system against overload, overheating and a system of the “soft start”.

To supply the whole device with power, the power source, made according to the classical scheme of the transformer, is used.

The installation of such a vibration system enables to:

– indirectly assess the degree of the holes clogging in the perforated shell of the priller;

– clean the holes in the perforated shell without stopping the priller and production as a whole;

– if it is necessary, the system lets to control the priller operation, using a PC;

– obtain the high-qualitative fractional composition of the final product;

– simplify technical service of the priller;

– use more reliable prilling system in the production.

All control elements are on the front panel. The printed boards of the device are treated with a protective varnish. The device has the built-in system, which lets to leave the "hangup" state if there are any failures in the program (as a rule, caused by the external factors – by welding, strong electromagnetic field, etc.).

The electric intellectual cleaning system scheme of perforated shell holes in the priller is demonstrated in figure 10.

The scheme works in the following way.

The input current $I_{in}$=4…20mA is converted into the voltage $V_{in}$=0.4…2V on the resistor $R_1$. The input voltage $U_{in}$ comes to the microcircuit $DA_1$ point 4 and is converted into the frequency according to the equations (2) and (3). If the control (control panel) is supplied with a voltage of about 0V, the frequency will be changed depending on $I_{in}$ by the equation (2). If the control (control panel) is supplied with a voltage of 10 V, the transistor $TV_1$ will be opened and resistor $R_3$ will be shorted out and the equation (3) will be used in the predetermined range (cleaning mode).

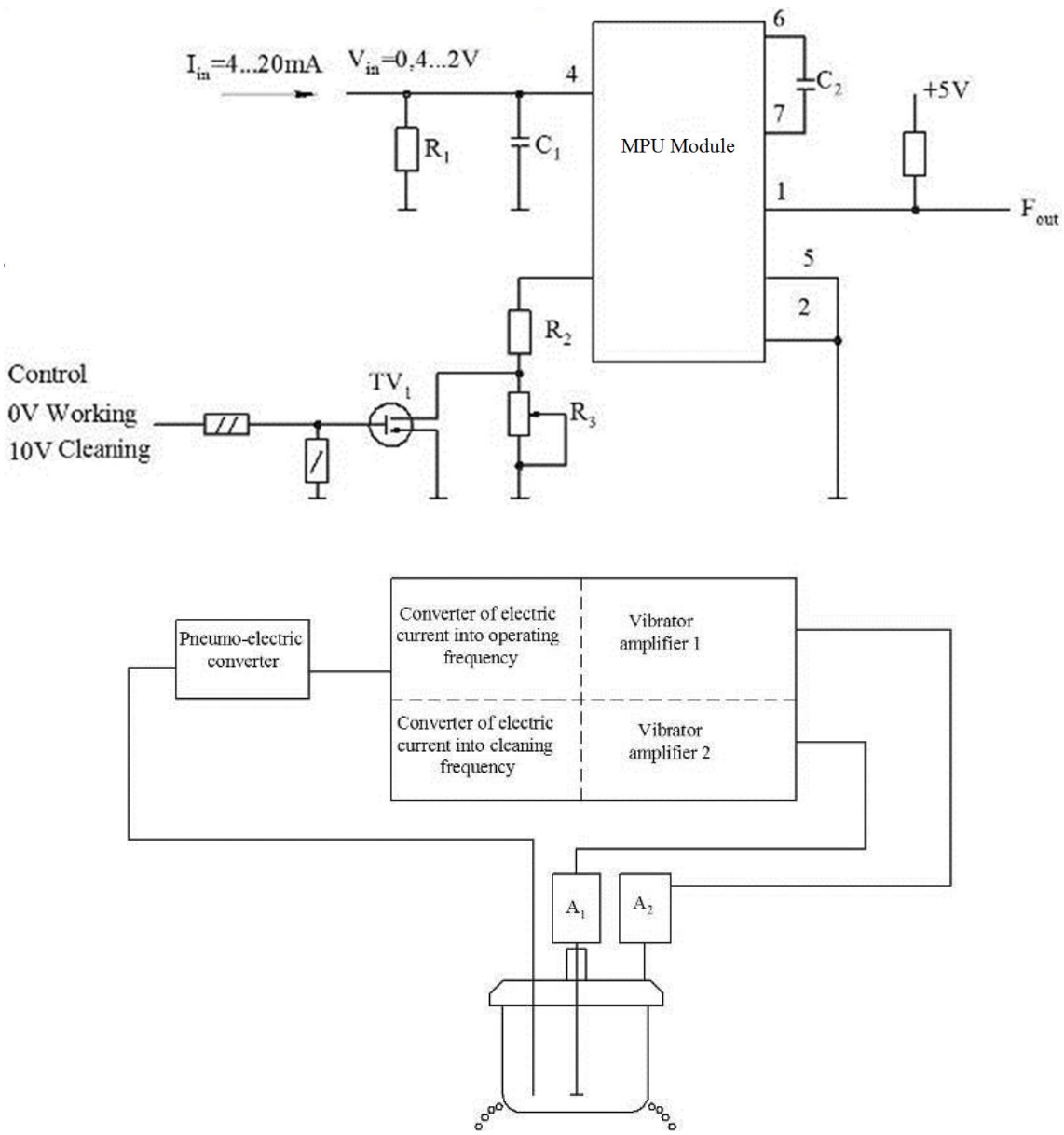


Figure 10 – The scheme of the vibrator operation

$$F_{out} = \frac{U_{in}}{10(R_2 + R_3)C_2}, \tag{27}$$

$$F_{in} = \frac{U_{in}}{10R_2C_2}. \tag{28}$$

During the operation of the vibration priller owing to some additives the perforated basket is clogged in the fusion. It decreases the granulator productivity, worsens the fusion jet properties and increases dust formation. One of the most significant constituents of the nitrogen-containing fertilizers losses at the production stage is dust emission from fertilizers with cooling air into the atmosphere. For example, ammonium nitrate production unit AN - 60, with a gas flow rate of 300 thousand $m^3$/hour through the tower and containing the ammonium nitrate dust of 200-250 mg/$m^3$, annually emits over 1500 tons of the nitrogen fertilizer into the air. Therefore, the ammonium nitrate dust amount, which is in the air of the tower, can reach 0.8 g/$m^3$. It causes the product losses and requires additional cost for the purification of the air coming out of the tower. Together with an economic aspect, related to the energy- and resource cost, this problem has also an ecological one – pollution of the air basin, transfer of fertilizers into the surface and groundwater, accumulation of nitrites and nitrates in the plants and waters, that leads to the load on the ecosystem. The results of the experimental and industrial testings of the modified prillers with the proposed intellectual system in the ammonium nitrate production demonstrated the efficiency of the changes, introduced into the system, and enabled to reduce the economic and ecological damage in the production of the nitrogen mineral fertilizers. Using the control panel of the vibration frequency, the system lets to impose high-frequency oscillations on the perforated shell of the priller, which cause to the cleaning of holes from pollutions. The proposed electric intellectual system has been tested and ways of its further improvement have been outlined. Implementation of the improving electronic intellectual cleaning system of holes allowed reducing the error in the high-frequency oscillations on the perforated shell of the priller from 0,43 to 0,27, i.e. 1,6 times.

# 2 RESEARCH OF THE PROCESS OF THE GRANULATION AND DRYING OF MINERAL FERTILIZERS IN THE DEVICES WITH ACTIVE HYDRODYNAMICS

## 2.1 Operational regimes in the devices with active hydrodynamics

This report section is prepared in according to data [5-8].

Ansys CFX and Ansys Fluent (https://www.ansys.com) software is based on a finite-volume method of solving hydrodynamic equations and using a rectangular adaptive mesh with local grinding. In order to approximate curvilinear geometry with higher accuracy, the technology of geometry grid density is used. This technology enables to import geometry from CAD systems and to share information with finite element analysis systems. This technology has solved the problem of automatic mesh generation – in order to generate a mesh, it is enough to set only a few parameters, after which the mesh is automatically generated for a computational area that has the geometry of any complexity degree.

The calculation starts with some initial approximation set as the initial data. At each global iteration, the velocity and pressure fields, obtained after the time specified as the integration step, are calculated. The stationary solution of the problem is achieved after a sufficiently large number of global iterations corresponding to a long period of time.

When performing the calculation, the program automatically breaks the calculation area into separate subareas, subdomains, the size of which is proportional to the velocity of the appropriate processor. The calculation algorithm works in such a way that each processor calculates the flow only in its own subdomain, and after each global iteration, the resulting solution is “adhesion”. The parallelization algorithms used in modern software products let to achieve acceleration with an efficiency close to 100%. In other words, the calculation time is inversely proportional to the total computing power

As a rule, the adhesion condition is set as boundary conditions on all solid walls (the velocity is zero), the distribution of all velocity components in the inlet section, and the first derivatives (in the direction of flow) of the velocity components in the outlet section

are equal to zero. In practice, if the flow rate at the inlet is approximately uniform in the intersection, the user sets only the average velocity (or flow rate) at the inlet, and sets nothing at the output - it is assumed that the user chose the output section far enough from the areas of intensive restructuring of the flow.

*Vortex granulator*

**Regime I.** Gas flow filtering through the stationary layer of granules (figure 11a). The layer is motionless, gas flow passes through pores in the layer.

**Regime II.** Beginning of the granules layer motion (figure 11b). In this regime, the lower parts of the layer are partially weighted, while the upper parts of the layer are still motionless.

**Regime III.** Partially fluidized bed (figure 11c). Granules in the lower parts of the layer are in the weighted state and move along the circular trajectory with low intensity, the granules in the upper parts of the layer are motionless. At a certain gas velocity, the whole layer goes into the weighted state.

**Regime IV.** Fluidized bed with partial swirling (figure 11d). Granules in the weighted layer take the wave trajectory, which is characterized by the localized vortex motion, started in any random place of the layer. The vortex is spread in that part of the layer, which is above the gap of the gas-distributing device, and the rest of the area is in the suspended state. With an increase of the gas velocity, the growing number of granules is drawn into the vortex motion.

**Regime V.** Developed vortex fluidized bed (figure 11e). With further increase of the gas velocity, the process of waves formation is weakened, the weighted layer has the ordered vortex structure.

**Regime VI.** Stable ablation regime of granules (figure 11f). Space over the vortex weighted layer of the material is filled with the solid phase, and the difference between the vortex weighted layer and overlayer space consists only in the concentration of the solid material. There is a gradual reduction of the granules concentration in the overlayer space with an increase of the height. Granules leave the vortex layer; their ablation is caused by the domination of the upward flow gas force over the gravity force.

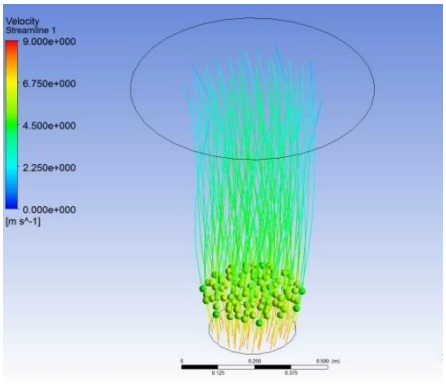


a

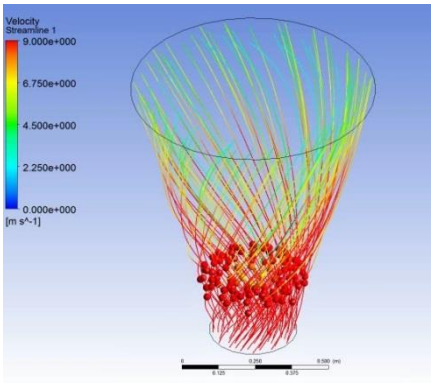


b

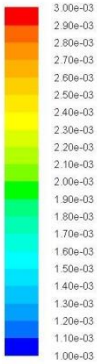


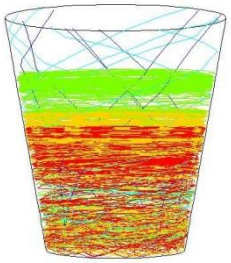

c

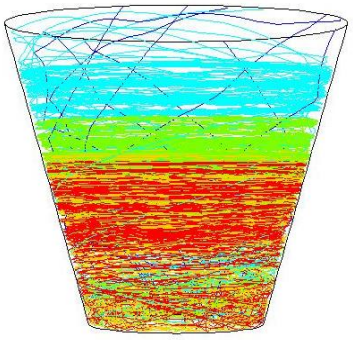

d

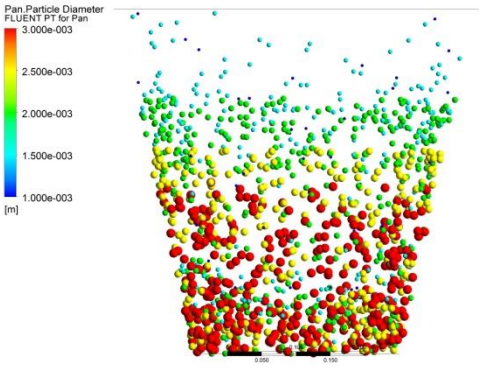


e

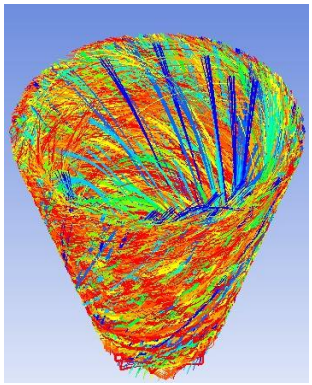

f

Figure 11 – Typical regimes of the vortex granulator operation: a – gas flow filtering through stationary layer of granules; b – beginning of the granules layer motion; c – partially fluidized bed; d – fluidized bed with partial swirling; e – developed vortex fluidized bed; f –stable ablation regime of granules

*Shelf multistage device with a weighted layer.*

In the upper section of the device the inclined shelves (angle of lean 30°) with ratio l/B (where l is the distance from the end of the shelf to the wall of the device; B – width of the device) in the amount of l/B=1 (free channel) to l/B=0.3 were installed. The results of the previous investigations, show that the efficiency to extract the small fraction (with the size less than 1 mm) into the ablation has the maximum value with the ratio l/B=0.5.

Thus, at the first stage of theoretical studies, it was necessary to find the optimal value of the free area in the shelf for the ablation efficiency of the fraction less than 1mm.

The results of the computer modeling show that the efficiency to extract the small fraction into the ablation is achieved with the reduction of the perforation degree of the shelf. While installing the solid shelf in the separation zone of the device, the whole gas flow guaranteedly passes through the outloading space. It defines the extraction of the small fraction of the material precisely in this zone. 5 % of perforation in the shelf causes the redistribution of the gas flow, directing its share through the hole in the shelf. Therefore, the gas flow intensively is interconnected with the material and not only in the outloading space zone but also on the shelf surface. It causes the increase of the fraction ablation efficiency, which is less than 1 mm.

The further increase of the free area of the inclined contact shelf is followed by the reduction of the small fraction extraction efficiency into the ablation. It is explained by the increased effect of the gas flow redistribution. The gas flow velocity in the outloading space decreases so much that the small fraction extraction process of the material in this zone is not very intensive. The total area of holes does not provide sufficient phase contact.

There are three perforated shelves in the drying (granulation) zone of the device. Moreover, while changing the distance between the end of the shelf and the wall of the device, it is possible to create different velocities of the gas flow

**Regime I.** Transition regime (figures 12a, 12b). The upward gas flow force in this regime causes the gradual change of its motion trajectory from the translational to the pulse-forward ones in direction of the outloading gap. Therefore the dispersed material starts to move into the weighted state, and the inertial force is compensated by the upward flow force of the drying agent.

**Regime II.** The weighted layer regime (figure 12c). The effect, made by the upward flow of the heat transfer agent in such regime leads to the creation of the stable weighted layer thanks to the compensation of the inertial force and the rolling-down force on the sloping surface. The gas flow velocity reaches the first critical value, then it increases and is within the range of the working velocity.

**Regime III.** The regime of the developed weighted layer (figure 12d). This regime is described by a dominant effect of the upward gas flow force on the dispersed material and by the increase of its displacement vertical component. Therefore, at first, the share of the dispersed material is taken out from the surface of the shelf and then it moves to the outloading gap.

In general, the algorithm to calculate the device with the directed fluidized bed can be represented by means of blocks (figure 13), which are logically interconnected between each other. The peculiarity of the algorithm includes its universality and ability of “flexible” implementation of separate blocks.

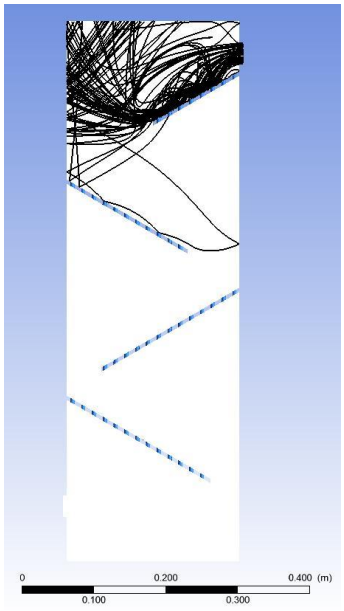


a

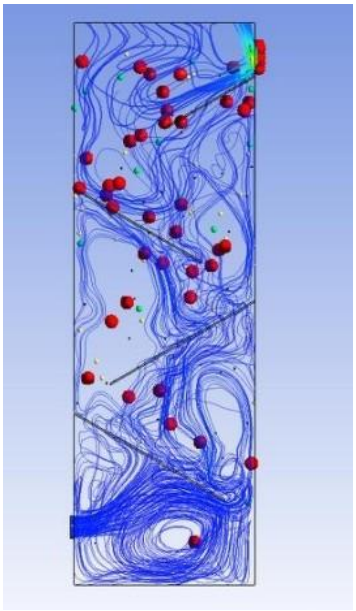

b

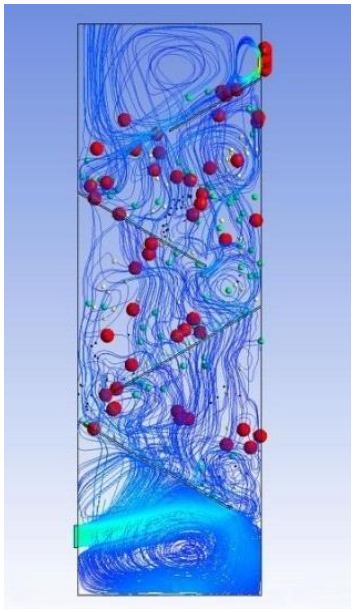

c

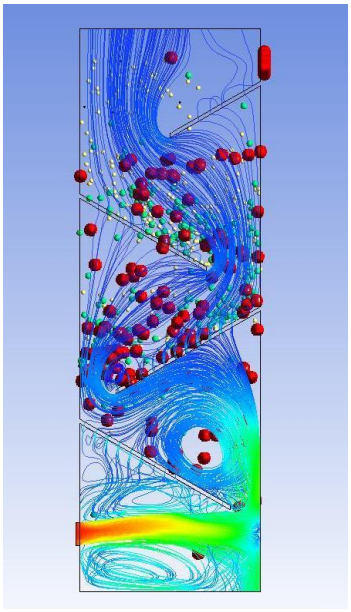

d

Figure 12 – Typical operation regimes of the shelf multistage device (dryer or granulator): a – separation of the small fraction in the shelf dryer (granulator); b – transition operation regime of the dryer (granulator); c –weighted layer regime of the dispersed material motion; d – developed weighted layer regime of the dispersed material motion

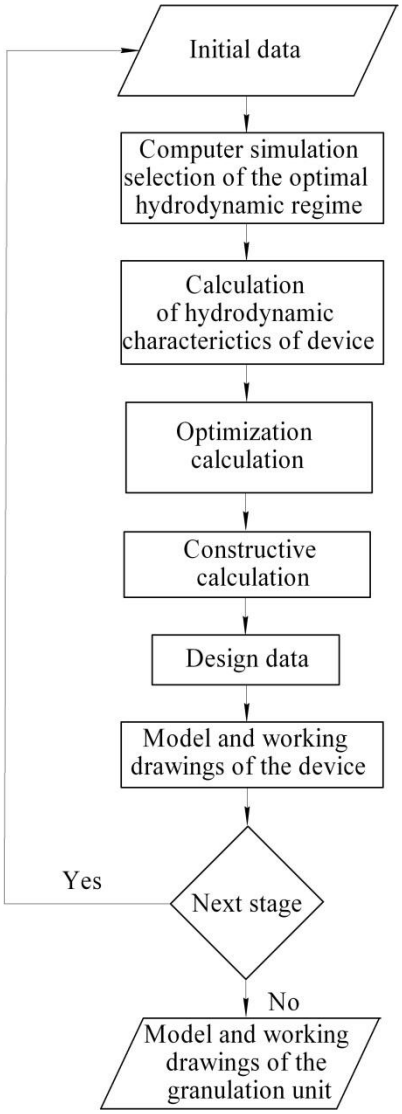


Figure 13 – Block-scheme of the granulation unit calculation

The modeling and calculation results with the use of authors' software, description of which is represented in the work [9], are exported to the cluster Granulation Unit© in the form of separate structural blocks (figure 14).


Figure 14 – Cluster Granulation Unit©

## 2.2 Convective drying in the multistage shelf dryers: theoretical bases

This report section is prepared in according to data [10-13].

The necessity to determine these features is due to the fact that before constructing an industrial sample of the gravitational shelf dryer it is necessary to determine its optimal design. In this case, the optimization criterion is to ensure the minimum required residence time of the dispersed phase in the working space of the dryer, which will let to complete the drying process to a predetermined humidity indicator. It is important to observe the condition, under which the “hydrodynamic” residence time of the dispersed phase in the workspace of the device should be no less than the “thermodynamic” time (this parameter is determined by the kinetics of the moisture removal process from the dispersed phase). Therefore, in order to keep the integrity of the dispersed particles, the "hydrodynamic" time should not exceed the "thermodynamic" time by more than 5-10%. By adjusting the hydrodynamic properties of the flow, an optimal construction of the

gravitational shelf dryer is achieved, which meets the requirements of the optimization criterion.

Thus, the optimization calculation of the dryer consists of three blocks: hydrodynamic calculation (calculation of the residence time of a particle on a stage), kinetic calculation (kinetic parameter of the moisture removal) and calculation of drying efficiency.

Initial data (figure 15):

– rate of gas flow $Q$, $m^3/s$;
– length of device $L$, m;
– overall width of device $h$, m;
– length of shelf $L_s$, m;
– degree of perforation (free area) $\delta$;
– perforation hole diameter $d$, m;
– the tilt angle of shelf $\gamma$, degr;
– the radius of the granule $r_{gr}$, m;
– granule density $\rho_{gr}$, $kg/m^3$;
– gas density $\rho_g$, $kg/m^3$;
– acceleration of gravity $g$, $m/s^2$;
– resistance coefficient $\xi$;
– volumetric content of a dispersed phase in a two-phase flow $\psi$;
– the coefficient that takes into account the tightness of the flow $m$;
– number of stages in dryer $i$.
– moisture of the material $i$-stage of the dryer $x$, kg of water/kg of material;
– moisture of the drying agent in $i$-stage of the dryer $b$, kg of water/kg of material;

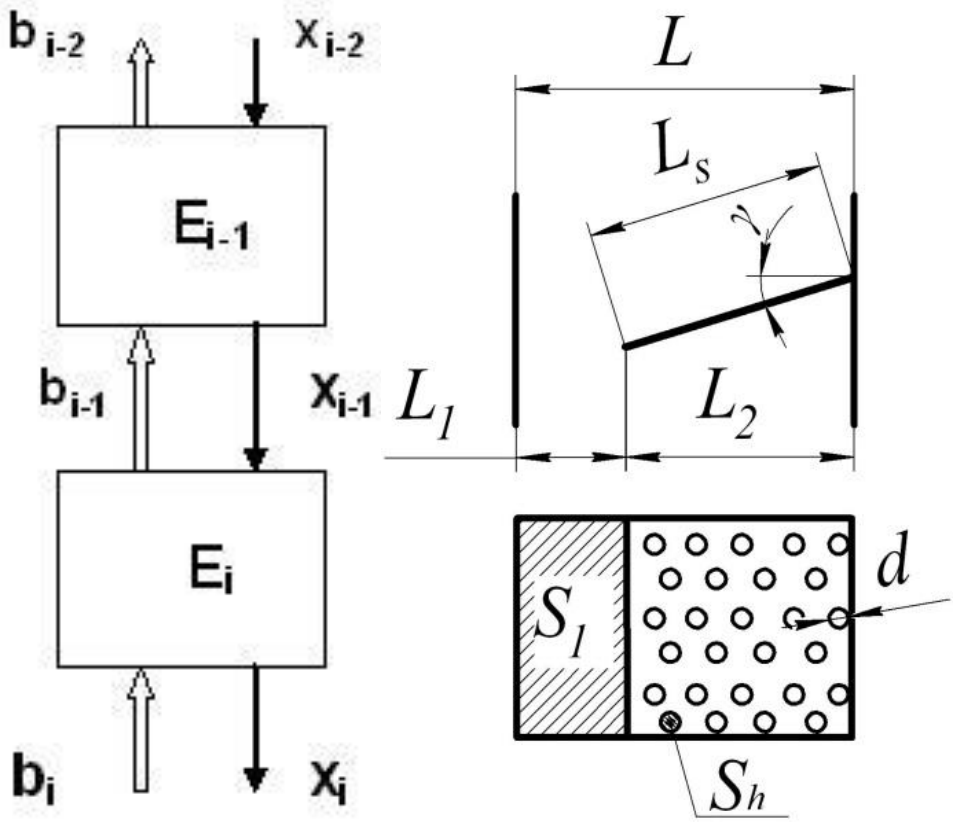


Figure 15 – A fragment of the calculation scheme for the multistage drying: left figure – change of flows' moisture; x– moisture of the disperse material; b – moisture of the drying agent), right figure – construction of dryer's workspace

*Hydrodynamic calculation*

Hole area on the shelf (horizontal position), $m^2$

$$S_h = \frac{\pi d^2}{4}. \tag{29}$$

The perforated area on the shelf (horizontal position of the shelf), $m^2$

$$\sum S_h = L_s \cdot h \cdot \delta. \tag{30}$$

Number of holes on the shelf

$$n = \frac{\sum S_h}{S_h}. \tag{31}$$

Area of outloading clearance, $m^2$

$$S_1 = (L - L_s \cos\gamma) \cdot h. \tag{32}$$

Area of the gas passage holes in the shelf (inclined position of the shelf), $m^2$

$$S_2 = \frac{\pi d^2}{4} \cdot n \cdot \cos\gamma. \tag{33}$$

The relative area of outloading clearance

$$S_1^r = \frac{S_1}{S_1 + S_2}. \tag{34}$$

The relative area of the gas passage holes in the shelf

$$S_2^r = \frac{S_2}{S_1 + S_2}. \tag{35}$$

Rate of the gas flow in outloading clearance, $m^3/s$

$$Q_1 = Q \cdot S_1^r. \tag{36}$$

Rate of the gas flow in holes in the shelf, $m^3/s$

$$Q_2 = Q \cdot S_2^r. \tag{37}$$

Gas velocity in holes in the shelf, m/s

$$V_{work} = Q_2 / S_2 . \quad (38)$$

Second critical velocity, m/s

$$V_{cr} = 1,63 \cdot \sqrt{\frac{\rho_{dr} \cdot g \cdot r_{gr}}{\xi \cdot \rho_g}}. \quad (39)$$

Velocity difference, m/s

$$\Delta V = V_{cr} - V_{work}. \quad (40)$$

Time of material residence on the shelf (free movement), s

$$\tau_f = \frac{L_s}{\Delta V \sin \gamma}. \quad (41)$$

The empirical function of the effect of compression on the residence time of the particle in the working space of the device

$$f_{e\tau}(\psi) = (1-\psi)^{-m}. \quad (42)$$

Time of material residence on the shelf (straitened movement), s

$$\tau_s = \frac{L_s \cdot f_{e\tau}(\psi)}{\Delta V \sin \gamma}. \quad (43)$$

The program Multistage fluidizer® used Hyper markup language HTML, cascading style sheet (CSS) and programing language JavaScript (including the library JQuery). HTML is presented as a tagging of web-based app, CSS pages formatting. JavaScript is used to calculate and to transfer data, to create animation and data validation effect. In the validation block of JavaScript, data accuracy is checked. In the block input info, basic data fields indices are accepted and they are written to the object of input_information. In the block, calculation computations are carried out by equations (29)-(43).

Index.html (figure 16) is the main page of the web-based app. It is responsible for reflection of the main menu, for main calculation of gas flow and for jumping the other pages (an examples of such page is represented in the figure 17), where main dependencies between key features to calculate gas flow and resistance time of the material on the shelf, are calculated and dependencies diagrams are formed.

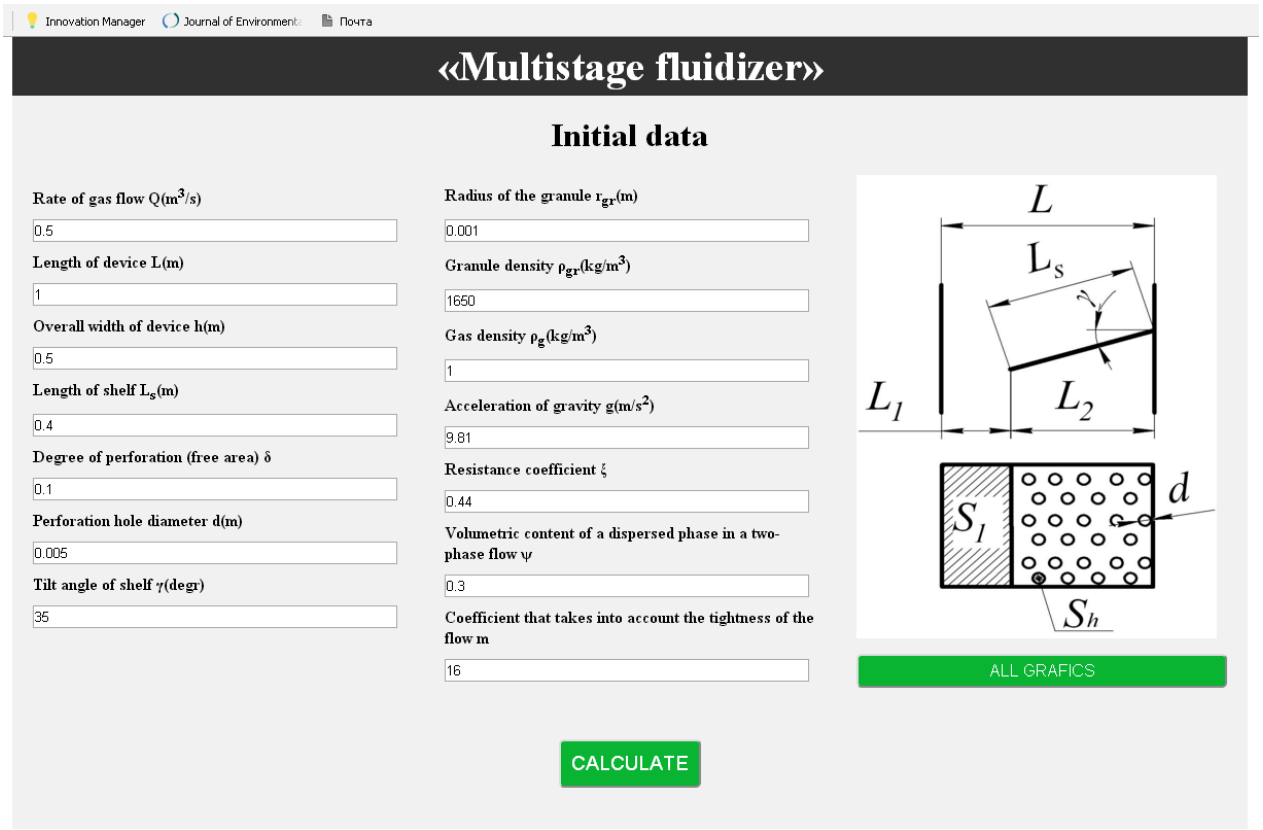


Figure16 – The main page of the Multistage fluidizer® software

Having inserted data, data validity is tested, if all data is correct, after keystroke CALCULATE data is processed given the above formulas and we receive the result in form of the computation table (figure 18).

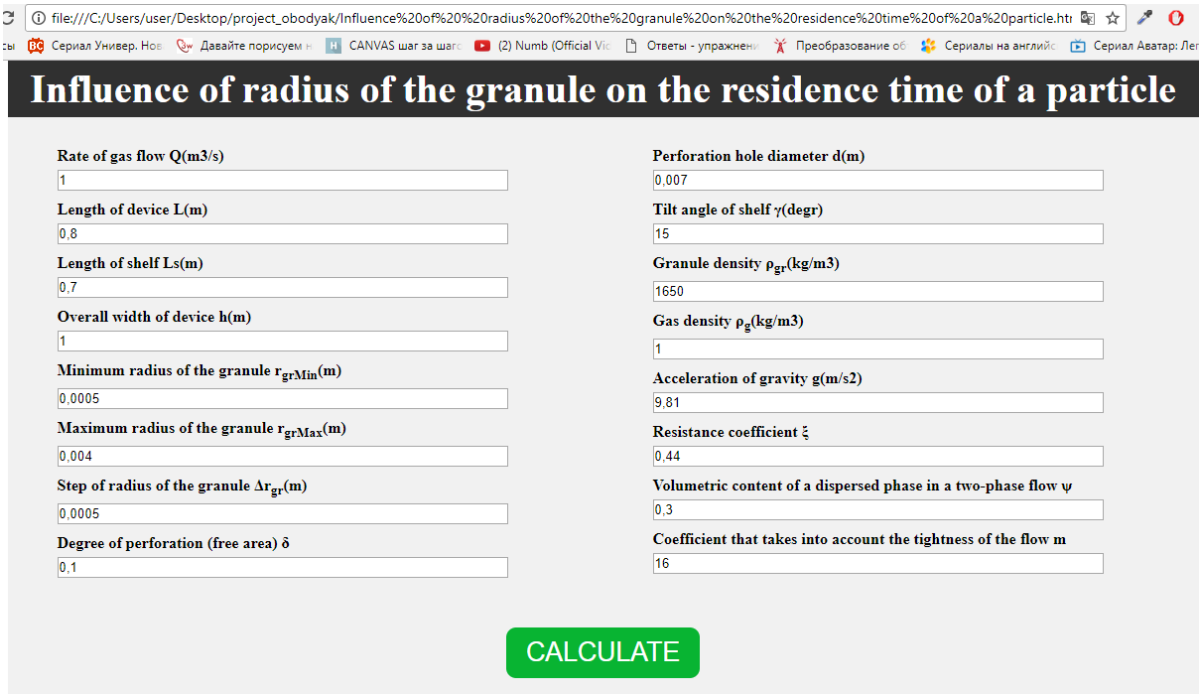


Figure 17 – Calculation page of various parameters impact on the particles resistance time in the device

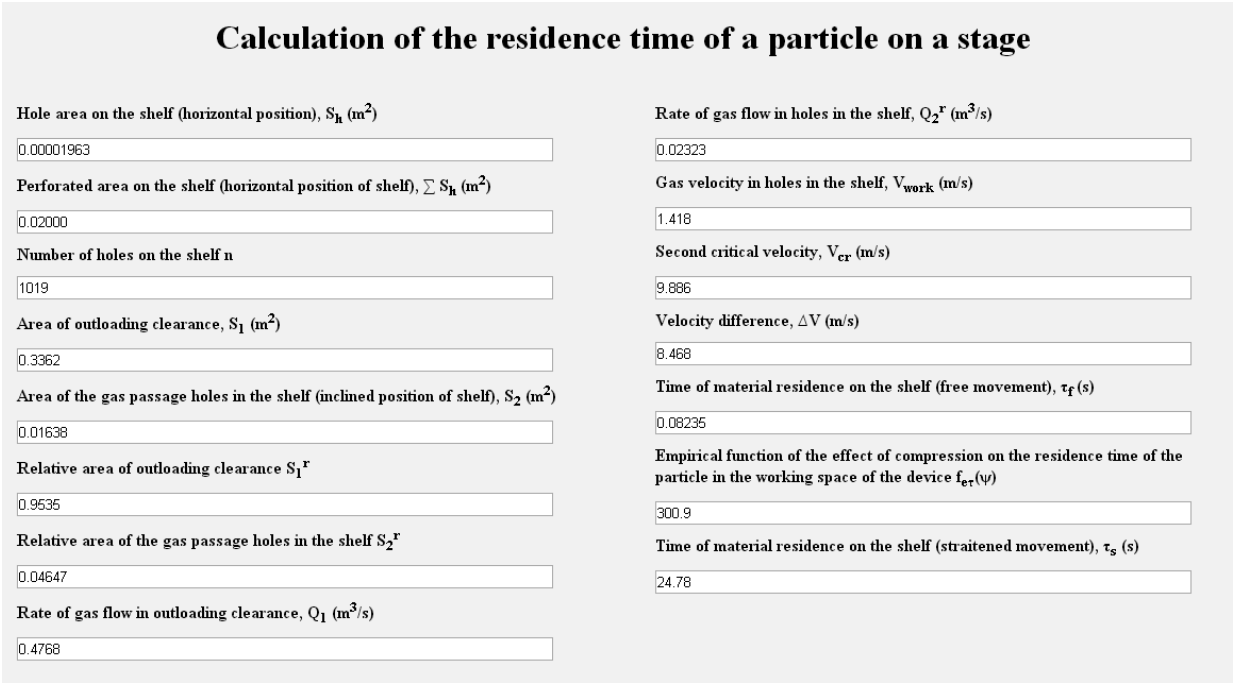


Figure 18 – Results of calculation

After changes of indices $l_f$ and $l_s$ it is possible to see how the animation appears while pressing the button show calculation (the example of distance length calculation, which particle takes on the shelf during the specified period of time, is shown in the figure 19). In order to create animation, functions clicker_lf and clicker_ls are implemented respectively for $\tau_f$ and $\tau_s$ animation.

In JavaScript one uses: libraries JQuery and table2excel, objects for data recording, methods .val(), .append() to read and to insert indices to fields, methods .removeClass() and .addClass() to delete and to add classes, method .animate() for work with animation lets to create an animation effect for any digital CSS feature of the element.

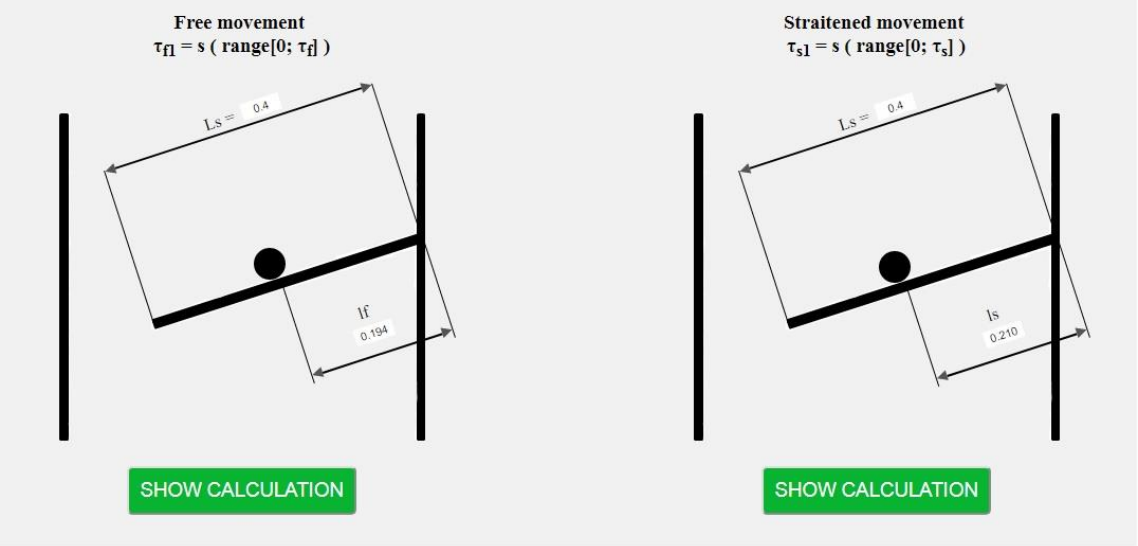


Figure 19 – Calculation of way length, which particle undergoes on the shelf during the specified period of time

In order to calculate the kinetic parameter of the moisture removal (the moisture-yielding capacity coefficient) let us use the following algorithm.

It is proposed to use the following equation for calculation of $\beta$:

$$\frac{\Delta U_m}{\tau} = \beta \cdot F \cdot \left( b_{fin} - \frac{b_{fin} + b_{in}}{2} \right) \cdot \rho_g , \qquad (44)$$

where $b_{in}$, $b_{fin}$, $\Delta U_m$ – the initial and final humidity of the drying agent, amount of the removed moisture from the material; $F$ – the surface of the mass transfer, which depends on the dryer's effective operation due to the disperse material and the residence time of the material in the dryer.

In general, the criteria equation of the drying process can be written as follows:

$$Sh = A_1 \cdot Sc^n \cdot \mathrm{Re}^m, \tag{45}$$

where $A_1$ – the equation coefficient;

$Sh = \beta \cdot d_{gre} / D$ – Sherwood criterion;

$d_{gre}$ – equivalent diameter of the particle (granule), m;

$Sc = \nu / D$ – Schmidt criterion;

$\mathrm{Re} = \left(V_{work} \cdot d_{gre}\right) / \nu$ – Reynolds criterion;

$D$ – diffusion coefficient of the gas flow, $m^2/s$;

$v$ – kinematic viscosity coefficient of the gas flow, $m^2/s$;

$m$, $n$ – indicators of the equation stages, which are evaluated through the graphical dependency $Sh / Sc^{0,33} = f(Re)$, obtained from the experimental data.

The drying process effectiveness on the i-stage of the dryer is presented by the ratio of differences between the moisture contents of the disperse material before and after the drying $x_{i-1}$-$x_i$ to the maximum possible (theoretical) difference between the moisture contents on the stage $x_{i-1} - b_i$, and also in the form of the function of the kinetic parameter of the moisture transfer $B_i$, the residence time of the material on the stage $\tau_i$ and the consumption ratio of the dispersed phase to the drying agent $G_i^{-1}$

$$E_i = \frac{\Delta x}{\Delta x_{\max}} = \frac{x_{i-1} - x_i}{x_{i-1} - b_i} = \frac{1 - \exp\left[-\beta_i \tau_i (1 + G_i^{-1})\right]}{1 + G_i^{-1}}. \tag{46}$$

Some graphic dependencies are shown in the figure 20. The program lets to receive two- and three-dimensional dependency graphs.

In general dependencies diagrams, features for free and constraint motion of particles have one functional dependence. The particle resistance time has enough narrow diapason at every stage (shelf) in free motion regime and is calculated by seconds units. In the constraint motion regime of particles, the residence time is greatly increased at every stage. The abundant ratio of particles in the two-phase system has a definite impact on this index. That is why, while defining the optimum performance of the device, it is necessary to define the workspace size of the granulating or drying device to high accuracy.

The impact made by some constructive features of the shelf dryer during the residence time of the dispersed material (figure 20) is shown below.

The change of the shelf tilt angle to the horizon affects the redistribution of the gravity components: enlargement of it leads to an increase of the gravity rolling component and vice versa. It should be mentioned that the tilt angle of the shelf may have a minimum value that complies with the natural slope angle of the material. As the tilt angle of the shelf decreases, the residence time of the dispersed material gradually increases. It leads to longer contact with the drying agent's flow.

Changing the gap between the edge of the shelf and the dryer's wall significantly influences the change of the residence time of the dispersed material on the shelf. If the gap increases, the contact time of the dispersed material with the drying agent will be reduced due to the decrease in the length of the material movement distance on the shelf. In this case, the operation of the rolling component of the dispersed material velocity lasts for a shorter period and at the end of the shelf is replaced by the full gravity. Thus, the material moves down and only the ascending gas flow force resists its fall.

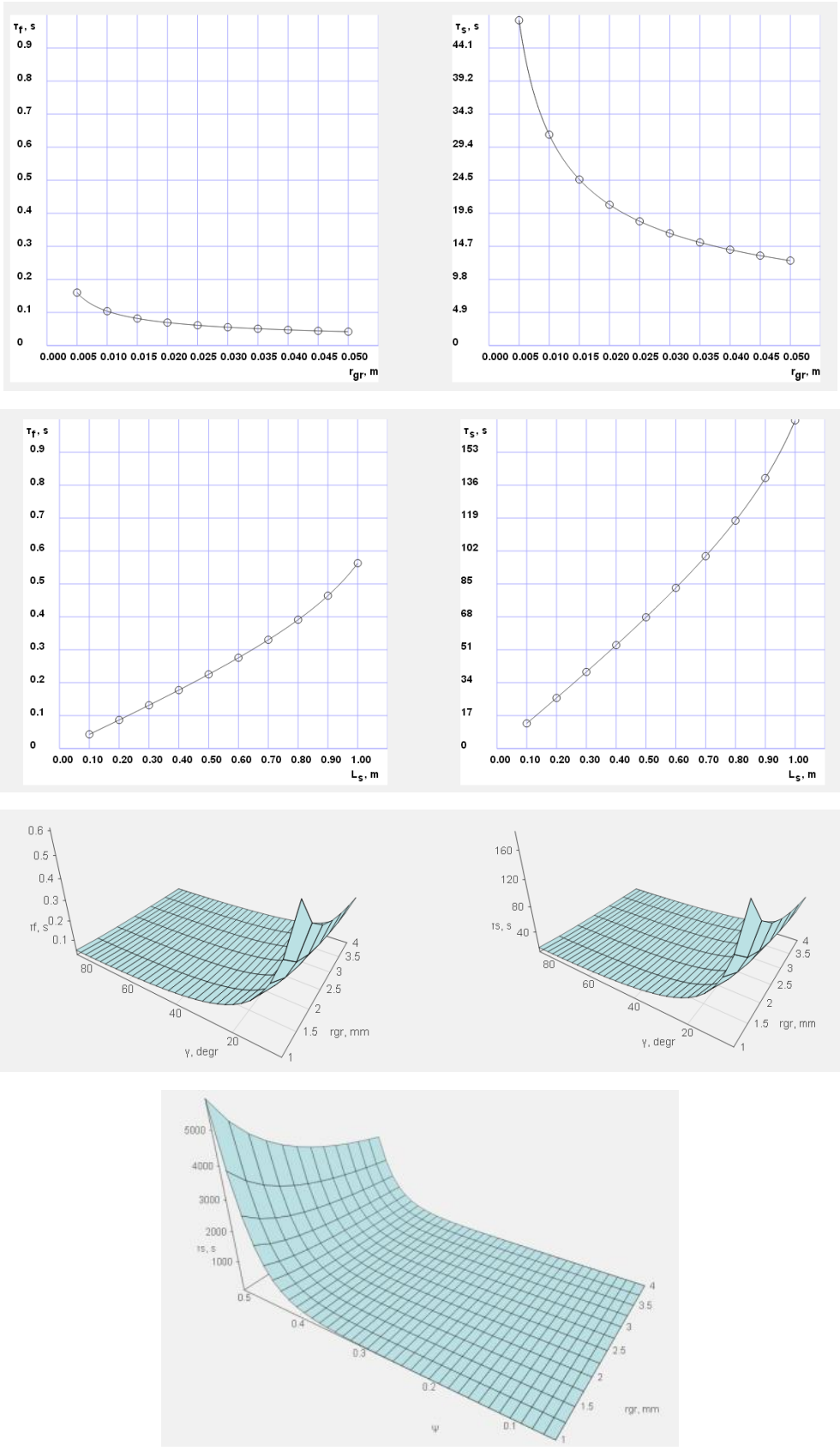


Figure 20 – Examples of calculation results

The analysis of the calculations regarding the effect, made by the free cross-sectional area of the shelf on the drying process efficiency showed the following. Reducing the free cross-sectional area of the shelf leads to an increase of the drying agent's ascending motion velocity in the holes. In this case, the action of the drying agent's ascending flow slows down the progressive motion of the dispersed material on the shelf, compensating for the rolling component of its gravity. The pulse component of the dispersed material displacement decreases and the trajectory changes to a pulse-forward one. The trajectory length of the dispersed material motion increases, the time of its contact with the drying agent is extended.

As the diameter of the perforation holes decreases, the effect of the drying agent's ascending flow increases, in which the pulse component of the dispersed material motion trajectory decreases, and the forward - increases. Thus, the trajectory length of the dispersed material motion increases and the contact time with the drying agent is extended. It should be noted that with the further reduction of the perforation holes diameter, the action of the drying agent's ascending flow begins significantly to outweigh the effect of the gravity rolling component. It leads to the formation of the second transitional mode and the ablation mode in the shelf dryer's operation.

The calculated values of the mass transfer coefficient β from the equation (44) depending on the velocity of the drying agent's motion, is demonstrated in figure 21.

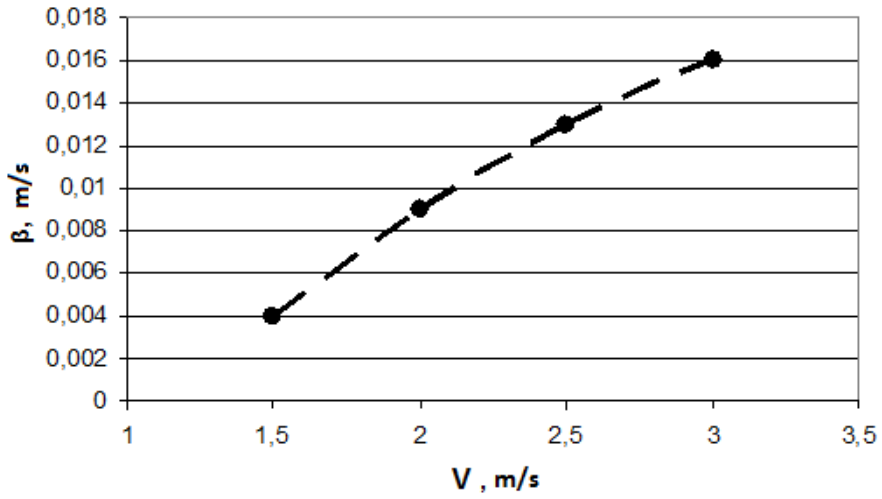


Figure 21 – Dependence of the mass transfer coefficient on the drying agent's motion velocity

The graphical dependency from the equation (45) shows (figure 22) that coefficient $A_1$= 0,008, $m$ = 0,47. The coefficient n is 0.33 for the situation when the drying agent's parameters were slightly changed during the experiment.

Taking into account the obtained values of the coefficient $A_1$ and equation stage $m$, the criterial value (46) will be as follows:

$$Sh = 0,008 \cdot Sc^{0,33} \cdot \mathrm{Re}^{0,47} \tag{47}$$

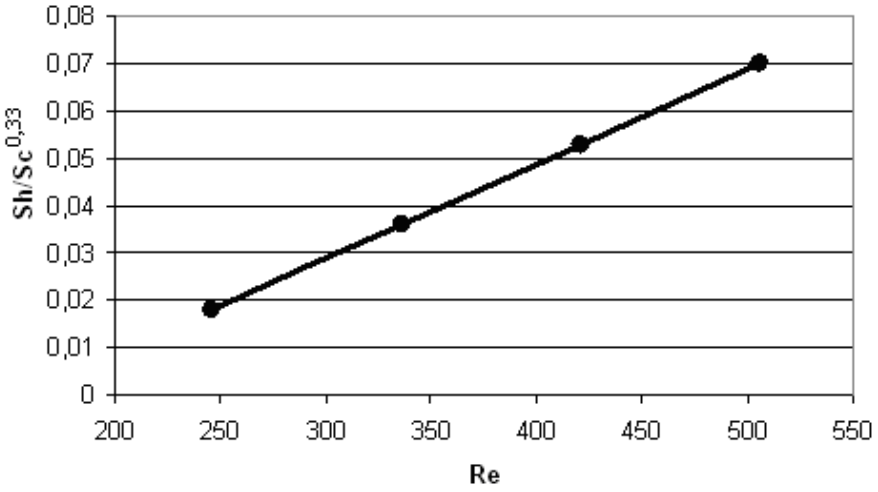


Figure 22 – Graphical dependency $Sh / Sc^{0,33} = f(Re)$ to define the coefficient $A_1$ and equation stage m.

The organization of the drying agent's motion may have a considerable influence on the quality indicators of the dried material and the properties of the drying agent. That has evolved several studies, the results of which are presented in figures 23-26. Their analysis enables us to select the method to organize the drying agent's motion, which consumes the least energy and ensures the necessary complete removal of moisture from the disperse material.

The analysis of the figures shows that the features of the dispersed material and the drying agent are changed according to one law; each of the technological indicators in the drying agent differently influences the intensity of the increase or decrease of parameters. The figures show that there is no function extremum on the graphical dependencies, which is explained by the regularities of the convective drying kinetics - the parameters

change of the contacting flows in each of the periods occurs monotonically with different intensity on separate sites depending on the dehydration conditions.

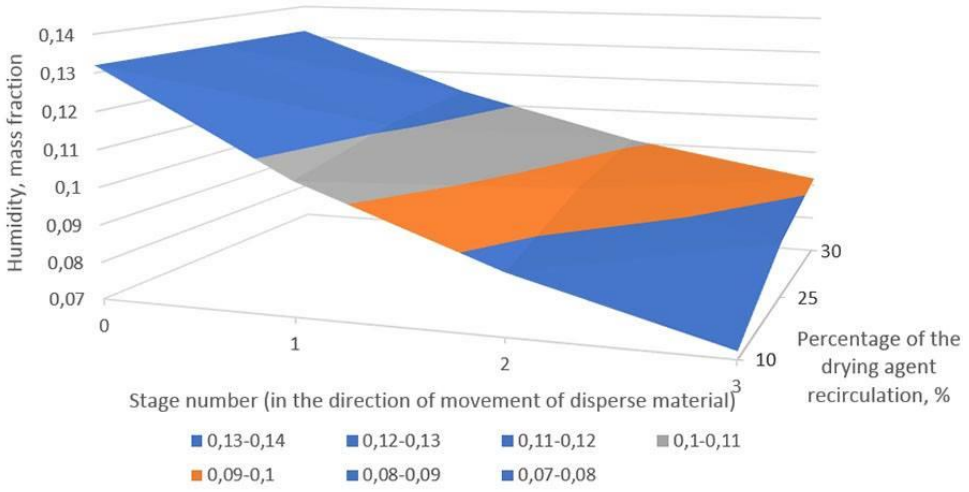


Figure 23 – Influence of the drying agent recirculation method on the change of the moisture content in the disperse material

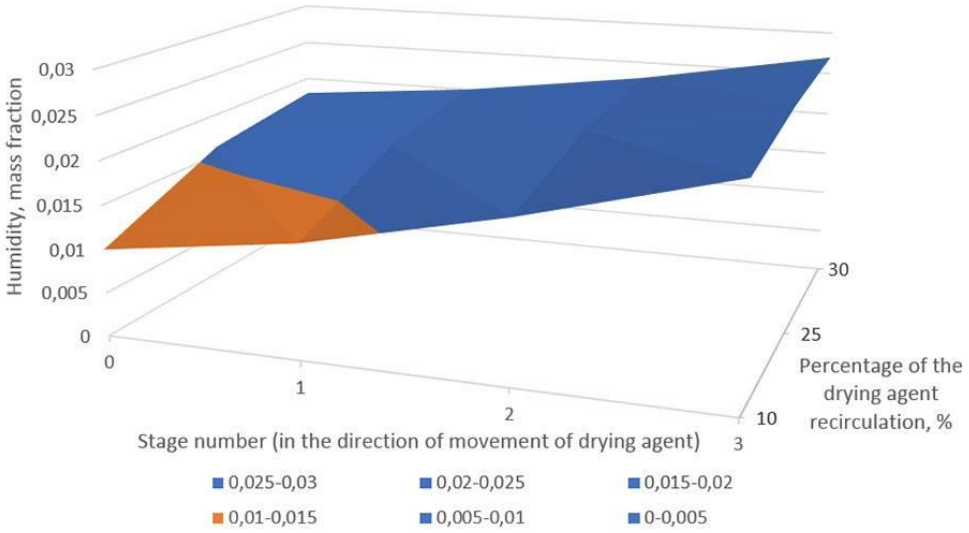


Figure 24 – Influence of the drying agent recirculation method on the change of the moisture content in the drying agent

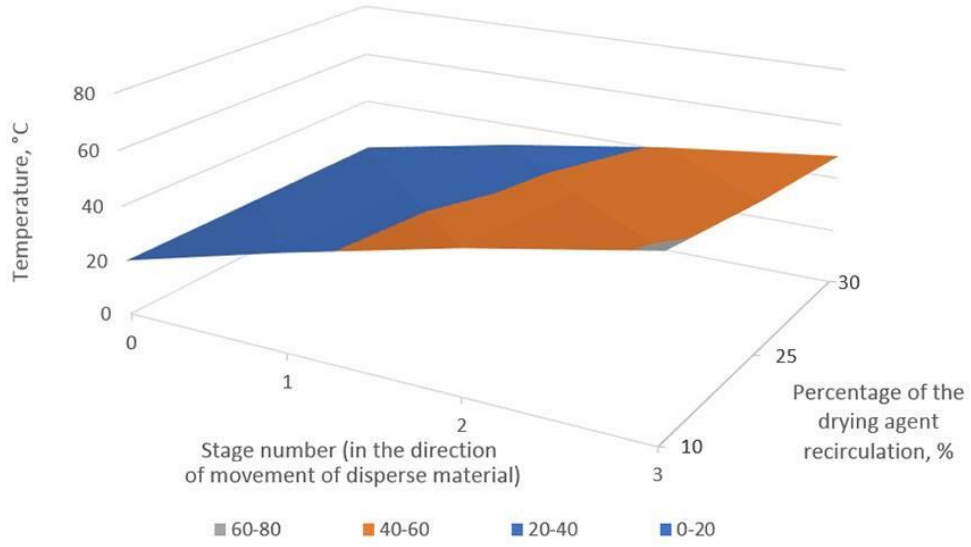


Figure 25 – Influence of the drying agent recirculation method on the temperature change of the disperse material

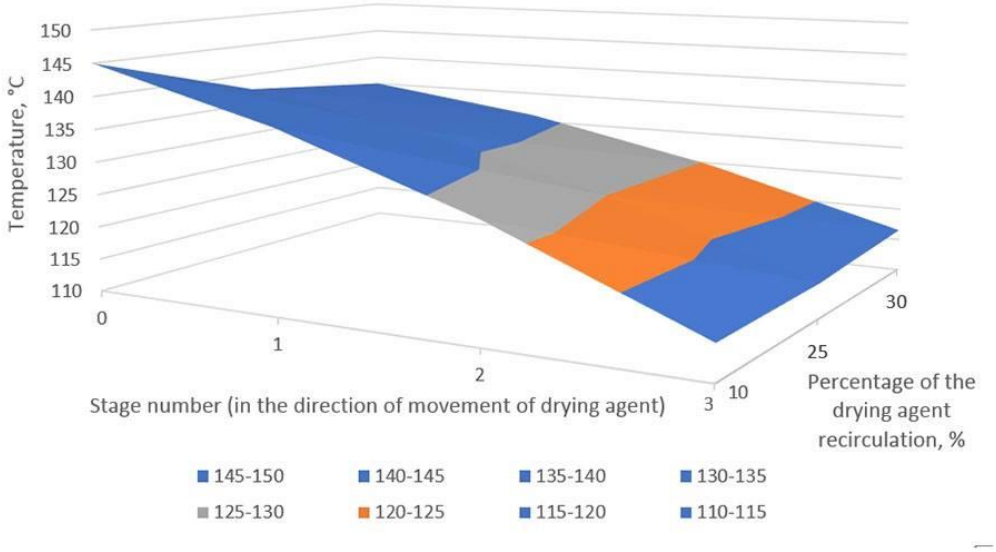


Figure 26 – An influence of the drying agent recirculation method on the temperature change of the drying agent

Block-scheme of the algorithm to calculate the multistage gravitational shelf dryer is represented in figure 27.

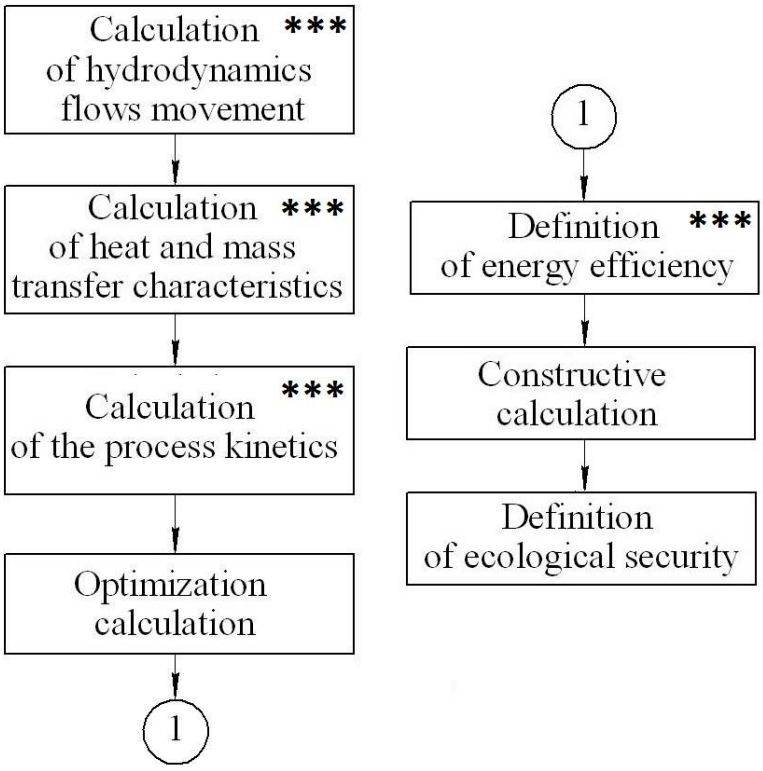


Figure 27 – Block-scheme of the algorithm to calculate the multistage gravitational shelf dryer (symbol *** shows the blocks which are described in this work).

# 3 THERMODYNAMIC CALCULATION OF VORTEX GRANULATOR OPERATION FOR PRODUCING OF AMMONIUM NITRATE WITH NANOPOROUS STRUCTURE

*This report section is prepared in according to data [15] and references in this work.*

According to the previous studies in the field of PAN granules production, thermodynamic and hydrodynamic conditions (temperature, gas velocity, time of contact of the granules with hot gas (air) environment) are the main factors which form the porous structure. In addition, having removed the bulk of the moisture and having formed the pores, the granules need to undergo some drying process to ensure the required strength. Otherwise, the granules can significantly lose their strength.

Thus, in the calculations, it is necessary to predict the kinetics description of granule heating and to determine the minimum drying time, the value of which exceeds the required time to warm the granules to the desired temperature.

The granule is a spherical body with pores, the peculiar size of which is the radius R and in terms of the physicochemical properties in the calculations - the structure of the granule's substance (including, moisture content as the main index).

In order to describe the influence of the thermodynamic parameters of the gas flow on the humidified granule, a physical model was investigated. It is based on the following principles:

- the selected diameter of the granules is determinant for the entire set of granules in the workspace, i.e. the formation of the porous structure in the granules with the selected diameter preferably defines the porous structure of the entire granules flow;

- the granule is washed by a stream of gas (air) which has a constant temperature.

Thus, one may accurately assume that the surface temperature of the granules during the whole residence time in the workspace will be constant;

- due to the fact that the granules are small in size from 1 mm to 4 mm, and the vast majority of granules obtained at nitrogen plants, are granules in size from 2 mm to 3 mm, we can suppose that due to the hygroscopicity of the granules, the humidification process

should be minimized. So, one may presuppose that moisture saturation occurs along the radius according to a linear law;

- the pore-formation starts consecutively from the top layer. The pore-formation front moves along the radius of the granule to its centre, representing a spherical surface;

- evaporating moisture is freely removed from the granule through the formed pores in the previous layers of the substance with a larger diameter, “external” layers (these layers are located closer to the surface of the granule) which form the granule;

- the proportionality of the formed pores in the granules with the steam extracted from moisture is the reason for the fact that the retention capacity of the granules is greater than the moisture content.

Based on the above assumptions, it is possible to create a mathematical model to determine the basic hydro- and thermodynamic parameters, the effect of which enables it to create a porous structure in the granules.

The temperature distribution in the PAN granule is described by the differential equation:

$$\frac{d}{d\tau}(rT(r,\tau)) = a\left(\frac{d^2}{dr^2}(rT(r,\tau))\right) \tag{47}$$

where r – current radius,

a – thermal diffusivity coefficient.

The solution of this equation will be the following:

$$T(r,\tau) = T_C - (T_C - T_0)\times \times\left(\sum_{n=1}^{\infty}\left(\frac{2(\sin(n\pi) - n\pi\cos(n\pi))R\sin\left(\frac{n\pi r}{R}\right)e^{\left(\frac{n^2\pi^2 a\tau}{R^2}\right)}}{(n\pi - \sin(n\pi)\cos(n\pi))rn\pi}\right)\right). \tag{48}$$

As a result of the drying process, the diameter of the granules increases due to the modification transitions and the porous structure formation.

Thus, the granule together with the heat transfer agent will be heated to a predetermined temperature, and only then the moisture will be removed. This factor increases the total required residence time of the granules in the device. The calculations of the above mathematical model showed that 8 seconds are required to complete the heating process of the granules with d = 2 mm at a temperature of 20 ° C - 120 ° C in a stream of heat transfer agent with a temperature up to 120°. If we perform a gradual calculation taking into account that with the introduction of granules or moistening the heat transfer agent is cooled, then gradual heating of the granules to a temperature of 120 ° will take a time interval 3-3.5 times longer than in the previous case. The results of experimental studies of the workspace heating kinetics in the vortex granulator under different conditions, which are given below, make the basis to determine the heat transfer agent's temperature with the gradual heating of the granules simultaneously with the heat transfer agent's flow.

Based on the value $dm$ of dry substance, the weight of the elemental volume $dV$ of granules, taking into account the presence of moisture, is

$$dm = \rho_{gr}(1 + U(r,\tau))r^2 \sin\theta d\theta d\phi dr\,, \tag{49}$$

where $dV = r^2 \sin\theta d\theta d\phi dr$ - elementary volume value.

On the other hand, the mass of "dry" granule with radius $R$ in general is

$$Msr = 2\int_0^R \int_0^\pi \int_0^\pi \rho_{gr} r^2 \sin(\Theta) d\Theta d\phi dr\,, \tag{50}$$

or after integrating

$$Ms = \frac{4}{3} \cdot \rho_{gr} \cdot \pi \cdot R^3 . \tag{51}$$

Given the fact that $U$ is a function from $r$ and drying time $\tau$

$$Mg_{n=\infty}(\tau) = \frac{4}{3}\rho_c \times \left( \int_0^R U_p + (U_0 - U_p) \left( \sum_{n=1}^{\infty} \left( \frac{2(\sin(n\pi) - n\pi\cos(n\pi)) R \sin\left(\frac{n\pi r}{R}\right) e^{\left(-\frac{n\pi m\tau}{R}\right)}}{(n\pi - \sin(n\pi)\cos(n\pi)) r n\pi} \right) \right) dr \right) \times \left( 1 + \frac{}{R} \right) \pi R^3 \tag{52}$$

where $m$ – diffusion coefficient.

Besides, the above equation takes into account the fact that the moisture content of the granule takes some average value, which is calculated based on the integral properties.

The calculations show that the sum of the first two components is significant in solving the differential equation describing the mass transfer during the drying process. Further calculation of the sum leads to a change in the result obtained in the seventh digit of the fractional part. Based on this conclusion, it is possible to calculate the first two coefficients of the sum. Thus, the equation to determine the change in humidity over time takes the following form

$$Us(\tau) = \frac{\int_0^R U_p + (U_0 - U_p \left( \frac{2R \sin\left(\frac{\pi r}{R}\right) e^{\left(-\frac{\pi^2 m\tau}{R^2}\right)}}{\pi r} - \frac{R \sin\left(\frac{2\pi r}{R}\right) e^{\left(-\frac{4\pi^2 m\tau}{R^2}\right)}}{\pi r} \right) dr}{R} \tag{53}$$

Integrating the obtained formula, it is possible to receive a dependency to find the mass of the granules at any time during the drying process

$$Mg(\tau)=\frac{4}{3}\rho_c\pi R^3\times$$
$$\times\left(1+\frac{\int_0^R U_p+\left(U_0-U_p\right)\left(\frac{2R\sin\left(\frac{\pi r}{R}\right)e^{\left(-\frac{\pi^2 m\tau}{R^2}\right)}}{\pi r}-\frac{R\sin\left(\frac{2\pi r}{R}\right)e^{\left(-\frac{4\pi^2 m\tau}{R^2}\right)}}{\pi r}\right)dr}{R}\right)+$$
$$+2R\left(\sum_{n=1}^{\infty}\left(\frac{\sin\left(\frac{n\pi r}{R}\right)(-\sin(n\pi)+n\pi\cos(n\pi))e^{\left(-\frac{n^2\pi^2 m\tau}{R^2}\right)}}{(n\pi-\sin(n\pi)\cos(n\pi))n}\right)U_p\right)dr. \quad (54)$$

Within the framework of the scientific work vortex granulator stand to obtain PAN granules (fig. 28) is used.

Devices and equipment:

– determine the hydrodynamic features of the flows motion – TES 1340 Hot-Wire Anemometer;

– temperature measurement in air heater – self-recording-register potentiometer;

– measurement of granulator workspace temperature – thermal imager Fluke Ti25;

– measurement of moisture granules – Multimeter DT-838;

– study of the microstructure of granules – microscope KONUSPIX-450X KONUS, scanning electron microscope VEGA3 XM and X-ray spectrometer with an energy dispersion.

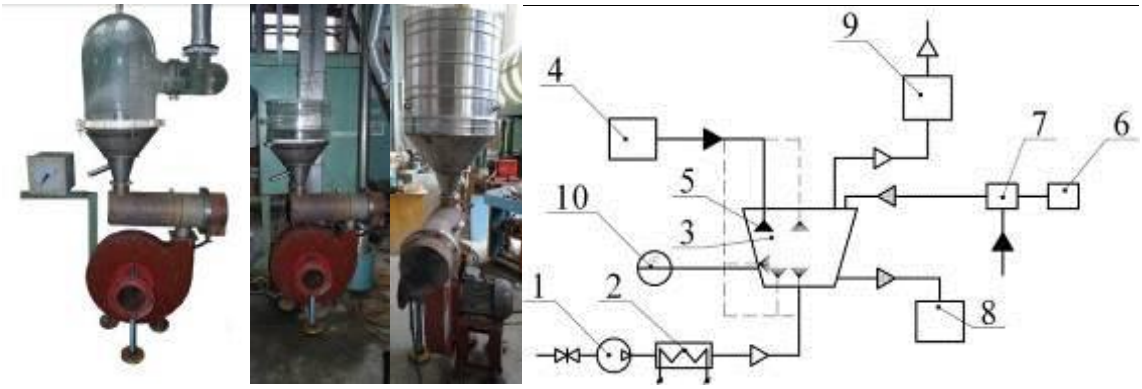


Figure 28 – The unit of the study on hydrodynamics of the vortex granulator workspace, thermodynamic conditions to obtain granules (with different configuration of the workspace): 1 - gas blower; 2 - heater; 3 - vortex granulator; 4 - container for preparation of the humidifier; 5 - nozzle; 6 - container of granules; 7 - container of pre-humidification (used when moistening); 8 – container for finished granules; 9 - the degree of purification of outgoing gases (bubbler); 10 - recording potentiometer. The dashed line shows the variants of the nozzle installation.

The results of the experimental study of the drying agent's temperature field in the vortex granulator workspace are presented in Fig. 29, 30. It should be noted that with the increase of the flow twisting degree one can observe the alignment of the temperature field in the granulator workspace. Intensification of the flow motion (turbulization due to the directed vortex movement) lets to distinguish an "active" zone, where the heat treatment process occurs with maximum intensity in the device.

Based on literature data, the heat-mass transfer processes occur with the highest intensity in the so-called "active" zone (heat-mass transfer zone, directly above the gas distribution device of the granulator or dryer with a fluidized bed. The height of this zone with the same features of the heat transfer agent depends on the type of gas-distributing device. Varying the design of the gas-distributing device (degree of the drying agent's flow twisting), it is possible to achieve an increase in the height of the "active" zone to that height of the zone of the predominant vortex motion of the granules.

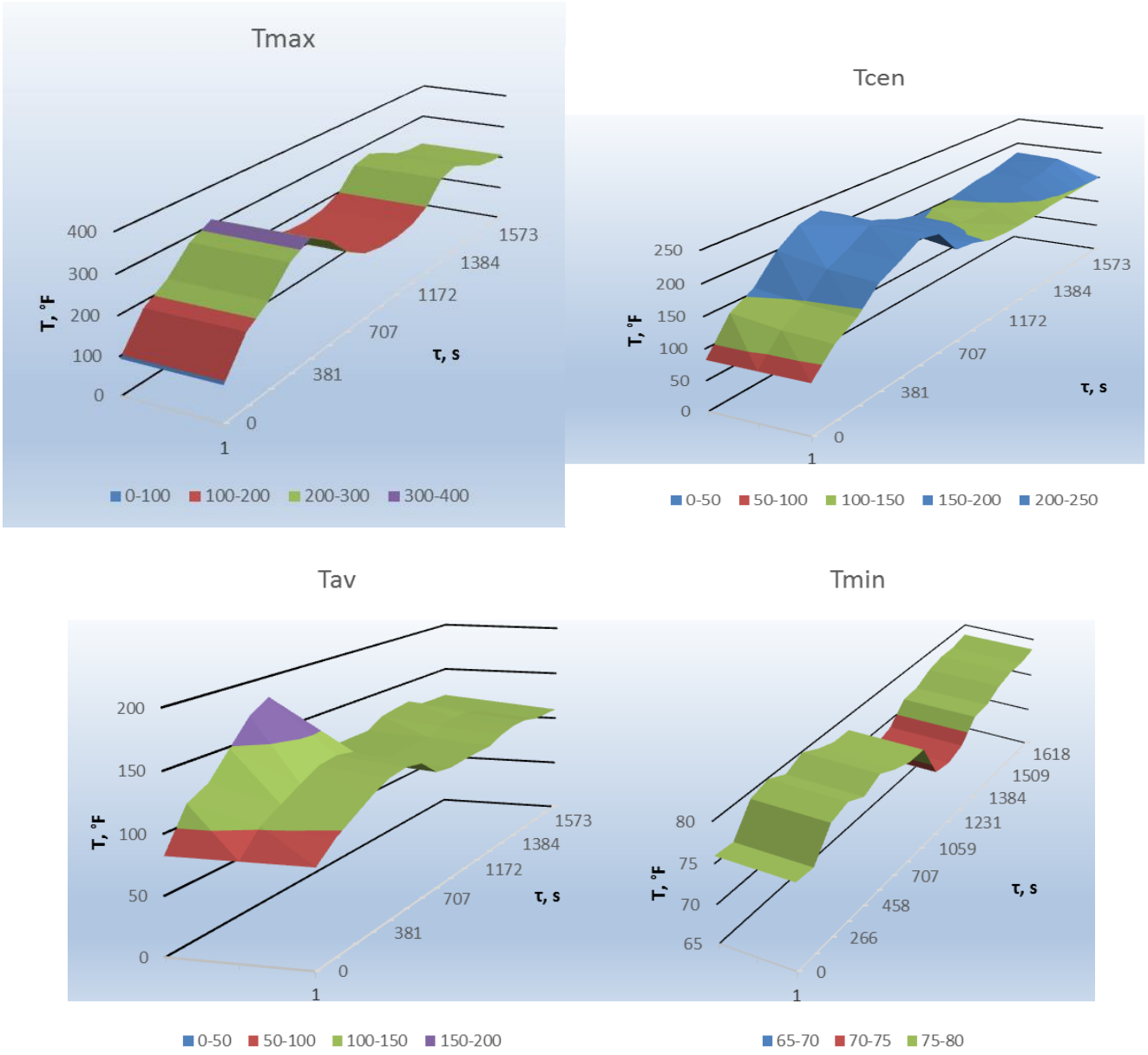


Figure 29 – Dynamics of the temperature change in the vortex granulator workspace depending on the intensity of solubilizer (drying agent) twisting (circular velocity of the drying agent 5.2-8.1 m/s) Temperature of the liquid agent: $T_{min}$ - minimum temperature; $T_{max}$ - maximum temperature; $T_{av}$ - average temperature; $T_{cen}$ - temperature in the center. Granule injection time is 650 s.

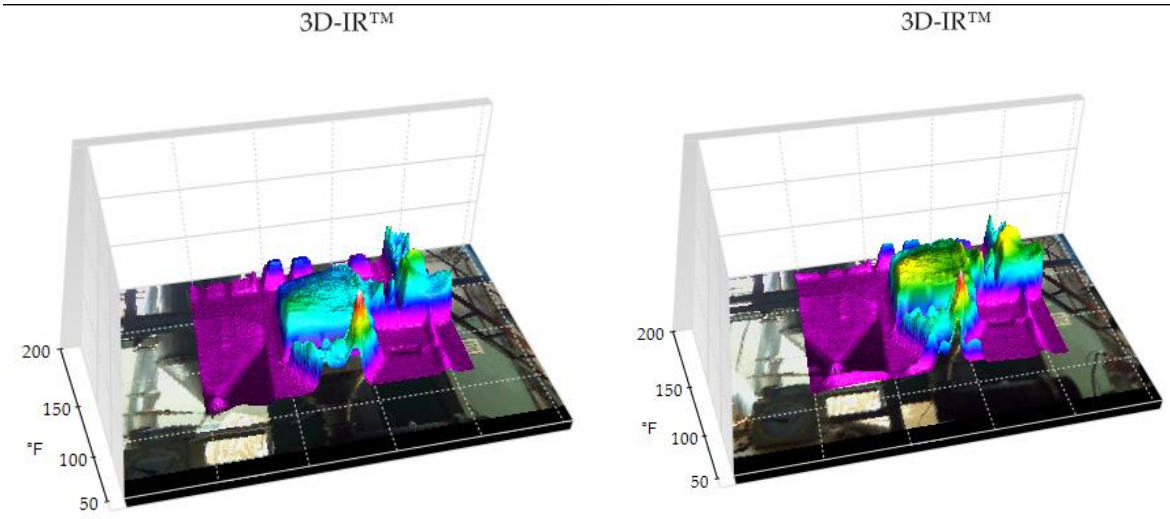


a b

Figure 30 – Data of thermal imaging studies of the vortex granulator workspace: a - access to the operating mode; b - operating mode

In order to confirm the experimental law regarding the temperature distribution in the vortex granulator workspace, in this work, a computer modelling of the temperature field of the twisted flow of a drying agent was carried out. The modelling results are presented in fig. 31. Satisfactory convergence between the experiment and modelling results in the operating (steady) mode of the vortex granulator operation is pointed out.

The model for calculation of the granule heating and drying kinetics proposed in the first section of the chapter, and the results to determine the drying agent's temperature field in a vortex granulator, let to carry out the thermodynamic calculation of the nanoporous structure obtaining process in the PAN granule. The received data of the temperature field are introduced to the calculation formulas in order to define the required time of the heat treatment process of PAN granules. Further, this paper presents constructive solutions regarding the methods to stabilize the drying agent's vortex flow, as well as the research findings of the nanoporous granule structure (nanoporous structure obtained at different twisting velocities of the drying agent).

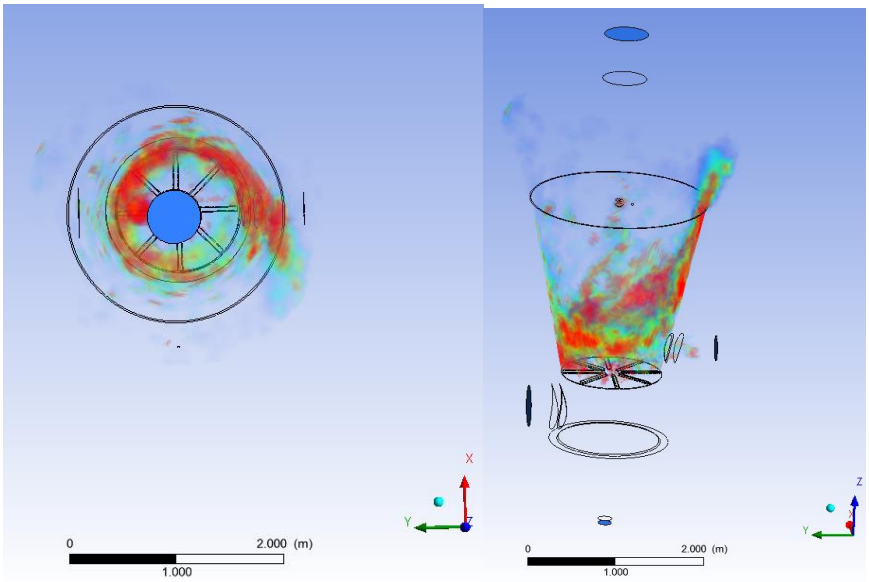


Figure 31 – The computer modelling results regarding the drying agent temperature field in the vortex granulator workspace

Fig. 32 demonstrates the construction of the gas-distributing unit in the vortex granulator without stabilization and with the stabilization of the drying agent's flow. The introduction of additional knots in the vortex granulator's construction practically does not complicate the production of the device and does not increase its price. However, as you can see below, such constructive solutions have a significant effect on the quality of the nanoporous surface in the PAN granules.

The nanoporous surface microscopy is performed in two steps. At the first stage, the effect of the temperature field (at different degrees of the drying agent's twisted flow in the same range as in fig. 29) on the nanoporous structure is investigated. The results of this microscopy are shown in fig. 33. The granules are obtained in a vortex granulator without stabilizing the drying agent's vortex flow.

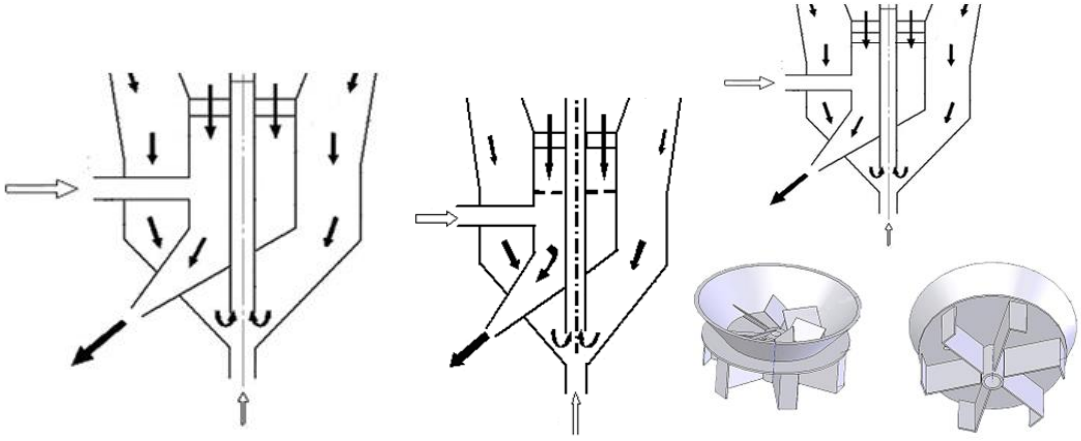

a b c

Figure 32 – The construction of the gas-distributing units in the vortex granulator: a - without stabilization of the drying agent ‘s flow motion; b - with stabilization grid under the vortex gas-distributing unit; c - with a two-stage swirler.

Data analysis fig. 33 confirms the assumption that the best quality of the nanoporous layer is obtained in the vortex granulator’s "active" zone. You can also clearly see an increase in the relative area of the nanoporous surface of the PAN granule with an increase in the degree of the drying agent flow twisting. A further increase in the drying agent’s twisting causes damages in the granule caused by the intensive collision of the granules with each other and with the walls in the granulator. Besides, an increase of the drying agent twisting degree over 8.1 m/s leads to an increase in heat loss in the granulator’s “active” zone through the wall of the device. Data from fig. 6 shows that the relative area of the nanoporous surface can be increased. Therefore, at the second stage of the research is devoted to the microscopy of granule samples obtained in granulators with stabilization of the drying agent’s vortex flow. The results of these studies are presented in fig. 7.

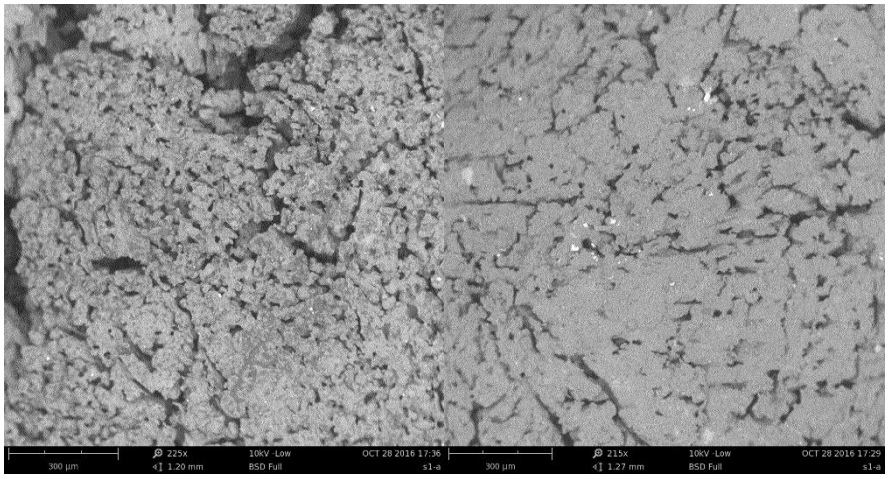


a

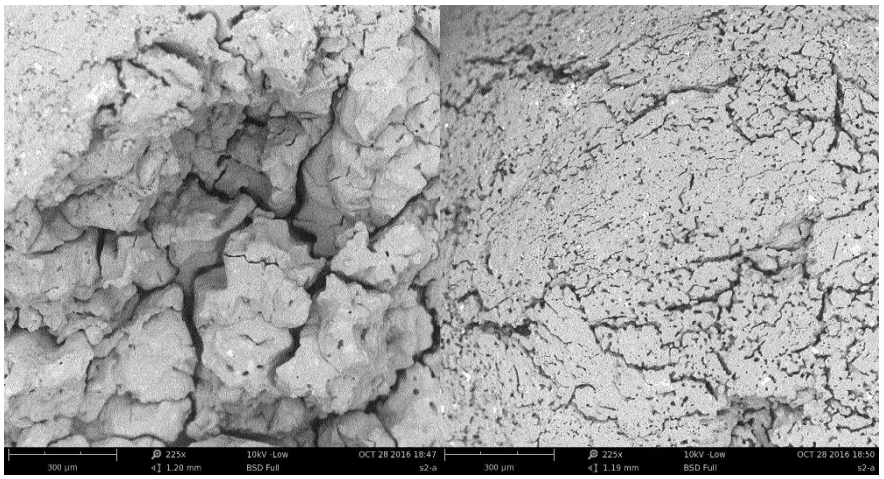


b

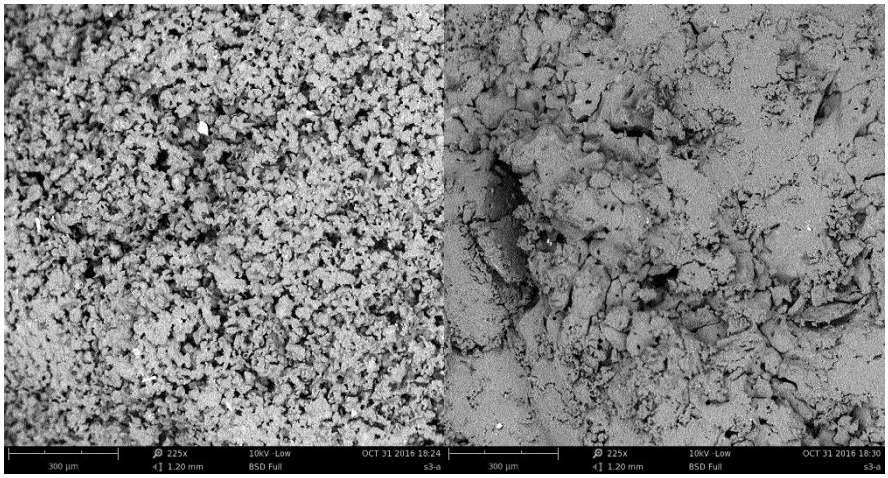


c

Figure 33 – Microscopy of the nanoporous surface in the granules obtained at different temperature distributions in the vortex granulator (according to fig. 2): a - circumferential velocity of 5.2 m/s; b - circumferential velocity of 6.5 m/s; c - the circumferential velocity 8.1 m/s. Left photo - PAN granule obtained in the "active" zone of the granulator, right photo - PAN granule obtained over the "active" granulator zone

Fig. 34 confirms the assumption about improving the nanoporous surface quality in the PAN granule due to the rational selection of a method to stabilize the vortex flow of a drying agent.

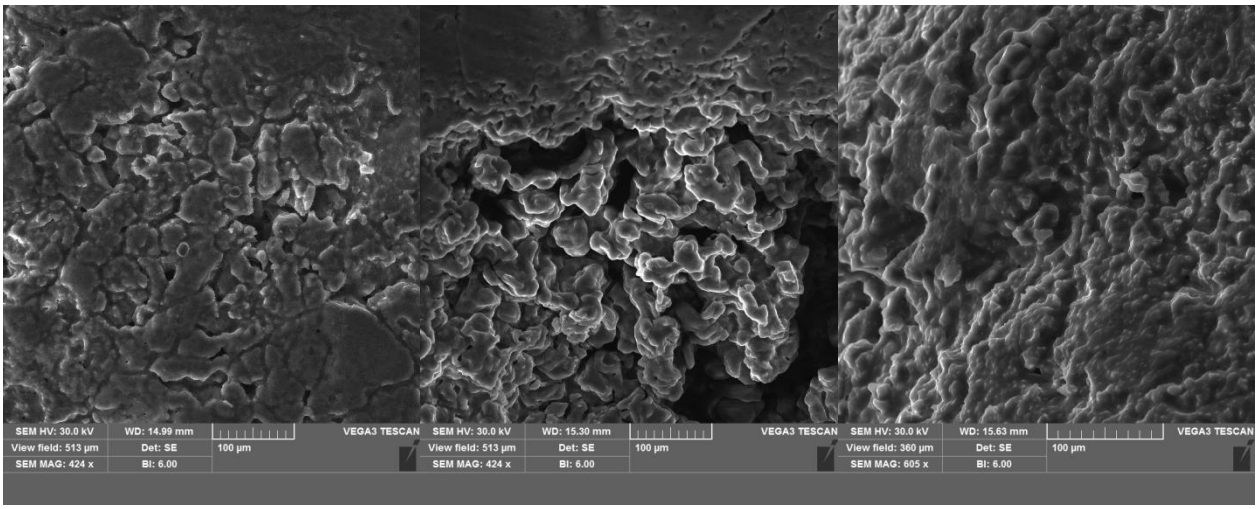


a b c

Figure 34 – Microscopy of the nanoporous surface of the granules obtained by using various methods of stabilizing the drying agent's vortex flow: a - granulator with a stabilization grid under the vortex gas-distributing unit; b - granulator with a two-stage swirler.

The data of experimental studies to define the relative area of the nanoporous surface in the PAN granule are summarized in Table 3.

Table 3 – Identification of the relative area in the nanoporous surface of the PAN granule

| Stabilization type | The relative area of the porous surface, $m^2/m^2$, at | | | | | |
|---|---|---|---|---|---|---|
| | V=5,2 m/s | | V=6,5 m/s | | V=8,1 m/s | |
| | in the "active" zone of the granulator | above the "active" zone of the granulator | in the "active" zone of the granulator | above the "active" zone of the granulator | in the "active" zone of the granulator | above the "active" zone of the granulator |
| Without stabilization | 0.36 | 0.25 | 0.39 | 0.28 | 0.41 | 0.3 |
| Granulator with stabilization grid under the vortex gas-distributing unit | - | - | - | - | 0.45 | - |
| Granulator with two-stage swirler | - | - | - | - | 0.48 | - |

Note: the “-” sign indicates the fields for which the studies were not carried out in view of determining the optimal conditions for the process to obtain the nanoporous layer on the PAN granule at the previous stages in the research

# 4 EFFECT OF TEMPERATURE ON FORMATION OF NANOPOROUS STRUCTURE OF GRANULE SHELL

*Report section "Introduction" is prepared in according to data [16] and references in this work.*

The two-layer granule with an organic shell is a solid core, that is, the primary granule of nitrogen fertilizers namely ammonium nitrate or urea. In the process of granulation in a fluidized bed, a layer of organic suspension, such as chicken manure, is applied on the core. By thermal drying of the granule outer shell, one obtains a porous shell of a certain structure. Size of pores, shape of their surface and nature of the curves, porosity of the shell depends on the temperature of the gas flow and duration of granules heating.

The process of heat transfer inside the granule, assuming its spherical shape, is described by the Fourier differential heat equation:

$$\frac{\partial t(r,\tau)}{\partial \tau} = a_T \left( \frac{\partial^2 t(r,\tau)}{\partial r^2} + \frac{2}{r} \frac{\partial t(r,\tau)}{\partial r} \right), \tag{55}$$

where $t\,(r,\tau)$ is granule temperature at a point with the current radius $r$ during the time $\tau$, °C;

$r$ – current radius of the granule, m;

$a_T$ – coefficient of thermal conductivity of the granule material, $m^2/s$; $\tau$ – granule heating time, s.

The well-known solution of equation (55) at:

initial conditions (the initial temperature distribution over volume of the granule is considered to be uniform)

$$\tau > \tau_0, 0 < r < R, t(r,\tau_0) = f(r); \tag{56}$$

symmetry conditions

$$t(0,\tau) \neq \infty, \frac{\partial t(0,\tau)}{\partial r} = 0; \tag{57}$$

boundary conditions of the third kind, providing for the equality of heat flows from the gas to the surface of the granule and from it into the middle of the core

$$\lambda_T \frac{\partial t(r,\tau)}{\partial r} = \alpha \left[ t(r,\tau) - t_{med} \right], \tag{58}$$

look like:

$$\frac{t_{med} - t(r,\tau)}{t_{med} - t_i} = \sum_{n=1}^{\infty} A_n \frac{\sin\left(\mu_n \frac{r}{R}\right)}{\mu_n \frac{r}{R}} \exp\left(-\mu_n^2 \cdot Fo\right), \tag{59}$$

where $t_i$ is the initial temperature of the granule, °C;

$t_{med}$ – temperature of the gas medium, °C;

$R$ – granule outer radius, m;

$Fo$ – Fourier criterion;

$A_n$, $\mu_n$ – constant and root of the equation, $A_1=f(Bi)$, $\mu_1=f(Bi)$;

$Bi$ – Biot criterion;

$\lambda_T$ – thermal conductivity coefficient of the particle material, W/(m·K).

Since the process of granule heating during granulation is quite long ($Fo \geq 0.3$), the infinite series in equation (5) quickly converges and we can restrict ourselves to only the first member of the series ($n$=1) in this equation.

Then equation (59) takes the form:

$$\frac{t_{med} - t(r,\tau)}{t_{med} - t_i} = A_1 \frac{\sin\left(\mu_1 \frac{r}{R}\right)}{\mu_1 \frac{r}{R}} \exp\left(-\mu_1^2 \cdot Fo\right). \tag{60}$$

Equation (60) makes it possible to determine the temperature profile by the granule radius when it is heated with gas from the surface to the center of the granule. Then from equation (52), temperature of the granule along its current radius is:

$$t(r,\tau) = t_{med} - (t_{med} - t_i) A_1 \frac{\sin\left(\mu_1 \frac{r}{R}\right)}{\mu_1 \frac{r}{R}} \exp\left(-\mu_1^2 Fo\right). \tag{61}$$

Since the granules are small in size, within 1–4 mm, to determine the temperature profile it is enough to determine the temperature on the surface of the granule, in the center of the granule and the average integral in the volume of the granule.

In the first case, assuming $r=R$ (granule surface) from equation (61) we obtain the expression for determining the temperature on the granule surface

$$t_P(r,\tau) = t_{med} - (t_{med} - t_i) A_1 \frac{\sin \mu_1}{\mu_1} \exp\left(-\mu_1^2 Fo\right). \tag{62}$$

In the second case, assuming $r \to 0$ (center of the granule) from equation (61) we obtain the expression for determining the temperature in the center of the granule

$$t_C(r,\tau) = t_{med} - (t_{med} - t_i) A_1 \exp\left(-\mu_1^2 Fo\right). \tag{63}$$

Using the formula for the integral average temperature in the volume of the granule

$$t_{ia}(\tau) = \frac{3}{R^3} \int_0^R r^2 \cdot t(r,\tau)\, dr. \tag{64}$$

in the third case, one obtains the expression for determining the volume-averaged temperature of the granule:

$$t_{ai}(r,\tau) = t_{med} - (t_{med} - t_i) \frac{6A_2}{\mu_1^2} \exp\left(-\mu_1^2 Fo\right). \tag{65}$$

The rate of granules heating and, accordingly, the rate of temperature profile change according to formula (61), is also determined by the thermal conductivity value of the granule material. This parameter is included in the Biot criterion and in the Fourier criterion through the thermal conductivity coefficient.

It is important to present a significant picture of the thermal conductivity of the granule material dependence on the structural characteristics of the porous shell. Structure diagram of the two-layer granule “solid core – porous shell” (fig. 35) provides that the solid core occupies 70 % of the granule’s volume, and the porous layer – 30 % of the volume.

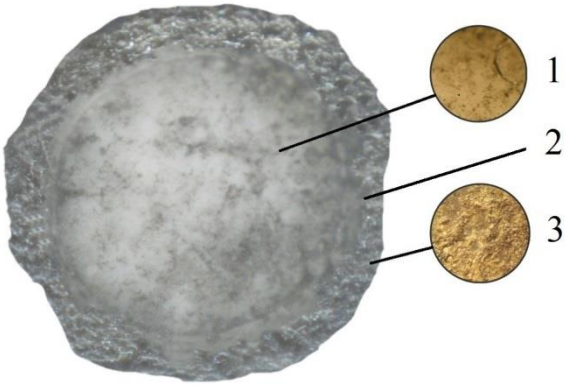


Figure 35 – Structure of organo-mineral granules: 1 – mineral core (urea); 2 – transition section; 3 – dry organic shell (chicken manure)

Based on the presented structure of the two-layer granule, it follows that the thermal conductivity of the granule material is not the same: the thermal conductivity is lower in the porous shell than that in the solid core, since in the porous layer the heat transfer by thermal conductivity decreases due to pores filled with gas. That is, in a porous shell, the resulting coefficient of thermal conductivity is always less than the corresponding coefficient in a solid body. This is explained by the following reasons:

1) part of the outer layer is covered with gas pores, wherin thermal conductivity of gas is considerably lower than the coefficient of thermal conductivity of a continuous body. Therefore, the heat flow taken relative to cross-sectional area of the porous shell

forms a certain fraction of the flow that would be transported in the absence of pores in the shell. This fraction is equal to the fraction of the free section of the total number of pores, that is, the porosity of the layer;

2) since pores are of irregular geometric shape, namely in the form of channels, alternating narrowing and expansion zones of the pore cross sections, additional resistance to heat transfer by thermal conductivity arises;

3) wavy porous channels lengthen the path of heat transfer by thermal conductivity through the gas layer;

4) the smaller the pore size, the greater the number of pores per unit volume of the granule with the same total porosity. It reduces value of the thermal conductivity coefficient.

Considering the above, the modified coefficient of "limited" thermal conductivity through the porous layer is

$$\lambda_{CT} = \frac{\lambda_E}{k_{sh} \cdot k_w \cdot k_p}, \tag{66}$$

where $\lambda_E$ is the effective coefficient of thermal conductivity, depending on the porosity of the layer $\varepsilon$, $\lambda_E = f(\varepsilon)$, $0<\varepsilon<1$;

$k_{sh}$ – pore shape coefficient;

$k_w$ – coefficient of pore weaving;

$k_p$ – pore size coefficient.

Thermal conductivity of the porous layer is an effective value that is intermediate between the thermal conductivity of the granule solid core and the thermal conductivity of the gas contained in the pores.

One proceeds from the simplified model of Kriescher, according to which the porous body in the section is alternating layers of a solid body and gas layers. In this case, the heat flow moves both parallel to the layers and perpendicular to them.

In the first case, one obtains:

$$\lambda_E = (1-\varepsilon)\lambda_T + \varepsilon\lambda_G. \quad (67)$$

In the second case:

$$\lambda_E = \frac{\lambda_T \cdot \lambda_G}{(1-\varepsilon)\lambda_G + \varepsilon\lambda_T}, \quad (68)$$

where $\lambda_T$, $\lambda_G$ – thermal conductivity of the granule material and gas in the pores, respectively, W/(m·K).

Then the average value of the effective thermal conductivity is

$$\lambda_E = \frac{0,5\left[(1-\varepsilon)\lambda_T + \varepsilon\lambda_G)\right]\left[(1-\varepsilon)\lambda_G + \varepsilon\lambda_T\right] + \lambda_T\lambda_G}{(1-\varepsilon)\lambda_G + \varepsilon\lambda_T}. \quad (69)$$

Analyzing equations (21)–(23), it can be seen that with increasing porosity of the layer, the thermal conductivity value decreases. Clarification of the nature and rate of this decrease is of a great interest, since thermal conductivity of the solid granule skeleton is tens of times higher than thermal conductivity of the gas inside pores. For example, mineral solid component parts of granules have thermal conductivity in the range of 0.15–0.45 W/(m·K), and thermal conductivity of air at 0°C is equal to 0.024 W/(m·K). Thermal conductivity of air is theoretically the lowest limit of the porous layer thermal conductivity. Values of the thermal conductivity coefficient can approach this limit when the heat transfer in the granule is minimized due to the presence of only touch contacts between the adjacent sections of the solid skeleton, i.e., in a layer with high porosity. These touch contacts have significant thermal resistance to heat transfer. Influence of the main solid skeleton is insignificant. Only at low porosity influence of continuous contact can be decisive, since a significant part of the heat flow is transferred inside the granule by its solid constituent parts.

Thus, considering these features, it should be noted that values of the coefficients $k_{sh}$, $k_w$, $k_p$ included in formula (66) should be greater than 1.

Formulas (55) and (69) are used to determine the surface temperature of a two-layer granule according to equation (62) and the temperature profile within $0.7R<r<R$ according to equation (61). When determining temperature in the center of the granule with equation (63) of the temperature profile for $r<0.7R$ using equation (61), the thermal conductivity $\lambda_T$ of the granule solid component is taken into account. When determining the volume-averaged temperature of a two-layer granule according to equation (19), the reduced thermal conductivity coefficient according to the equation is:

$$\lambda_R = 0,7\lambda_T + 0,3\lambda_E. \tag{70}$$

The results of mathematical modeling are obtained in comparison for a continuous granule with porosity $\varepsilon=0$ and a porous granule with values of $0.1\leq\varepsilon\leq0.7$.

The graph (fig. 36) shows the dependence $S_S=f(d_p)$, according to the equation

$$S_S = \frac{2\varepsilon}{d_p \cdot \rho_g}, \tag{71}$$

where $S_S$ is the total specific pore surface, $m^2/kg$;

$\varepsilon$ – granule porosity, $0<\varepsilon<1$;

$d_p$ – equivalent pore size, m;

$\rho_g$ – density of the granule material, $kg/m^3$.

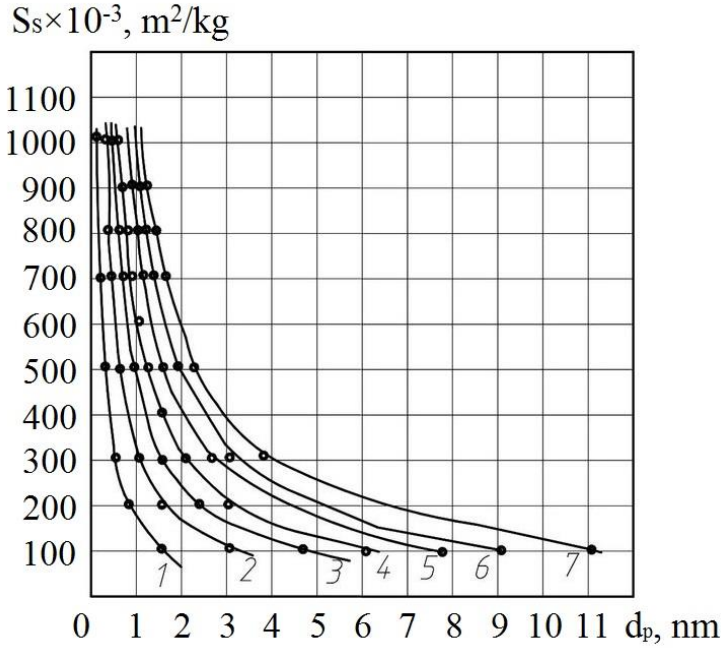


Figure 36 – Dependence of the specific pore surface on pore size: *1* – $\varepsilon$ = 0.1; *2* – $\varepsilon$ = 0.2; *3* – $\varepsilon$ = 0.3; *4* – $\varepsilon$ = 0.4; *5* – $\varepsilon$ = 0.5; *6* – $\varepsilon$ = 0.6; *7* – $\varepsilon$ = 0.7.

Graphs of the dependence $S_S=f(d_p)$ show definite relationship between the specific surface of pores with their size and granule porosity. With the specific pore surface in the range $(100–1000)\cdot10^{-3}$ m$^2$/kg and with $\varepsilon$=0.1–0.7, we have micropores with a size $d_p$=0.2–10 nm. With the decrease of the specific surface of pores to less than $10\cdot10^{-3}$ m$^2$/kg and at $\varepsilon$>0.5–0.7, there appear intermediate pores (mesopores) of size $d_p$=50–100 nm and we approach the initial boundary of appearing macropores of size $d_p$>100 nm.

Dependence of the effective coefficient of the granule thermal conductivity on its porosity, according to equation (69), first shows a rapid decrease of the thermal conductivity coefficient value during transition from the continuous structure of the granule ($\varepsilon$=0) to the beginning of the porous structure formation ($\varepsilon$=0.1), and then a proportional decrease in thermal conductivity within the change in the porosity of the granule $0.1<\varepsilon<0.7$.

The volume-averaged temperature of granule heating to a certain temperature is defined as

$$t = t_{med} - (t_{med} - t_i)\frac{6A_2}{\mu_1^2}\exp\left(-\mu_1^2\frac{\lambda_E \cdot \tau}{c \cdot \rho \cdot R^2}\right), \quad (72)$$

and granule heating time

$$\tau_h = \frac{R^2 \cdot c \cdot \rho}{\lambda_E \cdot \mu_1^2}\ln\left[\frac{6A_2}{\mu_1^2\left(\frac{t_{med} - t}{t_{med} - t_i}\right)}\right]. \quad (73)$$

where in addition to the above designations,

$c$ – the specific heat of the granule, J/kg·K;

$\rho$ – granule density, kg/m$^3$.

The numerical values of the constants $A_1$, $A_2$ and the root $\mu_1$ are found from the tables or graphically using the nomograms. This determination method makes it difficult to use a computer in an engineering calculation algorithm. Therefore, the authors using the least squares method processed the data of the monograph tables and obtained regression equations to determine the constants $A_1$, $A_2$ in the range $0.1<Bi<4.0$, which is typical for suspended and fluidized beds:

$$A_1 = 0.274(Bi) + 1.0, \text{ at } 0 < Bi \le 0.1; \quad (74)$$

$$A_1 = 0.29(Bi) + 1.0, \text{ at } 0.1 < Bi \le 1.0; \quad (75)$$

$$A_1 = 0.183(Bi) + 1.1, \text{ at } 1.0 < Bi \le 2.0; \quad (76)$$

$$A_1 = 0.13(Bi) + 1.22, \text{ at } 2.0 < Bi \le 4.0; \quad (77)$$

$$A_2 = 0.47(Bi) + 0.01, \text{ at } 0.1 \le Bi < 0.5; \quad (78)$$

$$A_2 = 0.325(Bi) + 0.06, \text{ at } 0.5 \le Bi < 1.0; \quad (79)$$

$$A_2 = 0.30(Bi) + 0.1, \text{ at } 1.0 \le Bi \le 2.0; \quad (80)$$

$$A_2 = 0.25(Bi) + 0.05, \text{ at } 2.0 < Bi \le 4.0. \quad (81)$$

Root $\mu_1$ is determined:

$$\mu_1 = \frac{в + \sqrt{в^2 - 4c}}{2}, \tag{82}$$

or

$$\mu_1 = \sqrt{\frac{Bi^2}{A_2} - Bi^2 + Bi}, \tag{83}$$

where

$$в = \frac{2Bi}{A_1}; \tag{84}$$

$$c = \frac{\left(Bi^2 - Bi\right)\left(2 - A_1\right)}{A_1}. \tag{85}$$

Dependence of the granule heating time on its porosity, according to equation (73), shows a sharp increase in the heating time of the granule (approximately 2 times) during the transition from a continuous granule ($\varepsilon$=0) to a granule with initial porosity ($\varepsilon$=0.1). Then heating time gradually increases and granule porosity reaches the level 0.1 <$\varepsilon$<0.3; further rapid increase of granule heating time causes porosity in range 0.3<$\varepsilon$<0.6. The latter is caused by a significant decrease of areas of the granule solid skeleton, that have less resistance to the heat conductivity process. This is proved by the nature of curves in the dependence $t=f(\tau)$ (fig. 37) during heating of granules in the gas medium with an initial temperature of 65°C.

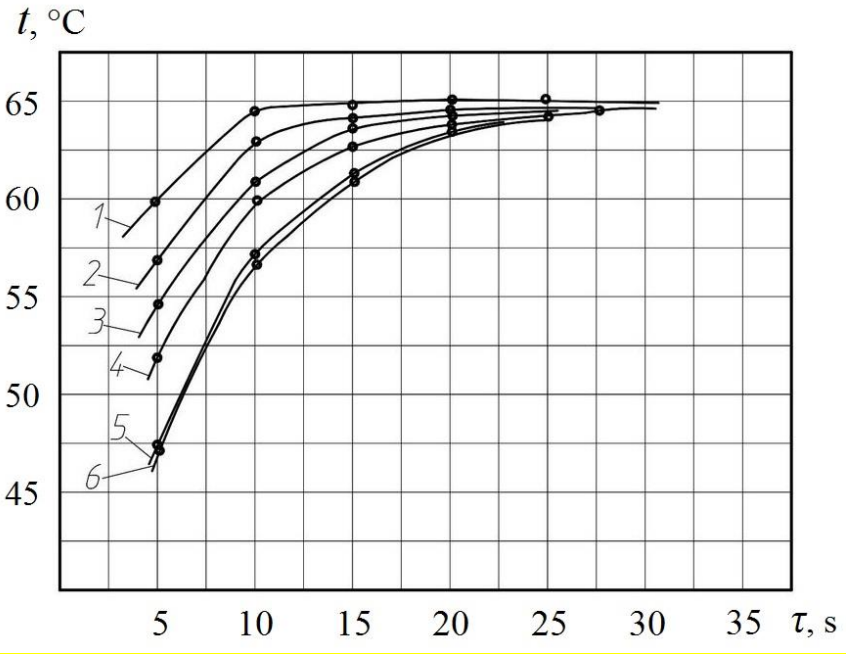


Figure 37 – Dependence of the granule heating temperature on time: *1* – $\varepsilon$ = 0.1; *2* – $\varepsilon$ = 0.2; *3* – $\varepsilon$ = 0.3; *4* – $\varepsilon$ = 0.4; *5* – $\varepsilon$ = 0.5; *6* – $\varepsilon$ = 0.6.

During laboratory studies film coating of an organic suspension was applied on mineral granules and temperature of gas medium in the fluidized bed of granules was maintained in the range of 40–80°C. The following temperature conditions of the granulation process were established experimentally:

1. At the temperature within 40–50°C, droplets of the suspension do not spread over the surface of the granule, but attach to one side of the granule, and form a big growth which is as big as a drop itself (fig 38, a).

2. When temperature of the fluidized bed is 60–65°C, droplets of the suspension spread over the surface of the mineral granules and liquid starts to evaporate intensively, forming a thin solid layer of dry organics (fig 38,b). As it can be seen from the graphs in Fig. 3, at 20–25 seconds of heating the granules, their temperature reaches 65°C and then remains constant, that is, the indicated value is the limiting temperature of granule heating. Moreover, the granule outer shell is of sufficiently dense structure with micro- and mesopores on its surface.

3. Increase of the fluidized bed temperature above the limiting value, namely, up to 70–80°C, causes the formation of irregular surface with deep cracks which is

accompanied with chipping of organic substance in separate places of the granules and thus new organic cores appear (fig 38, c). The porosity of such granules increase, macropores are formed.

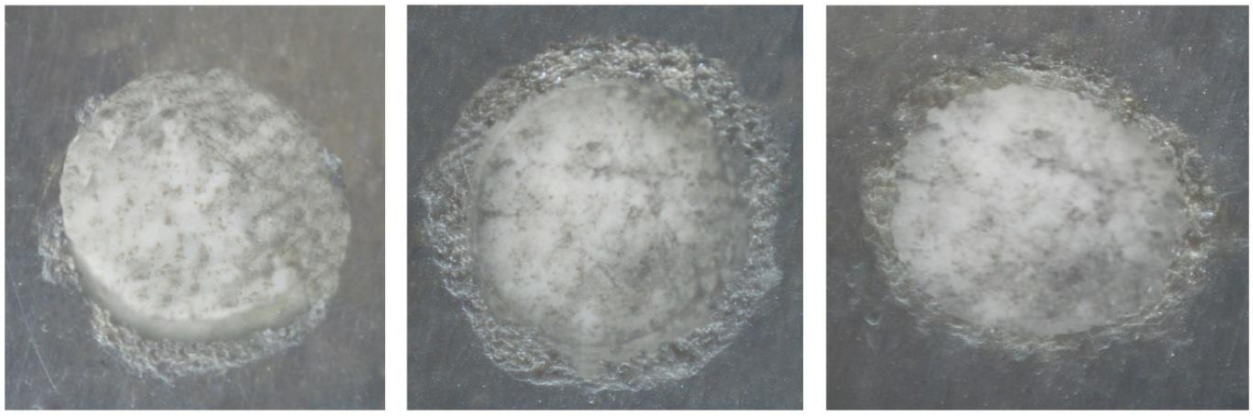

a b c

Figure 38 – Cut of the carbamide granule, encapsulated with chicken manure at the appropriate temperature: a – 40–50°C; b – 60–65°C; c – 70–80°C.

# 5 EFFECT OF THE INTENSITY OF AMMONIUM NITRATE GRANULES HUMIDIFICATION ON THE QUANTITATIVE AND QUALITATIVE COMPOSITION OF THE FINAL GRANULES NANOPOROUS STRUCTURE

*This report section is prepared in according to data [15] and references in this work.*

The pore structure of the finished PAN granules is affected by such indices as the type of humidifier, the degree of granules humidification and the heat treatment mode. In literature data, the dependence of the qualitative and quantitative features of the PAN granules porous structure on the type of humidifier is investigated. For laboratory tests, a laboratory a vortex granulator unit is used (fig. 39).

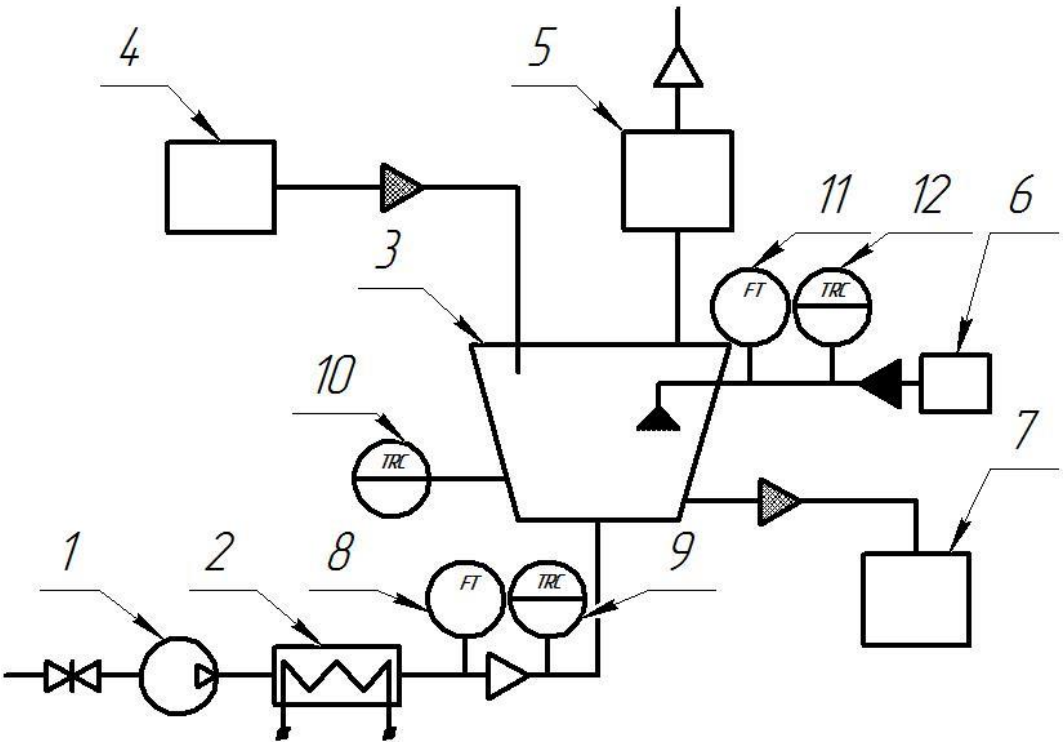


Figure 39 – The scheme of the laboratory vortex granulator unit:

1 – gas blower; 2 – heater; 3 – vortex granulator; 4 – container for granules; 5 – waste gas cleaning stage; 6 – container for preparation of humidifier; 7 – container of finished granules; 8 – automation device for measure the air flow; 9 – automation device for measure the temperature of air; 10 – automation device for measure the temperature of layer; 11 – automation device for measure the humidifier flow; 12 – automation device for measure the temperature of humidifier

The batch of the initial ammonium nitrate granules is heated to a predetermined temperature, then the granules are moistened (humidifier - water) and subsequent heat

treatment is carried out (8 minutes at a temperature of a layer - 108 ° C, thermodynamic parameters are taken according to the results of previous studies). Samples of finished PAN granules are studied by microscope (scanning electron microscope eTescan Vega 3, formation of the carbon film on the granule surface - Carbon evaporation head CA7625 and SC7620 high resolution, manual Sputter Coater).

It is important to determine the first and second critical velocities (the rate of fluidization beginning and the rate of the granules ablation) for the fluidized bed. The first critical velocity is calculated by the formula:

$$\omega_1 = \frac{\mathrm{Re} \cdot \mu_{fa}}{\rho_{fa} \cdot d} \tag{86}$$

where $Re$ - the Reynolds criterion,

$\mu_{fa}$ - the viscosity of the fluidizing agent,

$\rho_{fa}$ - the density of the fluidizing agent,

$d$ - the diameter of the fluidized bed particles (PAN granules).

The Reynolds criterion is calculated by the formula:

$$\mathrm{Re} = \frac{Ar}{1400 + 5,22 \cdot \sqrt{Ar}}, \tag{87}$$

where $Ar$ – Archimedes criterion.

Archimedes criterion is calculated by the formula:

$$Ar = \frac{d^3 \cdot \rho_{fa} \cdot g \cdot \rho_{fbp}}{\mu_{fa}^2}, \tag{88}$$

where $\rho_{fbp}$ – density of the fluidized bed particles (PAN granules)

The second critical velocity is calculated by the formula:

$$\omega_2 = \frac{\mu_{fa}}{d \cdot \rho_{fa}} \cdot \left( \frac{Ar}{18 + 0,575 \cdot \sqrt{Ar}} \right). \quad (89)$$

At the stage of the granule's humidification, their diameter remains the same, but the mass increases. It leads to an increase in the density of the granules $\rho_{fbp}$, to an increase in the value of the Archimedes criterion *Ar*, an increase in the values of the first and second critical velocities. Thus, humidifying the granules, it is necessary gradually to increase the solubilizer's motion velocity.

The range of the granulator stable operation (critical velocities of fluidization) for a vortex fluidized bed of dry granules and granules humidified to a predetermined humidity, is calculated using the author's software product (fig. 40). The literature data also show the main hydrodynamic indices of a vortex granulator operation, used in the experimental and industrial production line of PAN.

Depending on the granules humidification mode during the modification of the PAN granules in the vortex granulator, the qualitative and quantitative features of the porous structure in the finished granules are changed.

During the tests and analysis of their results, the following humidification modes are distinguished (fig. 41):

– The uneven humidification mode (less than 50 g of water per 1 kg of ammonium nitrate granules);

– Optimal humidification mode (50 – 150 g of water per 1 kg of ammonium nitrate granules);

– High humidification mode (150 – 300 g of water per 1 kg of ammonium nitrate granules);

– Excessive humidification mode (more than 300 g of water per 1 kg of ammonium nitrate granules).

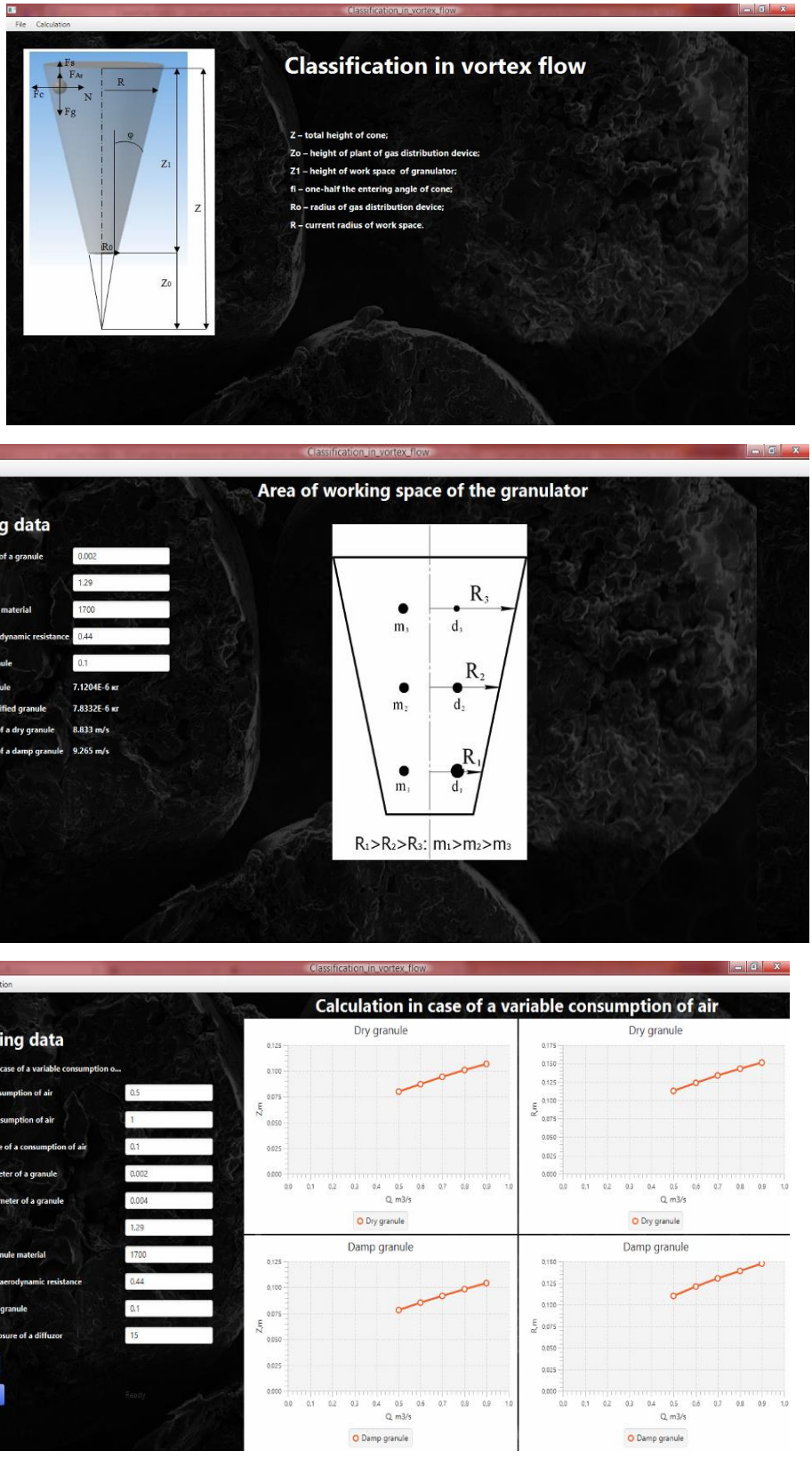


Figure 40 – The software product Classification in vortex flow© : calculation block for the vortex granulator stable operation range

When using the uneven humidification mode, the finished PAN granules have an undeveloped porous structure (fig. 42). The number and size of pores of the finished granules do not almost differ from the initial granules. Under conditions of low humidity of the granules and their subsequent heat treatment, there are local areas with the melted surface.

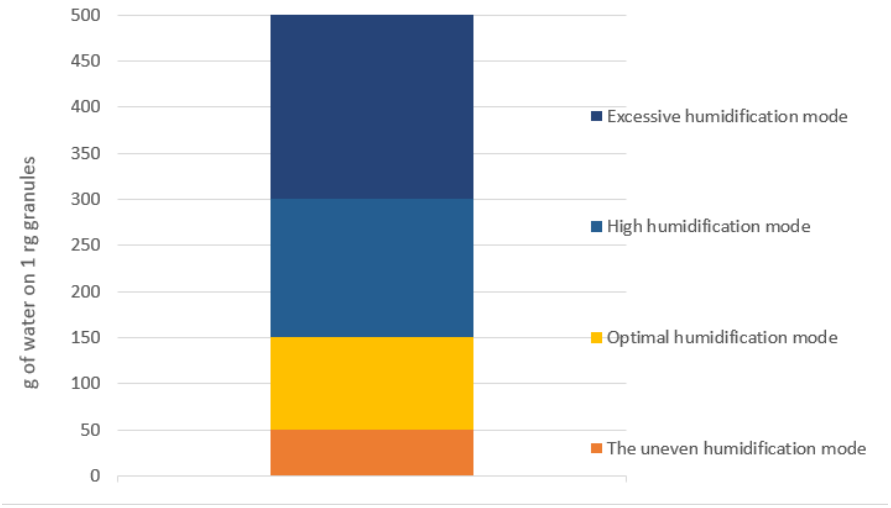


Figure 41 – Diagram of humidification modes (depending on the amount of humidifier)

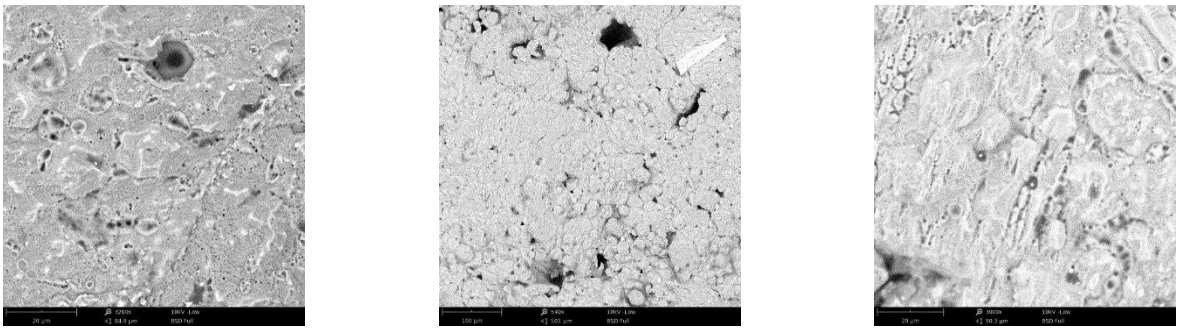

Figure 42 – The surface of the PAN granules (uneven humidification mode) with undeveloped porosity and local areas with a melted surface

Under conditions of the optimal humidification mode, the finished PAN granules have a developed porous structure with a large number of macropores (more than 50 nm)

and mesopores (2 – 50 nm) (fig. 43). There are no areas with melted surface or local sections with undeveloped porous structure.

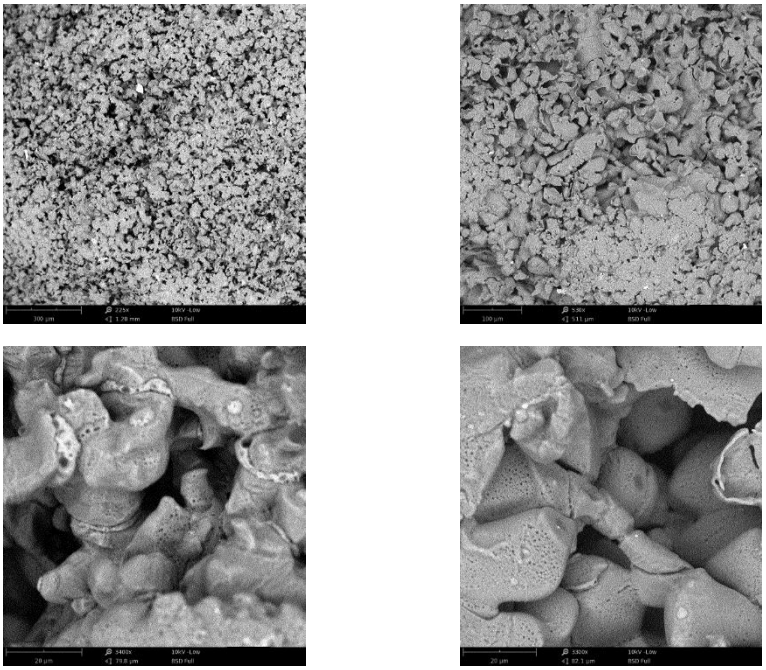

Figure 43 – The surface of the PAN granules (optimal humidification mode) with developed porous structure with macropores and mesopores

Further increase in the intensity of humidification (the high humidification mode) leads to the over-humidification of PAN granules. During subsequent heat treatment, significant destructive phenomena (cracks and chips) occur due to considerable pore-formation (fig. 44). Besides, increasing the moisture intensity, the tendency of granules to agglomeration increases, which impairs the qualitative features of the finished product.

When the intensity of the granules humidification increases, their destruction and partial dissolution occur. The fluidized bed of granules in the vortex granulator loses its stability and "falls", causing the necessity to stop the unit and clean it.

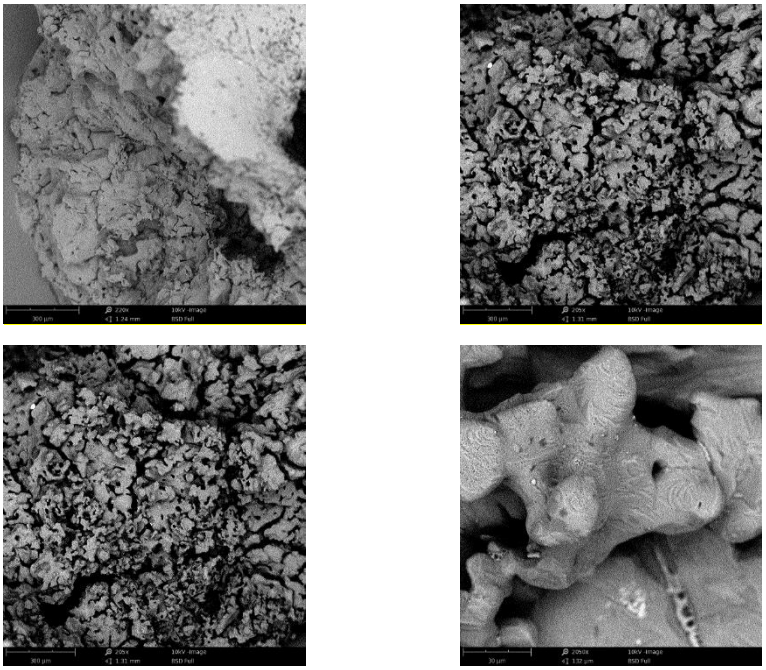

Figure 44 – The surface of the PAN granules (high humidification mode) with a lot of chips and cracks, granule agglomeration tendency

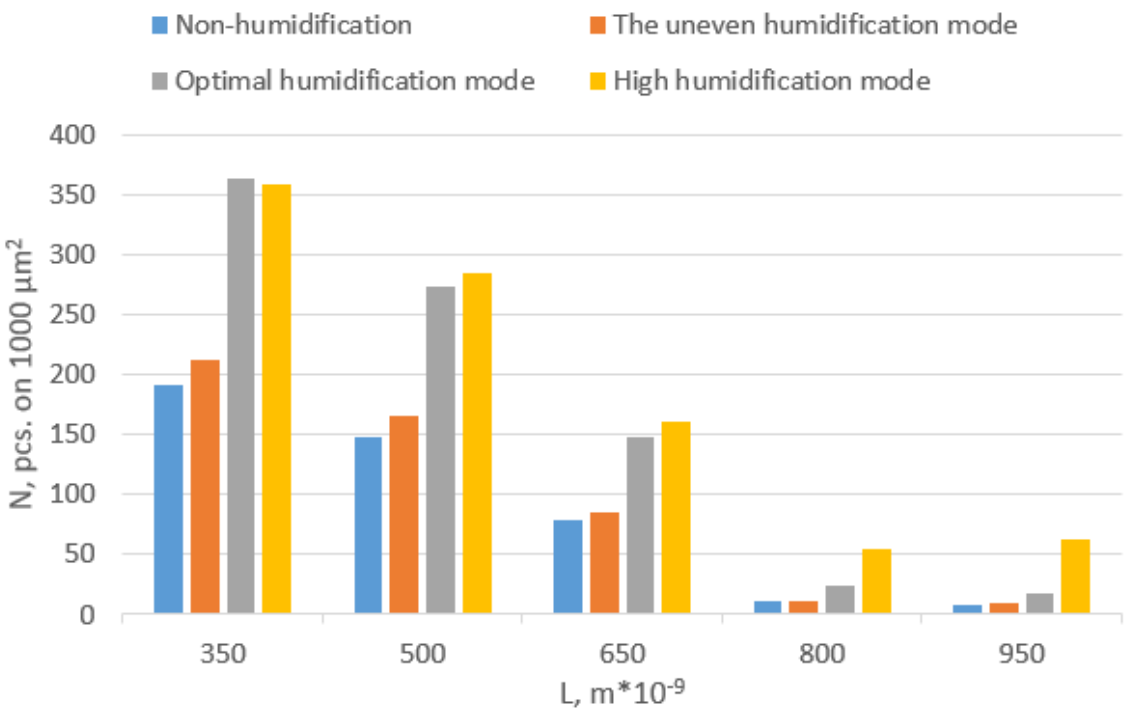


Figure 45 – Dependence of qualitative and quantitative features of PAN granules porosity on moisture intensity (surface layers)

The graphical dependence of the qualitative and quantitative porosity features of the PAN granules on the moisture intensity is shown in fig. 45 (surface layers) and fig. 46 (inner layers).

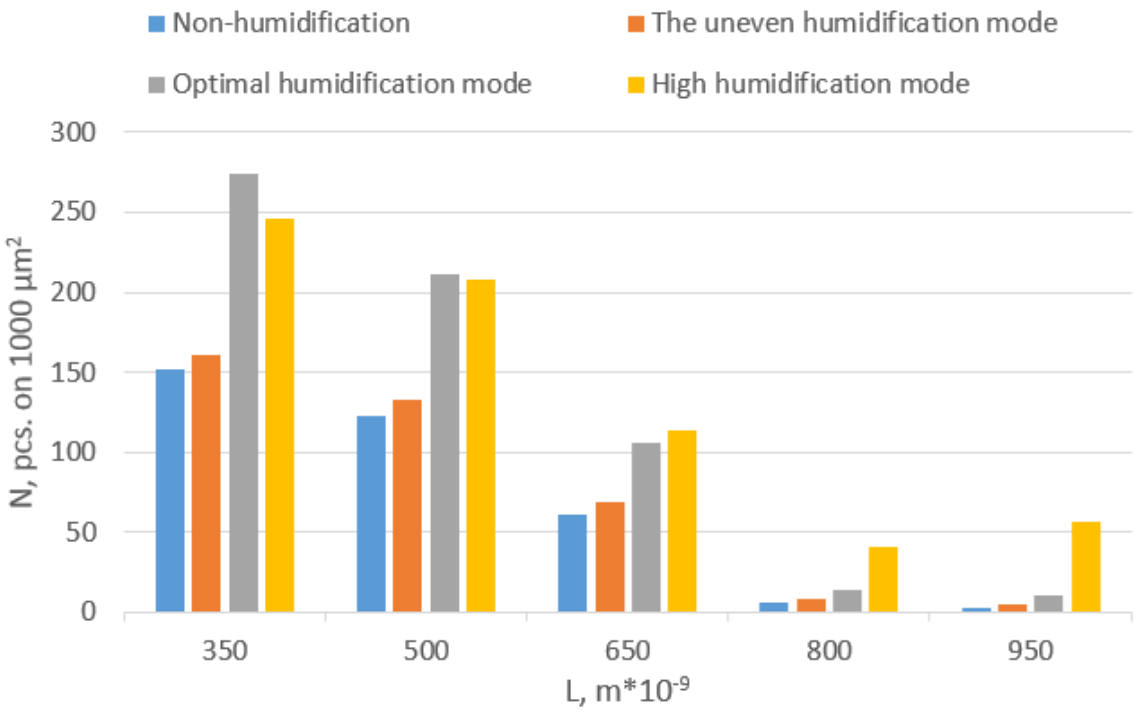


Figure 46 – Dependence of qualitative and quantitative features of PAN granules porosity on moisture intensity (inner layers)

# 6 COMPARATIVE EXERGY ANALYSIS OF UNITS FOR THE POROUS AMMONIUM NITRATE GRANULATION

*This section is prepared in according to data [17] and references in this work.*

Some chemical manufacturing units use energy to produce heat, electricity and raw materials which can amount to 85% of the production costs [18], making it possible to consider energy efficiency an essential component of the chemical unit design. The analysis in the research [19] enables to single out such initiative measures for increasing energy efficiency as improvement of existing processes; introduction (commercialization) of new processes; recycling; investments in renewable energy sources; creating products that save energy. However, the US chemical industry's share of the total energy consumed is 6% despite all the implemented advanced energy efficiency measures [20].

Analysis of the data [21-23] concludes that various heat exchangers make almost half of the chemical units' equipment. It is necessary to reduce the number of heat exchangers investigating new mechanisms for utilizing the temperature and humidity potential of flows to ensure energy efficiency in the units.

The estimated prime cost of chemical production shows that the cost of raw materials and their preparation, including its temperature potential change takes up to 70% of this indicator [24, 25]. This fact requires further revision to preparing raw materials and semi-finished products and recycling production waste in both physical and energy forms.

Granulation process as a method of forming various substances from solutions and melts are widely used in the chemical industry [26 – 31] and the pharmaceutical [29 – 32] and other industries, as well as in the production of granules with unique properties [33] (for example, porous ammonium nitrate, considered in this work). The high-temperature heat transfer agents and wet streams in granulation processes open the prospect of introducing and successfully implementing effective methods to utilize the temperature and humidity potential of granulation units.

The porous ammonium nitrate can be produced in granulation units by various methods described in the works of Cardarelli and Janssen [34, 38]. Analysis of the advantages and disadvantages of the existing methods for producing porous ammonium nitrate suggests a new approach. It is a combination of humidification and heat treatment of ordinary ammonium nitrate. Artyukhov and Artyukhova in their works [39, 40] describe in detail various stages of this process. One should note that the production of the porous ammonium nitrate can be improved by creating additional conditions for the utilization of heat and moisture of the used heat transfer agent (drying agent) and using the obtained temperature and humidity potential at other stages of getting a granular product in the same unit.

There are two large blocks of methods for improving the energy efficiency of chemical units:

Block 1. To improve the devices of the chemical unit and the organization of the flow motion inside them (internal efficiency).

Block 2. To improve the flow motion organization and methods for changing their potential in a chemical unit (external efficiency).

One can give the following examples of methods from the first block: investigations on the active hydrodynamic modes in devices represented by Artyukhov [39], the design of multistage and multifunctional devices were considered by Artyukhov [11, 41].

The key aspect in increasing the energy efficiency of the heat-mass transfer equipment provides the high specific indicators in the heat-mass transfer process (U value (factor), heat transfer coefficient, conductivity) and the required properties of heat-mass transfer surfaces. For example, the use of recuperators in which one or several heat carriers is transformed (condensed, evaporated, or boiled) can significantly increase the efficiency of the heat recovery process (according to the results of experimental studies GTI—Maisotsenko-Cycle Based Humidified Air Recuperator (HAR) and Water Heater Validation). For example, new thermodynamic prisnciples for air-evaporative cooling of a large amount of heat carrier in cooling towers will provide a significant economic effect [42] (GTI—Method and apparatus for dew point evaporative product cooling).

Besides, new materials and coating can be used to achieve these indicators and reach a new qualitative equipment level. Their implementation can significantly reduce energy consumption and increase equipment reliability, such as not using the pump working with highly efficient capillary-porous materials [43, 44]. Efficient heat and mass transfer equipment allow developing new solutions for many industrial processes and units.

The simplest solution in the second block of energy efficiency methods is to use a heat transfer agent's recirculation without additional preparation. The successful application of such a solution for multistage shelf dryers is presented in the study of Artyukhova [13]. However, there are more complex but more effective ways.

In the chemical industry, which simultaneously can use many flows with various substances with different thermal and caloric parameters, it is essential to ensure the most complete and positive effect of some processes on others. So, for example, in the utilization ejector module for the granulation scheme of porous ammonium nitrate [42, 46], in addition to the nitrogen oxides conversion into higher oxides (the main effect), there is a significant inflow of thermal energy (secondary energy resource), which can and should be used (heating, drying, humidification, electricity generation [47, 48]) for the needs of their chemical production or related enterprises/workshops or the population. It is advisable to organize a staged heat removal and recuperation since it will let more efficiently distribute energy between its consumers to ensure the available secondary energy resources use. In this regard, it is rational to use the evaporative indirect-regenerative cooling devices (M-cycle) since it allows removing heat effectively and obtaining highly enthalpy streams of highly humid air for their further humidification, heating or electricity generation. Besides, these devices use renewable energy from the environment [31] which, in addition to other renewable energy sources (e.g., solar), develops modules using the reverse sub-atmospheric Brayton cycle and makes a significant positive contribution to the overall scheme efficiency.

Some researchers and organizations (GTI, SoftInWay), who provide promising theoretical calculations results [48, 50], have studied the sub-atmospheric reverse Brayton cycle. Among the leading scientific and practical problems in implementing this cycle is

to develop a highly efficient heat and mass transfer device—a recuperator. The researchers propose to use a plate or spiral heat and mass transfer devices implementing the principles of evaporative indirect regenerative cooling (M-cycle). Therefore, it is relevant to study the potential of these devices in chemical production schemes to solve heat recovery and energy production problems.

Many methods can be used to efficiently analyze complex systems where various flows of heat, mass, and power are interdependent and interact pinch analysis, entropy generation minimization (EGM), exergy, thermoeconomic analysis and others. Pinch analysis (PA) shows its fast-developing nature for many fields of applications. PA offers a rational framework to identify energy saving targets and design efficient heat recovery networks, especially in the process industry [51, 52]. However, according to authors [53] PA is not suitable for processes dealing with changes in pressures and compositions of the materials. In our further investigations, it seems rational to consider a combined innovative approach proposed by [54] and adopt it for optimization operating processes of units for the porous ammonium nitrate granulation. Such a powerful tool as EGM is useful for optimization operating processes in various applications (cryogenics, heat storage, power generation, etc.) through minimization of the calculated entropy generation rate. However, one should relate the thermodynamic non-ideality degree of the design to the physical features of the system, namely to finite dimensions, shapes, materials, finite speeds and finite-time intervals of operation, to take the maximum advantage from EGM method [55, 56]. Thus, EGM will be more appropriate when the main operation modes and design of the elements, which are part of the complex system, will be defined. A similar situation is with thermoeconomic and exergo-economic analysis. It is complicated to obtain the necessary data for accurate calculation when the new layout of the unit for the porous ammonium nitrate granulation is considered, and new significant components are not designed or customized but considered black-box systems. Therefore, within the current investigation, we decided to provide an evaluative exergy analysis and amount only to the determination of system efficiency indicators [57].

Since the 50s of the last century, various industrial fields have implemented the exergy method of analysis that became one of the main ways to analyze, evaluate, and optimize the systems [58]. This approach is relatively flexible and universal for energy systems as a whole and their components [59-65]. The scheme components' analysis allows evaluating their effectiveness separately and determining the element that leads to a decrease in the system efficiency. In publication [66], the authors describe the fundamentals and recommendations for applying the exergy analysis device.

This method is based on an approach in which all its flows come to a single "measure," that is, "exergy", dividing them into costs and beneficial effect ("fuel and product") [66], and separating losses and exergy destruction [67]. If the initial data on the above flows are available at the design stage of the unit/device, it is possible to assess the exergy efficiency and, if necessary, to increase it.

Yukhimenko [68] demonstrates a technique for the exergy analysis of technological flows of the phosphorus-potassium fertilizer production, which uses the classical approach for the energy system. This technique defines product exergy due to its parameters. In this case, it is not entirely correct. The beneficial effect includes its quality, state and quantity at the output with minimal costs for its production, not the outcome thermodynamic parameters (affecting the exergy efficiency of the system) in the production of the material product.

A mixed exergy analysis is used to compare both schemes for porous ammonium nitrate production in the current work. This approach lets assess the efficiency of the schemes and the potential of secondary energy resources, which can be useful in this scheme or adjacent systems. The essence of the mixed exergy analysis is that the specific indicator, which is nothing more than the expenditure of specific exergy for production of a unit of mass of the product, is used for the assessment. It also allows determining the flows (energy, substandard, etc.) that can be utilized within the circuit design and minimize harmful emissions into the environment. For example, replacing an electric heater with an ejector recycling module to obtain the high temperatures required for the drying process leads to the fact that the residual heat is used to heat water and to generate

electricity in the sub-atmospheric Brayton cycle [49, 69, 70]. In the research Živić [71], the authors calculated the Brayton cycle with different features. As a result, the exergy efficiency was assessed, which, in contrast to the thermal efficiency (which includes various types of energies), showed the preferable operating parameters in the cycle. Thus, the exergy analysis of complex systems and comparison of their versions, given its flexibility and versatility, is of scientific and practical interest.

This section describes the circuit design and technological scheme of granulation (Figure 47). The presented system produces porous ammonium nitrate as a component of an explosive industrial ANFO (ammonium nitrate—fuel oil). The principle of operation is as follows.

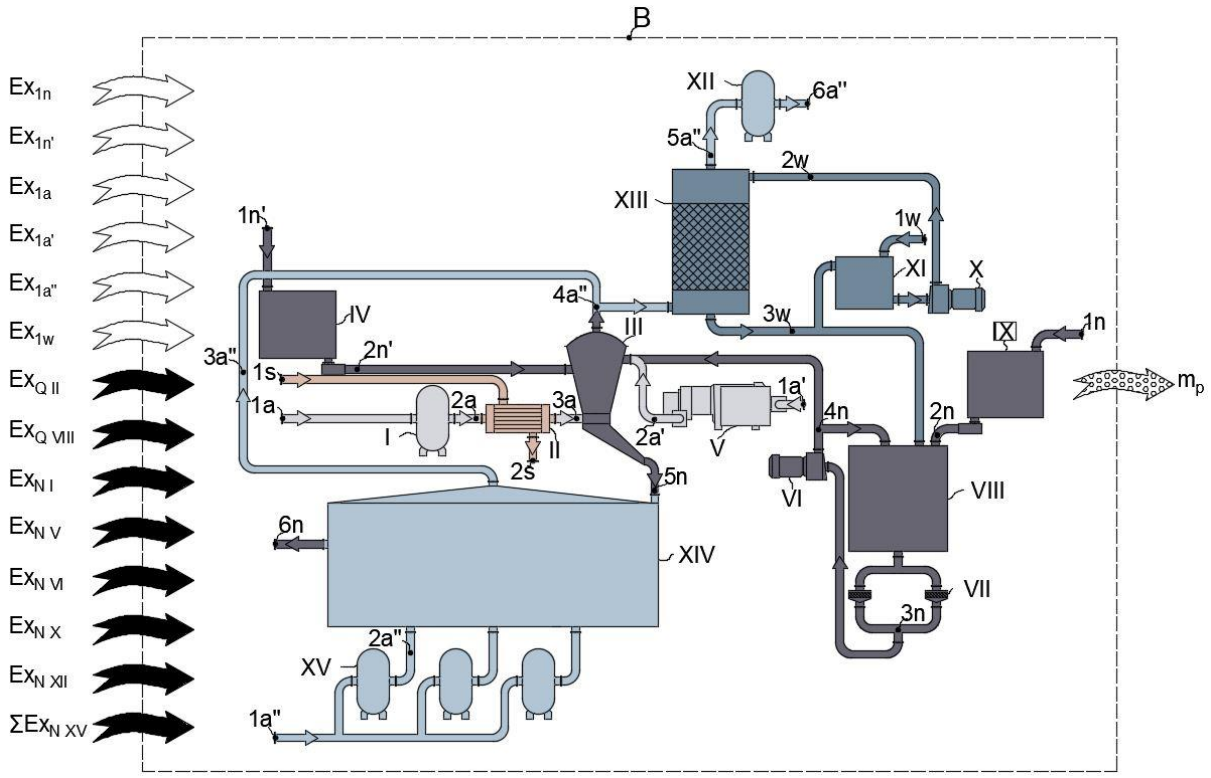


Figure 47 – Basic exergy contour in the technological scheme of porous ammonium nitrate granulation. I—gas blower; II—air heater; III—granulator; IV—bunker; V—compressor; VI—pump; VII—filter; VIII—capacity; IX—bunker; X—pump; XI—tank 2; XII—gas blower; XIII—absorber XIV—cooler; XV—gas blowers.

In the vortex granulator III, the seeding agents' granules (ordinary ammonium nitrate) are fed for further humidification with an ammonium nitrate solution coming from

mixer VIII and dehydration in the granulator with a stream of hot heat transfer agent (heated air) from the heat exchanger II. The saturated steam under pressure heats a hot heat transfer agent. Similarly, the ammonium nitrate solution is heated before it is applied to the seeding agent granule's surface. After humidification and heat treatment (drying), the porous ammonium nitrate granules are sent for cooling in the device XIV. The exhaust air is sent to device XIII for cleaning. The scheme provides the reuse of production waste to prepare a solution of small granules, the dust of ammonium nitrate and ammonia water after it absorbed waste from the used heat transfer agent.

The unit is implemented for thermomechanical processing of the product from seeding agent's granules with a solution applied on them to the productional granules with given physical parameters (density, humidity ratio content, porosity, hardness, geometric dimensions) with the maximum possible performance, and not to produce work, cold or heat. Thus, all incoming exergy streams are consumed to obtain a mass flow of the final product (granular ammonium nitrate). In this case, the exergy potential of the final product is not significant, and the mass flow rate mainly influences the efficiency of the scheme.

This section provides an approach to the unit's exergy analysis to produce the porous ammonium nitrate and the contour elements included in the system, restricting it with a conditional control contour "B" (Figure 48), crossed by supplied and removed exergy flows (mechanical/electrical, substance flow, chemical) of various amount, quality, and type. Exergy losses are also diverted through the control contour.

When performing an exergy analysis of any system, it is necessary correctly to determine the input and output exergy flows and their role. The general exergy balance Equation (90):

$$\sum \dot{E}x_{in} = \sum \dot{E}x_{out} + \sum \dot{E}x_{loss} + \sum \dot{E}x_{des} \qquad (90)$$

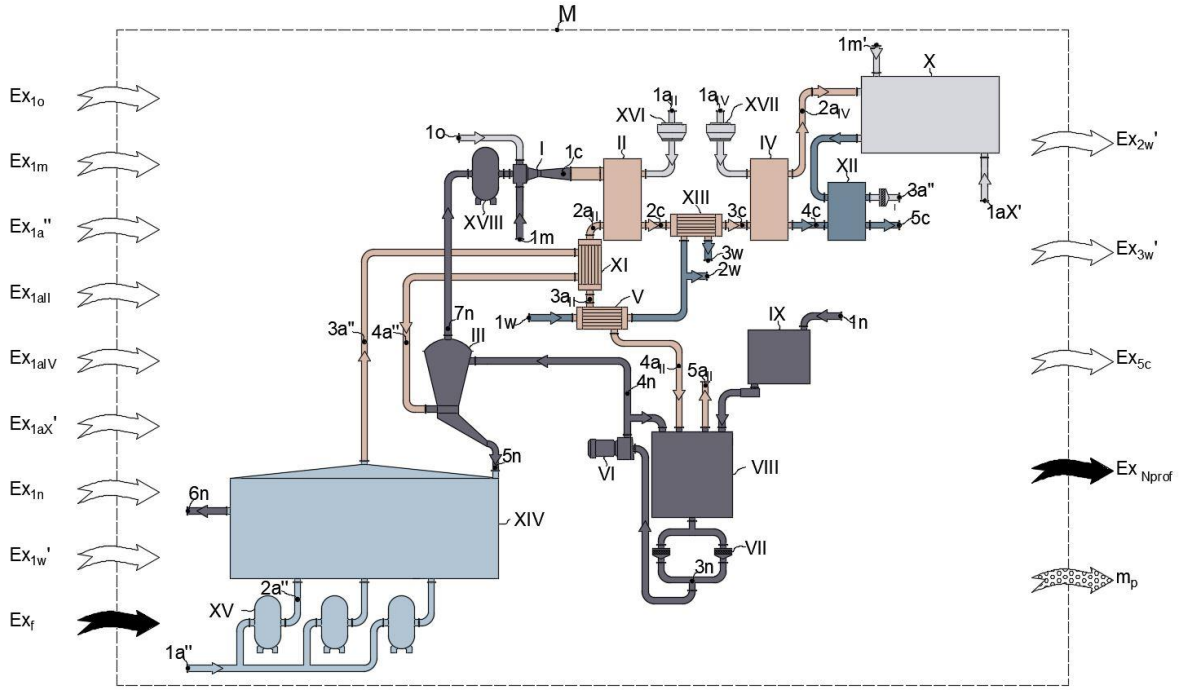


Figure 48 – Modified exergy contour in the technological scheme of porous ammonium nitrate granulation. I—ejector; II—HMX 1; III—granulator; IV—HMX 2; V—heat exchanger 1; VI—pump; VII—filter; VIII—tank; IX—bunker; X—Brayton's sub-atmospheric inverse cycle with HAR; XI—heat exchanger 2; XII—Reactor-Utilizer; XIII—heat exchanger 3; XIV—cooler; XV—gas blowers; XVI, XVII—fan; XVII—gas blower (compressor).

The exergy equation of a one-component substance flow is as follows:

$$\dot{E}x_j = \dot{m}_j \cdot ex_j = \dot{m}_j \cdot \left[h_j - h_0 - T_0 \cdot \left(s_j - s_0\right)\right] \quad (91)$$

Since humid air is one of the working substances in the system, we will observe it as a two-component substance (air and water vapor) for convenient calculation. Then, the equation of a two-component substance will be as follows:

$$\dot{E}x_{ha} = \dot{m}_j \cdot \left[ex_{j,da} + d_{j,ha} \cdot ex_{j,v}\right] = \quad (92)$$

$$= \dot{m}_j \cdot \begin{bmatrix} h_{j,da} - h_{0,da} - T_0 \cdot (s_{j,da} - s_{0,da}) + \\ + d_{j,ha} \cdot \left(h_{j,v} - h_{0,v} - T_0 \cdot (s_{j,v} - s_{0,v})\right) \end{bmatrix}$$

In the previous calculation model, humid air is considered a real mixture by Equation (92). The exergy equation can be rewritten for an ideal mixture as (93). The calculations of humidity ratio of water vapor in humid air are a prerequisite, omitting which one can get a false result:

$$\dot{E}x_{ha,j} = \dot{m}_j \cdot \begin{bmatrix} T_0 \cdot (c_{p,da} + d_j \cdot c_{p,v}) \left(\frac{T_{ha,j}}{T_0} - 1 - \ln \frac{T_{ha,j}}{T_0}\right) + \\ + R_v \left( (0.622 + d_j) \cdot \ln \frac{p_j (0.622 + d_0)}{p_0 (0.622 + d_j)} + d_j \cdot \ln \frac{d_{js}}{d_0} \right) \end{bmatrix} \quad (93)$$

We will use Equation (91) by introducing some transformations to calculate the exergy of a solid:

$$\dot{E}x_j = \dot{m}_j \cdot ex_j = \dot{m}_j \cdot c_p \left[ (T_j - T_0) - T_0 \cdot ln \left( \frac{T_j}{T_0} \right) \right] \quad (94)$$

One can use the approximate equation [58] to calculate the exergy of the fuel supplied to the system:

$$\dot{E}x_{Q_f} = m_f \cdot K \cdot HHV, \quad (95)$$

where $K = 0.95$—coefficient for gaseous fuels with more than one carbon atom in their molecules. This equation is used with coefficient $K = 0.975$ for liquid fuel.

It is permissible to use the approximate Equation (95) from the point of view of obtaining a quantitatively correct result since under the conditions, usual exergy losses

during combustion are so significant that the error related to the approximate methods turns out to be quite acceptable.

This section deals with assessing the effectiveness of both systems using the exergy analysis of mixed exergy indicators. This analysis allows us to amount all the production costs to a single dimension - "exergy". The exergy efficiency is one of the target functions for exergy analysis of energy systems designed to produce heat, cold or work (96). The target function for technological systems designed to create a material product is the ratio of the material product performance to the exergy expenditure for its production (97). The task is to minimize the value of $\sum \dot{E}x_{in}$ or to obtain an additional useful effect/product:

$$\eta_{ex} = \frac{\dot{E}x_{out}}{\dot{E}x_{in}} = \frac{\dot{E}x_{in} - \dot{E}x_{out}}{\dot{E}x_{in}} = 1 - \frac{\sum_{i=1}^{n}\left(\dot{E}x_{loss} + \dot{E}x_{des}\right)_i}{\dot{E}x_{in}} \quad (96)$$

Environmental parameters, which form the starting point for the substance flow exergy are pressure $p_0 = 101{,}325$ P$a$, temperature $T_0 = 293$ K.

The first stage of the analysis is to derive an equation of all flows brought to the system—costs, Equation (97):

$$e_m = \frac{\dot{m_p} + \dot{m_{NOx}}}{\sum \dot{E}x_{in} - \dot{E}x_{prof}} \quad (97)$$

Since the basic scheme does not provide for NOx recycling and does not generate electricity, thus Equation (98) for the basic scheme is:

$$e_m = \frac{\dot{m_p}}{\sum \dot{E}x_{in}{}^{b}} \quad (98)$$

Table 4 summarizes the exergy values included in Equation (99), Figure 49 shows the incoming exergy stream and outgoing one via Sankey diagram:

$$\sum \dot{E}x_{in}{}^{b} = \dot{E}x_{1n} + \dot{E}x_{1n'} + \dot{E}x_{1a} + \dot{E}x_{1a'} + \dot{E}x_{1a''} + \dot{E}x_{1w} + \dot{E}x_{Q\,II} + \\ + \dot{E}x_{Q\,VIII} + \dot{E}x_{N\,I} + \dot{E}x_{N\,V} + \dot{E}x_{N\,VI} + \dot{E}x_{N\,X} + \dot{E}x_{N\,XII} + \sum \dot{E}x_{N\,XV} \quad (99)$$

Table 4 – The values of exergy crossing the contour of the basic scheme

| Index | Mass Flow Rate $\dot{m}_j, \frac{kg}{h}$ | Temperature, $T_j, K$ | Pressure, $p_j, Pa$ | Humidity Ratio, $d, \frac{kg_w}{kg_{da}}$ | The Value of the Total Exergy, $E_j, kW$ |
|---|---|---|---|---|---|
| $\dot{E}x_{1n}$ | 1608 | 293 | 101,325 | - | 0 |
| $\dot{E}x_{1n'}$ | 835 | 293 | 101,325 | - | 0 |
| $\dot{E}x_{1a}$ | 15,000 | 293 | 101,325 | 0.00877 | 0 |
| $\dot{E}x_{1a'}$ | 453.6 | 293 | 101,325 | 0.00877 | 0 |
| $\dot{E}x_{1a''}$ | 12,000 | 293 | 101,325 | 0.00877 | 0 |
| $\dot{E}x_{1w}$ | 557 | 293 | 101,325 | - | 0 |
| $\dot{E}x_{Q\,II}$ | - | - | - | - | 120 |
| $\dot{E}x_{Q\,VIII}$ | - | - | - | - | 32 |
| $\dot{E}x_{N\,I}$ | - | - | - | - | 75 |
| $\dot{E}x_{N\,V}$ | - | - | - | - | 2.5 |
| $\dot{E}x_{N\,VI}$ | - | - | - | - | 3 |
| $\dot{E}x_{N\,X}$ | - | - | - | - | 3 |
| $\dot{E}x_{N\,XII}$ | - | - | - | - | 40 |
| $\sum \dot{E}x_{N\,XV}$ | - | - | - | - | 120 |
| $\dot{E}x_{1n}$ | 1608 | 293 | 101,325 | - | 0 |
| $\sum \dot{E}x_{in}{}^{b}$ | | | | | 395.5 |

The following Equation (97) finds the specific exergy expenditure to produce a product in the base system:

$$e_m^b = \frac{\dot{m}_p}{\sum \dot{E}x_{in}{}^{b}} = \frac{2400}{395.5} = 6.07 \frac{(kg/h)}{kW}$$

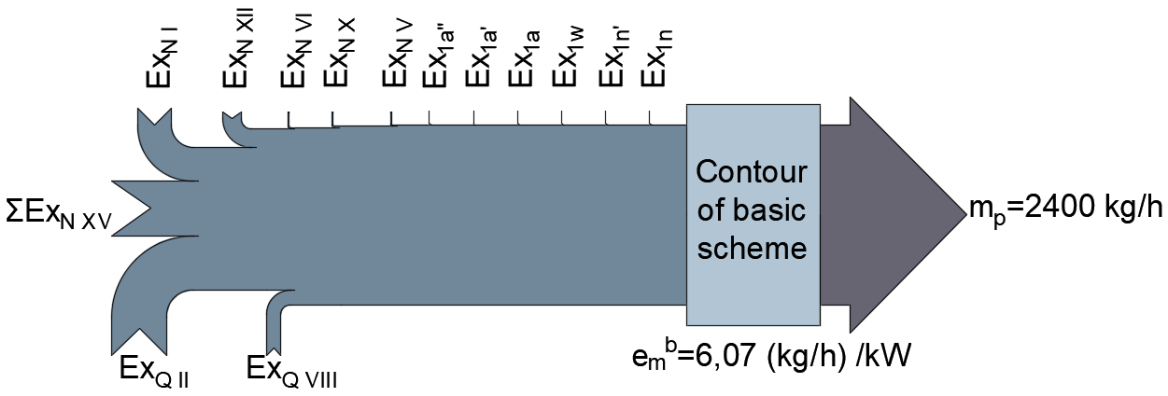


Figure 49 – Sankey diagram for basic scheme

The first stage of the analysis is to derive an equation of all flows brought to the system—costs, Equation (100). Due to the inclusion of Brayton's sub-atmospheric inverse cycle with Maisotsenko's humid air recuperator (HAR) in the production scheme, some electricity costs are compensated:

$$\sum \dot{E}x_{in}{}^{m} = \dot{E}x_{1o} + \dot{E}x_{1m} + \dot{E}x_{1a''} + \dot{E}x_{1aII} + \dot{E}x_{1aIV} + \\ + \dot{E}x_{1aX} + \dot{E}x_{1n} + \dot{E}x_{1w} + \dot{E}x_{N_{VI}} + \dot{E}x_{N_{XV}} + \dot{E}x_{N_{XVI}} + \dot{E}x_{N_{XVII}} + \dot{E}x_{N_{XVIII}} \quad (100)$$

Preliminary calculation of the parameters at the definite points of the modified scheme, thermal loads and electrical powers supplied or taken away in the elements of the scheme.

Thermal load on the device XI:

$$Q_{XI} = m_{2a\,II} \cdot (h_{2a\,II} - h_{3a\,II}) = \frac{18367}{3600} \cdot (188.5 - 120) = 350\ kW$$

Heat flux on the device V:

$$Q_V = m_{2a\,II} \cdot (h_{3a\,II} - h_{4a\,II}) = \frac{18367}{3600} \cdot (120 - 57) = 321\ kW$$

Water mass flow rate through device V:

$$m_{1w} = \frac{Q_V}{h_{2w} - h_{1w}} = \frac{321}{251.8 - 74.5} = 1.81 \frac{kg}{s}$$

The equation for the combustion reaction of natural gas with oxygen:

$$CH_4 + 2O_2 = CO_2 + 2H_2O$$

$$[1\ \text{mole}(\text{CH}_4) + 2\ \text{moles}(\text{O}_2) = 1\ \text{mole}(\text{CO}_2) + 2\ \text{moles}(\text{H}_2\text{O})]$$

$$[16\ \text{kg}(\text{CH}_4) + 64\ \text{kg}(\text{O}_2) = 44\ \text{kg}(\text{CO}_2) + 36\ \text{kg}(\text{H}_2\text{O})] \cdot \frac{8.4}{16}$$

$$8.4 + 33.6(\text{O}_2) = 23.1\text{kg}(\text{CO}_2) + 18.9(\text{H}_2\text{O})$$

33.6 kg of oxygen is required to burn 8.4 kg of natural gas. Heat flux on the device II:

$$Q_{II} = m_{1a\,II} \cdot (h_{2a\,II} - h_{1a\,II}) = \frac{18097}{3600} \cdot (188.5 - 42.4) = 734.4\ \text{kW}$$

The flow temperature “c” after device V:

$$t_{2c} = t_{1c} - \frac{Q_V}{m_{1c} \cdot \overline{c_{p\,c}}} =$$

$$= 600 - \frac{734.4}{\left(\frac{15000 + 270 + 42 + 8.4 + 33.6}{3600}\right) \cdot 1.195} = 428\ \ ^{o}C$$

Thermal load on the device XIII:

$$Q_{XIII} = m_w \cdot (h_{3w'} - h_{2w'}) = 1.81 \cdot (335.9 - 251.8) = 152.2\ kW$$

The flow temperature “c” after device XIII:

$$t_{3c} = t_{2c} - \frac{Q_{XIII}}{m_{1c} \cdot \overline{c_{p\,c}}} =$$

$$= 428 - \frac{152}{\left(\frac{15000 + 270 + 42 + 8.4 + 33.6}{3600}\right) \cdot 1.169} = 398 \ ^{o}C$$

Thermal load on the device IV:

$$Q_{IV} = m_{1c} \cdot \overline{c_{p\,c}} \cdot (t_{3c} - t_{4c}) =$$

$$= \frac{15000 + 270 + 42 + 8.4 + 33.6}{3600} \cdot 1.072 \cdot (398 - 20) = 1728 \text{ kW}$$

Humid air flow rate in the outlet of the device IV:

$$m_{2aIV} = \frac{Q_{IV}}{h_{2a\,IV} - h_{1a\,IV}} = \frac{1728}{1902.3 - 42.4} = 0.929 \frac{kg}{s} = 3344 \frac{kg}{h}$$

Air flow rate in the inlet of the device IV:

$$m_{1aIV} = \frac{m_{2aIV}}{1 + (d_{2aIV} - d_{1aIV})} =$$

$$= \frac{0.929}{1 + (0.5 - 0.00877)} = 0.623 \ \frac{kg}{s} = 2243 \frac{kg}{h}$$

Fans with electric motor power were selected for the obtained features of devices II and IV:

$$N_{II} = 7.6 \ kW \ N_{IV} = 0.2 \ kW$$

A preliminary calculation of the Brayton's sub-atmospheric inverse cycle with HAR [49] is carried out to determine the generated useful power. Its scheme and the cycle in h-s coordinates is shown in Figures 50 and 51, respectively.

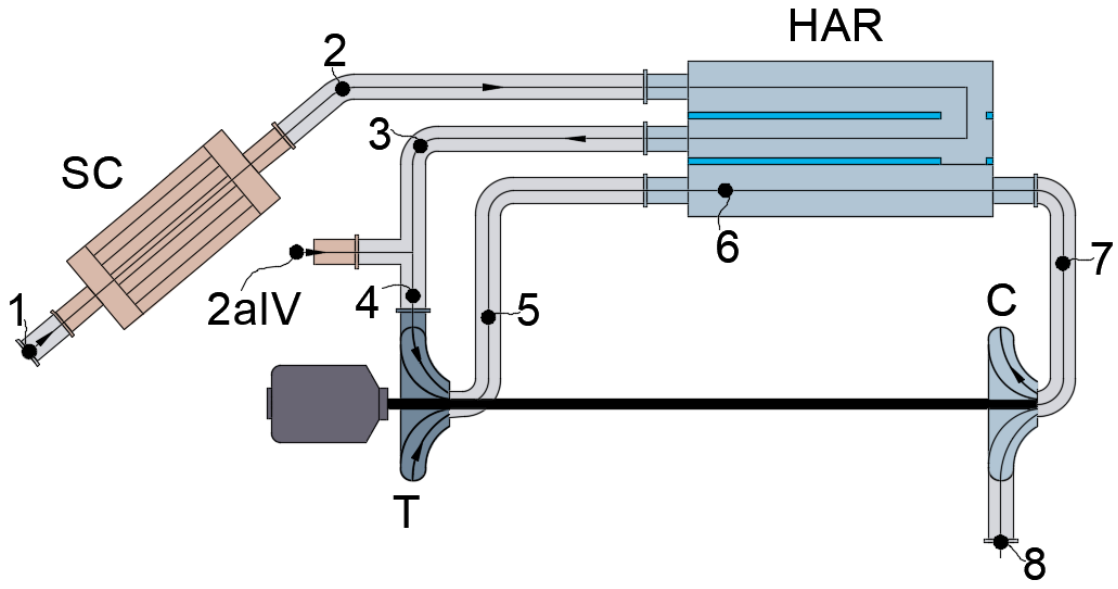


Figure 50 – Brayton's sub-atmospheric inverse cycle with HAR. SC—solar collector; HAR—humidified air recuperator; T—turbine; C—compressor.

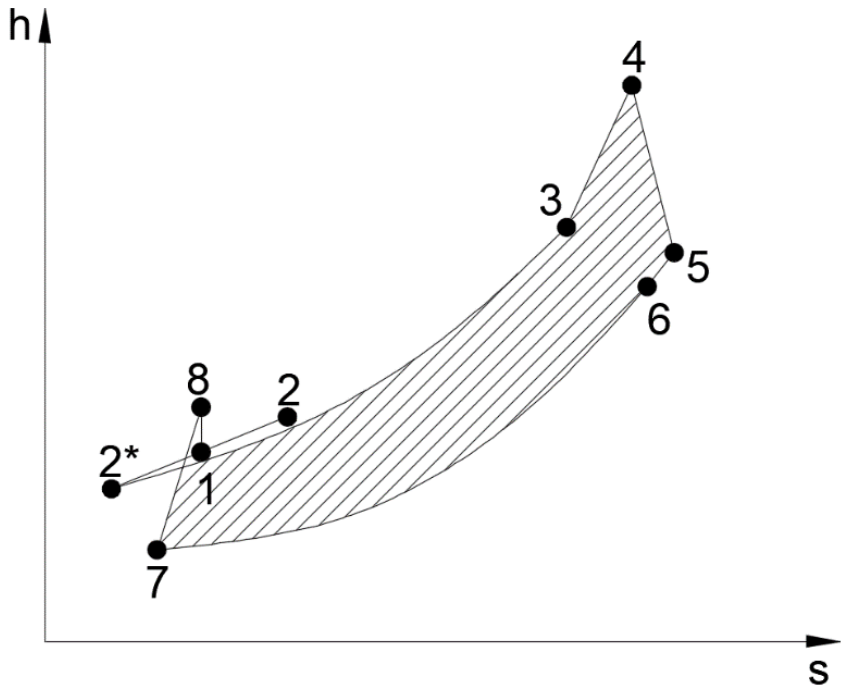


Figure 50 – Cycle of the unit in h-s coordinates.

Specific heat flow in the solar collector:

$$q_{SC} = h_2 - h_1 = 104.0 - 42.4 = 61.6\frac{kJ}{kg}$$

Specific heat flow on M device:

$$q_{HMX} = (h_3 - h_{2*}) - (h_2 - h_{2*}) =$$
$$= \big(1402.7 - 34.2(26)\big) - \big(104.0 - 34.2(25.6)\big) =$$
$$= 104.0 - 42.4 = 1299\frac{kJ}{kg}$$

Mass flow rate of air supplied to the cycle:

$$m_1 = \frac{m_{2aIV} \cdot (h_{2a\,IV} - h_4)}{h_4 - h_3} = \frac{0.929 \cdot (1902.3 - 1771.4)}{1771.4 - 1402.7} = 0.33\frac{kg}{s}$$

Mass air flow resulting from the mixing process:

$$m_4 = m_1 + m_{2aIV} = 0.929 + 0.33 = 1.259\frac{kg}{s}$$

Air parameters at the outlet of the turbine (T) are defined in the following way: adiabatic extension temperature is found $t_{5s}(s_4 = s_5)$. Then, considering the adiabatic efficiency of the turbine ($\eta_{t\,is} = 0.88$), temperature is calculated $t_5 = t_4 - (t_4 - t_{5s}) \cdot \eta_{t\,is}$:

$$t_5 = 77\ ^{o}C;\ p_5 = 14475\ Pa; d_5 = 0.5\frac{kg_w}{kg_{da}}$$

Specific work of the turbine:

$$l_t = h_4 - h_5 = 1771.4 - 1400 = 371.4\ \frac{kJ}{kg}$$

The parameters of the air at the outlet of the HMX are determined as follows: according to the recommended humidity ratio at the outlet of the product channels [49] $d_8$ the saturated humid air temperature is calculated.

$$t_8 = -35\ ^oC;\ p_8 = 14475\ Pa;\ d_8 = 0.001\frac{kg_w}{kg_{da}};\ h_8 = -32.7\ \frac{kJ}{kg}$$

The parameters of the air at the outlet of the compressor are determined as follows: air is compressed from $p_8$ to $p_9$with the temperature $t_9$ reached by removing heat during the compression by the cooling agent.

$$t_9 = 35\ ^oC;\ p_5 = 101325\ Pa;\ d_9 = 0.001\frac{kg_w}{kg_{da}};\ h_9 = 37.8\ \frac{kJ}{kg}$$

Compressor power:

$$N_c = m_4 \cdot \big(1 - (d_5 - d_8)\big) \cdot l_c =$$
$$= 1.259 \cdot \big(1 - (0.5 - 0.001)\big) \cdot (37.8 + 32.7) = 44.5\ kW$$

Net electrical power output produced in a cycle is:

$$N_{prof} = (N_t - N_c) \cdot \eta_g = (468 - 44.5) \cdot 0.98 = 415\ kW$$

Table 5 comprises exergy values, included in (100). Figure 50 demonstrates the supplied exergy flows and production supplied flow via Sankey diagram.

Table 5

| Index | Mass Flow Rate $\dot{m}_j, \frac{kg}{h}$ | Temperature, $T_j, K$ | Pressure, $p_j, Pa$ | Humidity Ratio, $d, \frac{kg_w}{kg_{da}}$ | The Value of the Total Exergy, $E_j, k$ |
|---|---|---|---|---|---|
| $\dot{E}x_{1o}$ | 33.6 | 293 | 101,325 | - | 0 |
| $\dot{E}x_{1m}$ | 8.4 | 293 | 101,325 | - | 110.8 |
| $\dot{E}x_{1a''}$ | 12,000 | 293 | 101,325 | 0.00877 | 0 |
| $\dot{E}x_{1aII}$ | 18,097 | 293 | 101,325 | 0.00877 | 0 |
| $\dot{E}x_{1aIV}$ | 2243 | 293 | 101,325 | 0.00877 | 0 |
| $\dot{E}x_{1aX}$ | 1188 | 293 | 101,325 | 0.00877 | 0 |
| $\dot{E}x_{1n}$ | 2442 | 293 | - | - | 0 |
| $\dot{E}x_{1w'}$ | 6516 | 291 | 101,325 | - | 0 |
| $\dot{E}x_{N_{VI}}$ | - | - | - | - | 3 |
| $\dot{E}x_{N_{XV}}$ | - | - | - | - | 120 |
| $\dot{E}x_{N_{XVI}}$ | - | - | - | - | 7.6 |
| $\dot{E}x_{N_{XVII}}$ | - | - | - | - | 0.2 |
| $\dot{E}x_{N_{XVIII}}$ | - | - | - | - | 385 |
| $\sum \dot{E}x_{in}^{m}$ | | | | - | 626.5 |
| $\dot{E}x_{prof}$ | | | | | 415.0 |

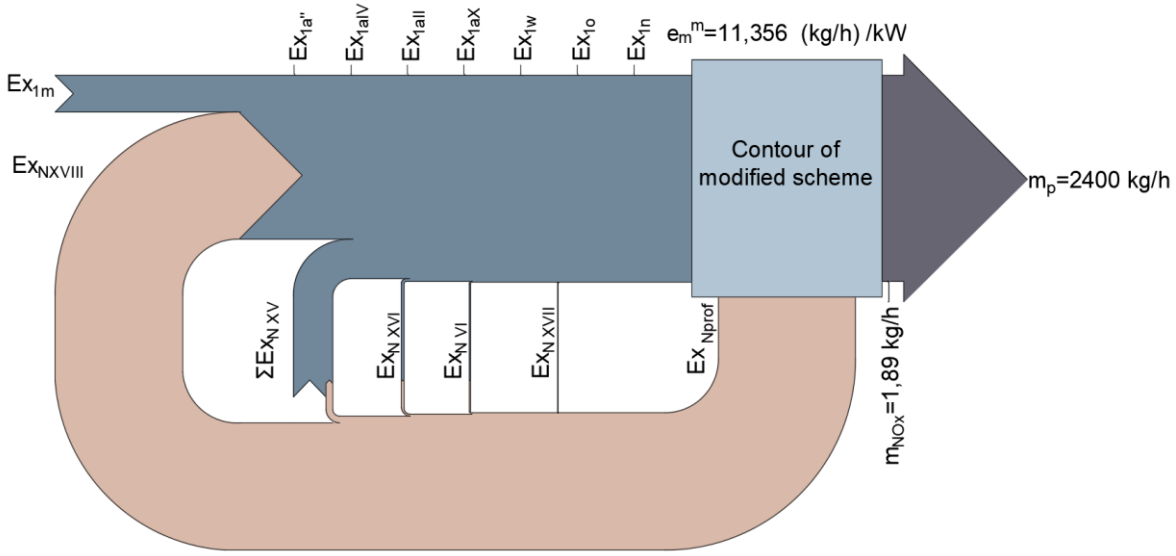


Figure 51 – Sankey diagram for the modified scheme.

The specific exergy expenditure to produce a product in a modified system is found by the equation:

$$e_m^m = \frac{\dot{m}_p + m_{NOx}}{\sum \dot{E}x_{in} - \dot{E}x_{prof}}$$

$$= \frac{\dot{m}_p + m_{NOx}}{\dot{E}x_{1m} + N_{VI} + N_{XV} + N_{XVI} + N_{XVII} + N_{XVIII} - N_{prof}} =$$

$$= \frac{2400 + 1.89}{110.7 + 3 + 120 + 7.6 + 0.2 + 385 - 415} = 11.356 \frac{kg/h}{kW}$$

The obtained results assume that it is reasonable to consider in more detail the elements in the modified scheme, their mutual influence, and dependence on the operating mode of the granulator. It is rational to analyze the exergy efficiency of the basic and modified schemes in dynamics, namely, at different operating modes of the granulator and/or other types of granulators. It is due to the fact that changes in the granulator's operating modes (its performance) entail a chain of significant changes in the operating modes of the related components in the scheme: if the granulator performance is changed (for example, reduced) → there is lower consumption of the recovered stream "d" → lower consumed amount of natural gas for recycling of lower oxides in the ejector module "I" → lower heat flow removed in heat and mass transfer (II, IV) device and recuperators (V, XI, XIII).

A problem with the calculation of heat and mass exchangers and the heat recovery reactor causes difficulty in identifying the composition of the flow "c" after the ejector module. Thus, with a significant decrease in the temperature of the flow "c" caused by stepwise heat removal, it is difficult to determine the nature of the heat and mass transfer processes occurring in device IV since condensation and chemical interaction between the components of the flow "c" are possible. Hence, the following problem arises with determining the composition, state parameters and the ongoing physical and chemical processes in the waste heat reactor (XII).

As a result of the exergy analysis of the basic and modified granulation schemes for porous ammonium nitrate, the following indicators of their specific efficiency are obtained:

$$e_m^b = 6.07 \frac{(kg/h)}{kW}, e_m^m = 11.356 \frac{(kg/h)}{kW}.$$

Thus, the use of an ejector recycling module (as a way to recycle substandard ammonium nitrate and nitrogen oxide of the formula NxO), a sub-atmospheric cycle inverse (as a way to recycle excess heat and generate energy) and two heat and mass exchangers according to the Maisotsenko cycle (as a way to humidify ammonium nitrate in a highly humid air flow and organizing a more efficient heat recovery process) increase the efficiency of the basic scheme by:

$$\frac{e_m^m - e_m^b}{e_m^b} \cdot 100\% = \frac{11.356 - 6.070}{6.070} \cdot 100\% = 87\%$$

A porous ammonium nitrate granulation workshop often is located within a nitrogen fertilizer plant. Therefore, it is worth noting that the basic scheme should be modified in terms of the amount and cost of resources available at the enterprise and the present mass and energy flows from adjacent industries/workshops. The task of further research is theoretical modeling and experimental operation of the HMX (IV) and the waste heat reactor (XII), concerning the effect of the incoming flows on operation modes of these devices.

Within this work, the authors proposed a modified scheme of the installation for porous ammonium nitrate granulation. They showed the potential for the energy efficiency of the new system compared to the basic one (used in practice) through the exergy analysis. The study of heat and mass exchange processes, chemical transformations, and changes in the phase composition of flows in these devices is of particular interest. One of the directions for further research is to improve the method for obtaining porous ammonium nitrate, particularly the organization of the optimal technological and constructive solution for the humidification and drying stages.

The main innovative solutions in the modified scheme are vortex granulator with the new organization of flows' interactive, an ejector module for the utilization of substandard flow; the use of heat and mass exchangers of indirect regenerative evaporative cooling as recuperative, cooling and humidifying equipment; a power

generation and heat recovery module based on a sub-atmospheric inverse Brayton cycle. The calculations showed a significant energy efficiency of the proposed solutions.

Further directions of study are:

- optimization of flow arrangement in the vortex granulator as a core device in the scheme to provide additional utilization of fine fraction of ammonium nitrate;
- consideration of various combinations of operating modes in the same workspace of the device to meet the drying agent's optimal heat potential;
- detailed calculations of the proposed scheme and its further study are required, considering the design features, materials and processes inside the equipment;
- experimental investigation of devices for indirect regenerative evaporative cooling;
- detailed analysis of the proposed sub-atmospheric inverse Brayton cycle and other cycles as a core for power generation and heat recovery module.

After the detailed study of the mentioned components in the new scheme, it seems rational to conduct its optimization concerning economic indicators.

# CONCLUSIONS

*This section is prepared in according to data [1-3, 14-17].*

- a mathematical model was derived to calculate hydrodynamic properties of the melt jet expiration process from a perforated shell;

- influences of the hole diameter and melt properties on the radial velocity field were determined and shown;

- optimal conditions for prilling in a rotating vibration granulator for a given capacity of 37 t/h are defined: the rotation velocity of the basket (60 rpm), the diameter of holes in the perforated shell (1.2 mm), the melt temperature (185 $^{o}$C), the frequency range of the actuator's oscillation (340-400 Hz);

- the experimental studies and mathematical modeling provided possibilities for construction of a modernized rotating vibration granulator;

- industrial tests of the modernized vibrating granulator confirmed optimal conditions of the prilling resulting in the improved product.

- the proposed electric intellectual system has been tested and ways of its further improvement have been outlined. Implementation of the improving electronic intellectual cleaning system of holes allowed reducing the error in the high-frequency oscillations on the perforated shell of the priller from 0,43 to 0,27, i.e. 1,6 times;

- various hydrodynamic regimes to weigh particles of a material by a gas flow, depending on the constructive parameters of shelf contacts was showed;

- the effectiveness of the shelf device to carry out the drying and dedusting processes of granular and powder materials simultaneously was experimentally proved;

- the nanoporous structure quality of the PAN granules largely depends on the thermodynamic operation mode of the vortex granulator. Rational selection of the drying agent's flow twisting degree and the twisting stabilization method lets us achieve an extended network of nanopores on the surface in the granules, which provide access to the internal pores (where the diesel distillate will be retained). During the creation of an optimization calculation algorithm, the change in the nanoporous structure of the ammonium nitrate granule in the

specified temperature ranges and the intensity of the fluidizing agent motion was taken into account. An optimal thermodynamic range (main modes) of the vortex granulator work which enables to obtain $NH_4NO_3$ granules with branchy net of pores with required size on the surface of the sample and inside it is proposed$

- nanoporous structure of organic fertilizer granules is described and the presence of micropores with a size of 0.2–10 nm and mesopores with a size of 50–100 nm in the solid skeleton of the granules are grounded. Influence of granule solid skeleton porosity on the process of its thermal conductivity during heating of the granule in a gas medium is shown. One proposed formulas for determining the effective coefficient of thermal conductivity depending on the porosity of the granule and true thermal conductivity coefficients of the solid skeleton and gas in the hollow sections of the granule. Decrease of heat conductivity with increasing of granule porosity is shown. Analytical expressions for determining of the temperature profile and granule heating time, taking into account its porosity are obtained. It is explained that high granule porosity cause increase of the heating time and decrease of the granule temperature$

- in order to obtain PAN granules with a developed porous structure, it is necessary to use the optimal humidification mode, technological parameters of which are demonstrated in this research. If this mode is not kept, the humidification and heat treatment stages will be ineffective (the uneven humidification mode), or the commodity qualities of the finished product will be deteriorated (high humidification mode);

- the authors proposed a modified scheme of the installation for porous ammonium nitrate granulation. They showed the potential for the energy efficiency of the new system compared to the basic one (used in practice) through the exergy analysis. The study of heat and mass exchange processes, chemical transformations, and changes in the phase composition of flows in these devices is of particular interest. One of the directions for further research is to improve the method for obtaining porous ammonium nitrate, particularly the organization of the optimal technological and constructive solution for the humidification and drying stages;

- the main innovative solutions in the modified scheme are vortex granulator with the new organization of flows' interactive, an ejector module for the utilization of substandard flow; the use of heat and mass exchangers of indirect regenerative evaporative cooling as recuperative, cooling and humidifying equipment; a power generation and heat recovery module based on a sub-atmospheric inverse Brayton cycle. The calculations showed a significant energy efficiency of the proposed solutions.

## REFERENCES (2019)

1. Sklabinskyi V.I., Artyukhov A.E., Kononenko N.P., Krmela J. Decay of melt stream of during dispersion in granulation devices / Hemijska industrija. – 2019. - 73(4). – pp. 239-248.

2. Kreber [E-text type]. Location of document: https://www.kreber.nl/markets/prilling-nitrates date of access 22.12.2019.

3. Research Institute at the Chemical plant [E-text type]. Location of document: https://www.niichimmash.ru/ date of access 22.12.2019.

4. Sklabinskiy V., Skydanenko M., Kononenko M., Artyukhov A. Improving of the Electronic Intellectual Cleaning System of Holes in Perforated Shells of the Priller / Proceedings of the International Conference on Modern Electrical and Energy Systems, MEES 2019. – 2019. - pp. 70-73.

5. Artyukhov A., Sklabinskiy V., Ivaniia A. Electrical intelligent system for controlling the formation of monodisperse droplets in granulation devices based on magnetostrictive actuator / Proceedings of the International Conference on Modern Electrical and Energy Systems, MEES 2017, – 2017. - pp. 280-283.

6. Artyukhov A., Artyukhova N., Krmela J. Computer Simulation of the Aerodisperse Systems Hydrodynamics in Granulation and Drying Apparatus In: Process Analysis / Design and Intensification in Microfluidics and Chemical Engineering. – IGI Global, USA. – 2019. – pp. 277-321.

7. Obodiak V., Artyukhova N., Artyukhov A. Calculation of the residence time of dispersed phase in sectioned devices: Theoretical basics and software implementation / Lecture Notes in Mechanical Engineering. – 2020. - pp. 813-820.

8. Artyukhov A.E., Krmela J., Gavrylenko O.M. Evaluation of the Impact Made by the Hydrodynamic Regime of the Granulation Equipment Operation on the Nanoporous Structure of $N_4HNO_3$ Granules / J. Nano- Electron. Phys. – 2019. – 11 No 3, 03033-1-03033-4.

9. Рішення про реєстрацію договору, який стосується права автора на твір № 4357 Україна. Комп'ютерна програма «Granulation Unit»/ А.Є. Артюхов, Я. Крмела, В.К, Ободяк, А.О. Горішняк. – опубл. 20.05.2019.

10. Ivaniia A.V., Artyukhov A.Y., Olkhovyk A.I. Hydrodynamic and thermodynamic conditions for obtaining a nanoporous structure of ammonium nitrate granules in vortex granulators / Springer Proceedings in Physics. – 2019. – 221. – pp. 257-268.

11. Artyukhov A.E., Artyukhova N.O. Technology and the main technological equipment of the process to obtain $N_4HNO_3$ with Nanoporous Structure / Springer Proceedings in Physics. – 2019. – 221. – pp. 585-594.

12. Artyukhov A., Artyukhova N., Ostroha R., Yukhymenko M. Bocko J., Krmela J. Convective drying in the multistage shelf dryers: theoretical bases and practical implementation / Drying Unit Operations. – IntechOpen, UK, 2019. – pp. 140-163.

13. Artyukhova N.O., Krmela J. Nanoporous structure of the ammonium nitrate granules at the final drying: The effect of the dryer operation mode / Journal of Nano- and Electronic Physics. – 2019. – 11(4). – 04006-1-04006-4.

14. Artyukhov A.E., Lytvynenko A.V., Krmela J., Krmelova V. Thermodynamic Calculation of Vortex Granulator Operation for Producing of Ammonium Nitrate with Nanoporous Structure / Nanomaterials and Nanocomposites, Nanostructure Surfaces, and Their Applications. Springer Proceedings in Physics, vol. 246, p. 203-217 (2021)

15. Yukhymenko M., Ostroha R., Artyukhov A., Bocko J. Effect of Temperature on Formation of Nanoporous Structure of Granule Shell in Technology of Obtaining Organo-mineral Fertilizers / Nanooptics and Photonics, Nanochemistry and Nanobiotechnology, and Their Applications. Springer Proceedings in Physics, vol. 247, p. 159-169(2020).

16. Ivaniia A.V., Artyukhov A.E., Olkhovyk A.I., Potapov D.R. The Effect of the Intensity of Ammonium Nitrate Granules Humidification on the Quantitative and Qualitative Composition of the Final Granules Nanoporous Structure / Nanomaterials and Nanocomposites, Nanostructure Surfaces, and Their Applications. Springer Proceedings in Physics, vol. 246, p. 397-407 (2021).

17. Levchenko, D., Manzharov, A., Artyukhov, A., Artyukhova, N., Krmela, J. Comparative exergy analysis of units for the porous ammonium nitrate granulation / Energies, 2021, 14(2), 280.

18. Carole, T.; Scheihing, P.; Sousa, L. Energy Efficiency and Use in the Chemical Industry. ACEEE Proc. 2001, 267–275.

19. Fawkes, S.; Oung, K.; Thorpe, D. Best Practices and Case Studies for Industrial Energy Efficiency Improvement. In An Introduction for Policy Makers; UNEP DTU Partnership: Copenhagen, Denmark, 2016; p. 173.

20. Patt, J.J.; Banholzer, W.F. Improving Energy Efficiency in the Chemical Industry. Bridg. Energy Effic. 2009, 39, 15–21.

21. Duroudier, J.-P. Heat Transfer in the Chemical, Food and Pharmaceutical Industries; Elsevier: Amsterdam, The Netherlands, 2017; ISBN 978-1-78548-188-8.

22. Hipple, J. Chemical Engineering for Non-Chemical Engineers; Elsevier: Amsterdam, The Netherlands, 2017; ISBN 978-1-119-30965-9.

23. Kapustenko, P.O.; Kukulka, D.J.; Arsenyeva, O.P. Intensification of heat transfer processes. Chem. Eng. Trans. 2015, 45, 1729–1734, doi:10.3303/CET1545289.

24. Beller, M.; Böhland, T.; Demtröder, D.; Ebenhoech, J.; Ernst, S.; Ewers, J.; Haber, S.; Hoer, R.; Hirth, T.; Jahn, D.; et al. Change in the Raw Materials Base; GDCh: Frankfurt, Germany, 2010.

25. Ali, M.F.; Ali, B.M.; Speight, J.G. Handbook of Industrial Chemistry: Organic Chemicals; McGraw-Hill Education: New York, NY, USA, 2005; ISBN 9780071410373.

26. Stahl, H.; Van Vaerenbergh, G. Single-Pot Processing. In Handbook of Pharmaceutical Granulation Technology, 2rd ed.; 2005; pp. 311–332 ISBN 9780849354953.

27. Litster, J.; Ennis, B. The Science and Engineering of Granulation Processes; 31 March 2004; Springer: Berlin/Heidelberg, Germany, 2004; ISBN ISBN 978-94-017-0546-2.

28. Stahl, H. Comparing Granulation Methods; GEA Pharma Systems: Hürth, Germany, 2010.

29. Muralidhar, P.; Bhargav, E.; Sowmya, C. Novel Techniques of Granulation: A Review. Int. Res. J. Pharm. 2016, 7, 8–13, doi:10.7897/2230-8407.0710114.

30. Stahl, H. Comparing Different Granulation Techniques. In Pharmaceutical Technology; PharmTech: Muellheim, Germany, 2004; pp. 22–33.

31. Sahoo, C.K.; Rao, S.R.M.; Sudhakar, M.; Bhaskar, J. Advances in granulation technology. Res. J. Pharm. Technol. 2016, 9, 571–580, doi:10.5958/0974-360X.2016.00108.6.

32. Athar, M. A technical note on granulation technology: A way to optimise granules. Int. J. Pharm. Sci. Rev. Res. 2013, 4, 55–67.

33. Artyukhov, A.Y.; Sklabinskiy, V.I. Experimental and industrial implementation of porous ammonium nitrate producing process in vortex granulators. Nauk. Visnyk Natsionalnoho Hirnychoho Universytetu 2013, 6, 42–48.

34. Cardarelli, F. Fuels, Propellants, and Explosives. In Materials Handbook; Springer International Publishing: Cham, Switzerland, 2018; pp. 1465–1496 ISBN 3527302107.

35. Janssen, T.J. Explosive Materials: Classification, Composition and Properties; Nova Science Publishers: New York, NY, USA, 2011; ISBN 1617611883.

36. Artyukhov, A.E.; Sklabinskiy, V.I. Investigation of the Temperature Field of Coolant in the Installations for Obtaining 3D Nanostructured Porous Surface Layer on the Granules of Ammonium Nitrate. J. Nano-Electron. Phys. 2017, 9, 01015, doi:10.21272/jnep.9(1).01015.

37. Artyukhova, N.O. Morphological Features of the Nanoporous Structure in the Ammonium Nitrate Granules at the Final Drying Stage in Multistage Devices. J. Nano-Electron. Phys. 2020, 12, 04036, doi:10.21272/jnep.12(4).04036.

38. Artyukhov, A., Obodiak, V., Boiko, P., Rossi, P. Computer modeling of hydrodynamic and heat-mass transfer processes in the vortex type granulation devices. In CEUR Workshop Proceedings; ICTERI: Kyiv, Ukraine, 2017; pp. 33–47.

39. Artyukhov, A.E., Ivaniia, A.V. Obtaining porous ammonium nitrate in multistage and multifunctional vortex granulators. Nauk. Visnyk Natsionalnoho Hirnychoho Universytetu 2017, 7, 68–75.

40. Levchenko, D.; Yurko, I.; Artyukhov, A.; Baga, V. Maisotsenko cycle applications for multistage compressors cooling. IOP Conf. Ser. Mater. Sci. Eng. 2017, 233, 012023, doi:10.1088/1757-899X/233/1/012023.

41. Levchenko, D.; Pavlenko, I.; Shulumei, A.; Ochowiak, M.; Manzharov, A. Parameter Identification of the Capillary Rising Process in Nanomaterials for Evaporative Cooling Applications. In Design, Simulation, Manufacturing: The Innovation Exchange; Springer, Cham, Switzerland, 2020; pp. 201–215.

42. Choi, C.-H.; Krishnan, S.; TeGrotenhuis, W.; Chang, C.-H. Capillary Rise of Nanostructured Microwicks. Micromachines 2018, 9, 153, doi:10.3390/mi9040153.

43. Levchenko, D.O.; Artyukhov, A.E.; Yurko, I.V. Maisotsenko cycle applications in multi-stage ejector recycling module for chemical production. IOP Conf. Ser. Mater. Sci. Eng. 2017, 233, 012024, doi:10.1088/1757-899X/233/1/012024.

44. Buyadgie, D.; Buyadgie, O.; Drakhnia, O.; Brodetsky, P.; Maisotsenko, V. Solar low-pressure turbo-ejector Maisotsenko cycle-based power system for electricity, heating, cooling and distillation. Int. J. Low-Carbon Technol. 2015, 10, 157–164, doi:10.1093/ijlct/ctv012.

45. Khalatov, A.A.; Severin, S.D.; Brodetsky, P.I.; Maisotsenko, V.S. Brayton's subatmospheric inverse cycle with regeneration of output heat by Maisotsenko's cicle. Rep. Natl. Acad. Sci. Ukr. 2015, 72–79, doi:10.15407/dopovidi2015.01.072.

46. Mahmood, M.H.; Sultan, M.; Miyazaki, T.; Koyama, S.; Maisotsenko, V.S. Overview of the Maisotsenko cycle—A way towards dew point evaporative cooling. Renew. Sustain. Energy Rev. 2016, 66, 537–555, doi:10.1016/j.rser.2016.08.022.

47. Kozlov, A.; Chudnovsky, Y. Combined Cooling, Heating And Power System. U.S. patent 16/297928, 12 September 2019.

48. Piacentino, A. Thermal analysis and new insights to support decision making in retrofit and relaxation of heat exchanger networks. Appl. Therm. Eng. 2011, 31, 3479–3499, doi:10.1016/j.applthermaleng.2011.07.002.

49. Asante, N.D.K.; Zhu, X.X. An Automated and Interactive Approach for Heat Exchanger Network Retrofit. Chem. Eng. Res. Des. 1997, 75, 349–360, doi:10.1205/026387697523660.

50. Safder, U.; Ifaei, P.; Yoo, C. A novel approach for optimal energy recovery using pressure retarded osmosis technology: Chemical exergy pinch analysis—Case study in a sugar mill plant. Energy Convers. Manag. 2020, 213, 112810, doi:10.1016/j.enconman.2020.112810.

51. Bejan, A. Method of entropy generation minimization, or modeling and optimization based on combined heat transfer and thermodynamics. Rev. Générale Therm. 1996, 35, 637–646, doi:10.1016/S0035-3159(96)80059-6.

52. Korpyś, M.; Gancarczyk, A.; Iwaniszyn, M.; Sindera, K.; Jodłowski, P.J.; Kołodziej, A. Analysis of entropy production in structured chemical reactors: Optimization for catalytic combustion of air pollutants. Entropy 2020, 22, 1017, doi:10.3390/e22091017.

53. Besagni, G. Ejectors on the cutting edge: The past, the present and the perspective. Energy 2019, 170, 998–1003, doi:10.1016/j.energy.2018.12.214.

54. Бродянский, В.; Фратшер, В.; Михалек, К. Эксергетический метод и его приложения; Энергоатом.; Москва, Россия, 1988; ISBN 5-283-00152-0.

55. Morosuk, T.; Tsatsaronis, G. Advanced exergy-based methods used to understand and improve energy-conversion systems. Energy 2019, 169, 238–246, doi:10.1016/j.energy.2018.11.123.

56. Sayadi, S.; Tsatsaronis, G.; Morosuk, T.; Baranski, M.; Sangi, R.; Müller, D. Exergy-based control strategies for the efficient operation of building energy systems. J. Clean. Prod. 2019, 241, 118277, doi:10.1016/j.jclepro.2019.118277.

57. Athari, H.; Soltani, S.; Rosen, M.A.; Gavifekr, M.K.; Morosuk, T. Exergoeconomic study of gas turbine steam injection and combined power cycles using fog inlet cooling and biomass fuel. Renew. Energy 2016, 96, 715–726, doi:10.1016/j.renene.2016.05.010.

58. Fazelpour, F.; Morosuk, T. Exergoeconomic analysis of carbon dioxide transcritical refrigeration machines. Int. J. Refrig. 2014, 38, 128–139, doi:10.1016/j.ijrefrig.2013.09.016.

59. Jannatkhah, J.; Najafi, B.; Ghaebi, H. Energy and exergy analysis of combined ORC – ERC system for biodiesel-fed diesel engine waste heat recovery. Energy Convers. Manag. 2020, 209, 112658, doi:10.1016/j.enconman.2020.112658.

60. MOROSUK, T.; TSATSARONIS, G. A new approach to the exergy analysis of absorption refrigeration machines. Energy 2008, 33, 890–907, doi:10.1016/j.energy.2007.09.012.

61. Morosuk, T.; Tsatsaronis, G. Advanced exergy analysis for chemically reacting systems—Application to a simple open gas-turbine system. Int. J. Thermodyn. 2009, 12, 105–111, doi:10.5541/ijot.245.

62. Morosuk, T.; Tsatsaronis, G. Splitting physical exergy: Theory and application. Energy 2019, 167, 698–707, doi:10.1016/j.energy.2018.10.090.

63. Shargut, Y. Exergy; in Russian; Shargut, R.P., Ed.; Energiia: Moscow, Russia, 1968.

64. Yukhimenko, N.; Vakal, S. The exergy analysis of energy efficiency of the technology of granulated phosphorus-potassium fertilizers. Eastern-European J. Enterp. Technol. 2016, 5, 4–10, doi:10.15587/1729-4061.2016.77182.

65. Quoilin, S.; Lemort, V. Technological and Economical Survey of Organic Rankine Cycle Systems. In Proceedings of the 5th European Conference Economics and Management of Energy in Industry, Algarve, Portugal, 14–17 April 2009; Volume 278, p. 12.

66. Madhawa, H.; Golubovic, M.; Worek, W.; Ikegami, Y. Optimum design criteria for an Organic Rankine cycle using low-temperature geothermal heat sources. Energy 2007, 32, 1698–1706, doi:10.1016/j.energy.2007.01.005.

67. Živić, M.; Galović, A.; Avsec, J.; Holik, M. Exergy analysis of a Brayton cycle with variable physical properties and variable composition of working substance. Teh. Vjesn. Tech. Gaz. 2016, 23, 801–808, doi:10.17559/TV-20160208112755.